INSTITUTO POTOSINO DE INVESTIGACIÓN CIENTÍFICA Y TECNOLÓGICA, A.C.

POSGRADO EN NANOCIENCIAS Y MATERIALES

The potential of reduced graphene oxide decorated with magnetite nanoparticles in the physical and biological processes of bioenergy production

Tesis que presenta

Itzel Covarrubias García

Para obtener el grado de

Doctor(a) en Nanociencias y Materiales

Codirectores de la tesis:

Dr. José Luis Rodríguez López
División de Materiales Avanzados

Dra. Sonia Lorena Arriaga García
División de Ciencias Ambientales

San Luis Potosí, S.L.P., abril de 2021

Constancia de aprobación de la tesis

La tesis **"The potential of reduced graphene oxide decorated with magnetite nanoparticles in the physical and biological processes of bioenergy production"** presentada para obtener el Grado de Doctor(a) en Nanociencias y Materiales fue elaborada por **Itzel Covarrubias García** y aprobada el día **12 de abril de 2021** por los suscritos, designados por el Colegio de Profesores de la División de Materiales Avanzados del Instituto Potosino de Investigación Científica y Tecnológica, A.C.

_____
Dr. José Luis Rodríguez López
Codirector de tesis

_____
Dra. Sonia Lorena Arriaga García
Codirectora de tesis

_____
Dr. Armando Encinas Oropesa
Miembro del Comité Tutoral

_____
Dr. Aitor Aizpuru
Miembro del Comité Tutoral

_____
Dr. Guillermo Quijano Govantes
Miembro del Comité Tutoral

Institutional acknowledgement

The present work thesis was developed in the Bio-Nanomaterials laboratory of Advanced Materials Division and in the Environmental Biotechnology laboratory of the Environmental Sciences Division of Instituto Potosino de Investigación Científica y Tecnológica, A.C (IPICyT); under the direction of PhD. José Luis Rodríguez López and PhD. Sonia Arriga García.

During the accomplishment of this work, the author received an academic grant from the National Council of Science and Tecnnology (No. 333080) and finantial support from IPICyT;
And has also been financed by the CONACYT project (No. CB -2014-01-239622).

As a part of this study, the author made a research stay at Institute National de la Recherche Scientifique-Eau Terre Environnement (INRS-ETE) at Université du Québec in Canada. The research stay was under the supervision of PhD. Antonio Avalos Ramirez and PhD. Satinder Kaur Brar. The academic stay was funded by Programme des futurs leaders dans les Amériques (PFLA, No. 509) and Beca mixta-CONACYT scholarship. The results of such stay are shown in chapter IV of this work.

Créditos Institucionales

Esta tesis de doctorado fue elaborada en el laboratorio de Bio-Nanomateriales de la División de Materiales Avanzados y en los laboratorios de Biotecnología Ambiental de la División de Ciencias Ambientales del Instituto Potosino de Investigación Científica y Tecnológica, A.C; bajo la dirección del Dr. José Luis Rodríguez López y la Dra. Sonia Arriaga García.

Durante la realización del trabajo la autora recibió una beca académica del Consejo Nacional de Ciencia y Tecnología (No. 333080) y apoyos financieros del Instituto Potosino de Investigación Científica y Tecnológica, A.C., y también ha sido financiado por el proyecto CONACYT (No. CB-2014-01-239622).

También, como parte de este trabajo se realizó una estancia de investigación en el Institute National de la Recherche Scientifique-Eau Terre Environnement (INRS-ETE) de la Universidad de Quebec en Canadá, bajo la supervisión del Dr. Antonio Avalos Ramírez y la Dra. Satinder Kaur Brar. La estancia fue financiada por el Programa Líderes Emergentes en las Américas (PFLA, No. 509) y Beca mixta-CONACYT. Los resultados de la estancia se presentan en el capítulo IV de la presente tesis.

IPICYT

Instituto Potosino de Investigación Científica y Tecnológica, A.C.

Acta de Examen de Grado

El Secretario Académico del Instituto Potosino de Investigación Científica y Tecnológica, A.C., certifica que en el Acta 019 del Libro Primero de Actas de Exámenes de Grado del Programa de Doctorado en Nanociencias y Materiales está asentado lo siguiente:

En la ciudad de San Luis Potosí a los 15 días del mes de abril del año 2021, se reunió a las 09:00 horas en las instalaciones del Instituto Potosino de Investigación Científica y Tecnológica, A.C., el Jurado integrado por:

Dr. Armando Encinas Oropesa	**Presidente**	**IPICYT**
Dr. José Luis Rodríguez López	**Secretario**	**IPICYT**
Dra. Sonia Lorena Arriaga García	**Sinodal**	**IPICYT**

a fin de efectuar el examen, que para obtener el Grado de:

DOCTORA EN NANOCIENCIAS Y MATERIALES

sustentó la C.

Itzel Covarrubias García

sobre la Tesis intitulada:

The potential of reduced graphene oxide decorated with magnetite nanoparticles in the physical and biological processes of bioenergy production

que se desarrolló bajo la dirección de

Dra. Sonia Lorena Arriaga García
Dr. José Luis Rodríguez López

El Jurado, después de deliberar, determinó

APROBARLA

Dándose por terminado el acto a las 11:00 horas, procediendo a la firma del Acta los integrantes del Jurado. Dando fe el Secretario Académico del Instituto.

A petición de la interesada y para los fines que a la misma convengan, se extiende el presente documento en la ciudad de San Luis Potosí, S.L.P., México, a los 15 días del mes de abril de 2021.

Dr. Marcial Bonilla Marín
Secretario Académico

Mtra. Ivonne Lizette Cuevas Vélez
Jefa del Departamento del Posgrado

INSTITUTO POTOSINO DE INVESTIGACIÓN CIENTÍFICA Y TECNOLÓGICA, A.C.
IPICYT
SECRETARIA ACADEMICA

Para Amaia y Alithzé, la luz en mi corazón, mi alegría, mis niñas que siempre me hacen ver lo que realmente importa en la vida.

Para Joel, mi esposo, por ser el mejor, gracias por todo tu apoyo, tu que siempre estás a mi lado alentándome y apoyándome en todo.
Gracias por todo amor.

Para mis padres a los que les debo todo lo que soy.

Para Lili y Hugo, mis hermanos que siempre están ahí y son mi motivo para ser mejor.

Acknowledgements

I wish to express my sincere thanks to my thesis Codirectors; to PhD. Sonia Arriaga García for her constant support, dedication and commitment in this research; and to PhD. José Luis Rodríguez López for your commitment and feedback in this research.

My sincere thanks is expressed to the committee members, PhD. Aitor Aizpuru, PhD. Guillermo Quijano and PhD. Armando Encinas for their invaluable comments and attentions.

My special gratitude to PhD. José Luis Sanchez García from Universidad Autónoma de San Luis Potosí (FCQ) for his assistant in the synthesis of nanomaterials.

My gratitude to Laboratorio Nacional de Investigaciones de Nanociencias y Nanotecnología (LINAN). I am especially thankful to MC. Breatriz Adriana Rivera Escoto and MC. Ana Iris Peña Maldonado for your technical support and advices for XRD, Raman and SEM.
My gratitude is also expressed to PhD. Daniel Bahena from Laboratorio Avanzado de Nanoscopia y Electronica, who helped us with STEM characterization.
My gratitude to academic technicians from Environmental Sciences Division of IPICyT, MC. Juan Pablo Rodas Ortiz, PhD. Elizabeth Diane Isaacs Paez and MC. Guillermo Vidriales Escobar.

A special gratitude is expressed to PhD. Antonio Avalos Ramirez and PhD. Satinder Kaur Brar for the opportunity of the research stay at the University of Quebec Canada. Thank you for your time and experience. Also, thank you to PhD. Joanna Lecka and MC. Carlos Osorio for your important assistance and friendship.

The use of the infrastructure of Environmental Sciences Division from IPICyT and Scientist-Water Earth Environment Department form University of Quebec are also acknowledged.

I.C.G is thankful to all the funding: Beca Nacional CONACYT, Beca mixta scholarship and Emerging Leaders in the Americas Program Scholarship. I.C.G is also thankful for the finantial support from Advanced Materials Division of IPICyT.

Finally but not least, to my laboratory co-workers for their time and invaluable help. Edgardo, Joel, Rodolfo, Mariana, Erika, Nohemi and Monica.

Content

List of tables

Chapter I. Introduction

Chapter II: Reduced graphene oxide decorated with magnetite nanoparticles enhance biomethane enrichment

Chapter III: Nanostructured complex of reduced graphene oxide adorned with magnetite as an adsorbent for inhibitor compounds in wood hydrolysates

Chapter IV. Use of reduced graphene oxide adorned with magnetite nanoparticles to enhance the production of metabolites of interest from syngas fermentation

.

List of figures

Chapter I. Introduction

Chapter II: Reduced graphene oxide decorated with magnetite nanoparticles enhance biomethane enrichment

Chapter III: Nanostructured complex of reduced graphene oxide adorned with magnetite as an adsorbent for inhibitor compounds in wood hydrolysates

Chapter IV. Use of reduced graphene oxide adorned with magnetite nanoparticles to enhance the production of metabolites of interest from syngas fermentation

Abbreviations

BES	2-Bromoethanesulfonate
AD	Anaerobic digestion
AGS	Anaerobic granular sludge
CO_2	Carbon dioxide
CO	Carbon monoxide
COD	Chemical oxygen demand
$CHCl_3$	Chloroform
CLSM	Confocal laser scanning microscopy
DIET	Direct interspecies electron transfer
ESC	Electron shuttling capacity
EPS	Extracellular polymeric substances
FTIR	Fourier-transform infrared
FR	Furfural Removal
GWh	Gigawatt Hour
GR	Glucose removal
GO	Graphene oxide
Gt	Graphite
GtO	Graphite oxide
HTR	Hydraulic retention time
H_2	Hydrogen
MNPs	Magnetite nanoparticles
Fe_3O_4	Magnetite
MW	megawatt
CH_4	Methane
MWCNTs	Multi-wall carbon nanotubes
NPs	Nanoparticles
rGO	Reduced graphene oxide
SEM	Scanning electron microscopy
Q	sorption capacity
TOC	Total organic carbon
TEM	Transmission electron microscopy
VFA	Volatile fatty acid
XRD	X-ray diffraction

Resumen

En este trabajo se estudiaron los efectos de la adición óxido de grafeno reducido adornado/decorado con nanopartículas de magnetita (rGO-MNPs) en diferentes procesos biológicos para la producción de energía. El trabajo de tesis se divide en V capítulos. El Capítulo I presenta una visión general sobre procesos biológicos para la producción de energía en donde se han adicionado nanomateriales. En el Capítulo II se estudia la adición de rGO-MNPs en el enriquecimiento de biogás por microorganismos hidrogenotróficos y la adición de H_2. Se concluyó que el composito rGO-MNPs estimuló la producción de CH_4 en un 47%, 28% y 33% con 50, 100 y 200 mg/L del composito. La mejora se vinculó a la capacidad de sorción de H_2, a la mejora en la capacidad de transferencia de electrones (ESC), y al Fe^{2+} liberado al medio líquido. En cuanto a los cambios estructurales, los espectros Raman y los patrones de difracción de rayos equis (XRD) del rGO-MNPs recuperado indicaron una pérdida de cristalinidad. El Capítulo III presenta el uso de rGO-MNPs como adsorbente de compuestos inhibidores presentes en hidrolizados de madera. Los hidrolizados de madera provienen de biomasa lignocelulósica, una materia prima abundante y renovable que puede ser utilizada para la producción de biocombustibles. Durante la obtención del hidrolizado se pueden producir diferentes subproductos distintos de los azúcares, estos pueden causar inhibición microbiana en el subsecuente proceso de fermentación. Por tanto, rGO-MNPs se utilizó como adsorbente para desintoxicar el hidrolizado. rGO-MNPs pudo adsorber furfural y otros compuestos inhibidores derivados de la lignina con una pérdida mínima de azúcar de 5.9, 6.2 y 7.6%, para 10, 20 y 50 mg de composito. En el Capítulo IV se estudió la adición los nanomateriales en el proceso de fermentación de syngas para obtener metabolitos de interés como es el ácido acético. Se encontró que el óxido de grafeno reducido (rGO) y rGO-MNPs mejoraron la producción de ácido acético en un 32% y un 23% con 100 mg/L de material. Tal mejora se relacionó con la mayor capacidad de transferencia de electrones y la capacidad de sorción. Finalmente, en el Capítulo V se presentan las cocluciones, las perspectivas y las observaciones finales del trabajo de tesis.

Palabras Clave: grafeno; magnetita; biogás; syngas; hidrolizados de madera

Abstract

In this work, the effects of the addition of reduced graphene oxide adorned/decorated with magnetite nanoparticles (rGO-MNPs) were analyzed for bioenergy production. The thesis work is divided into V chapters. Chapter I is an overview of nanoadditives in biological processes to produce energy. Chapter II presents the effects of the addition of rGO-MNPs in the biogas enrichment process. Interestingly, rGO-MNPs boosted the CH_4 production by 47%, 28% and 33% relative to the control without nanomaterial for 50, 100 and 200 mg/L, respectively. The improving in CH_4 was linked to the sorption capacity of the nanomaterials, to the electron shuttling capacity (ESC) provided from conductive graphene, and to the release of Fe^{2+} in the media. Moreover, significant structural changes occurred in the rGO-MNPs composite after hydrogenotrophic tests. Raman spectra and XRD patterns of the recovered rGO-MNPs suggested a loss of crystallinity, and FTIR and Raman indicated that the material was oxidized during biological treatment. Chapter III explores the use of rGO-MNPs as adsorbent for inhibitor compounds present in wood hydrolysates. The importance of the use of wood hydrolysates lies in the fact that they come from lignocellulosic biomass, an abundant and renewable feedstock for biofuels. During the hydrolysis step, different by-products other than sugars, can cause microbial inhibition in the fermentation step. Therefore, rGO-MNPs was used to detoxificate the hydrolysate. It was conclude that rGO-MNPs can adsorb fermentation inhibitors such as, furfural, 5-hydroxymethyl-furfural, levulinic acid, vanillic acid and vanillin from wood hydrolysates with a minimal sugar loss of 5.9, 6.2 and 7.6%, for 10, 20 and 50 mg of the adsorbent. Then, Chapter IV shows that the addition of reduced graphene oxide (rGO) and rGO-MNPs can improve the production of acetic acid, a very important commodity in the chemical industry. rGO and rGO-MNPs enhanced the acetic acid production by 32% and 23% with 100 mg/L of nanomaterial added, respectively. Such improvement is linked to the higher electron shuttling capacity, the sorption capacity and the dosing of dissolved Fe^{2+} to the medium. Finally, chapter V presents the perspectives, conclusions and final remarks of the thesis work.

Keywords: graphene; magnetite; biogas; syngas; wood hydrolysates

Chapter I: Introduction

1. Introduction

Nowadays the world has confronted with two crises, i.e.; the fossil fuel depletion and environmental degradation. The widespread use of fossil fuels within the current energy infrastructure is considered as the largest source of anthropogenic emissions of carbon dioxide (CO_2), which is largely blamed for global warming and climate change (Letcher, 2019; Yoro and Daramola, 2020; Zanganeh and Shafeen, 2007). The primary anthropogenic source of CO_2 is the combustion of fossil fuels, with major contributors being electricity and heat production (42%), transport (23%), and industry (19%) (IEA, 2016). Therefore, the research of new technologies for energy development is necessary.

In this first Chapter the main components used in the thesis will be reviewed, such as concepts, processes, materials and approaches currently used in the development of new technologies for bioenergy production. Later, the justification of the work is presented, as well as the hypotheses and the general and specific objectives that motivated the thesis. The structure of the thesis is developed as follows: Chapter I, review of the related topics to nanomaterials and bioenergy production; Chapter II and III, articles already published; Chapter IV, article that will be forthcoming for peer review; and Chapter V, conclusions and perspectives.

1.1 Biogas

Biogas is the main vehicle for producing bioenergy from anaerobic digestion (**AD**) in the frame of modern bioeconomy and has been evaluated as one of the most energy efficient and environmentally beneficial technology (Fehrenbach et al., 2008; Koniuszewska et al., 2020; Zhang et al., 2016). It has been highlighted that AD is the only environmentally friendly renewable gas production technology at industrial scale from agricultural residues and organic wastes (O'Connor et al., 2021; Siegl et al., 2012, 2011). The purified and enriched version of biogas is a versatile renewable energy source, which can be used for replacement of fossil fuels in power and heat production, and it can be used also as gaseous vehicle fuel. Biogas is generated by microorganisms in the absence of air by a so called anaerobic metabolism. Industrial

biogas is produced at (1) sewage treatment plants (sludge fermentation stage), (2) landfills, (3) sites with industrial processing industry and (4) at digestion plants for agricultural organic waste, both mesophilic (35°C) and thermophilic (55°C) conditions (Jönsson et al., 2003; Koniuszewska et al., 2020). An overall scheme for AD of organic substrates to methane (CH_4) is indicated in **Figure 1**.

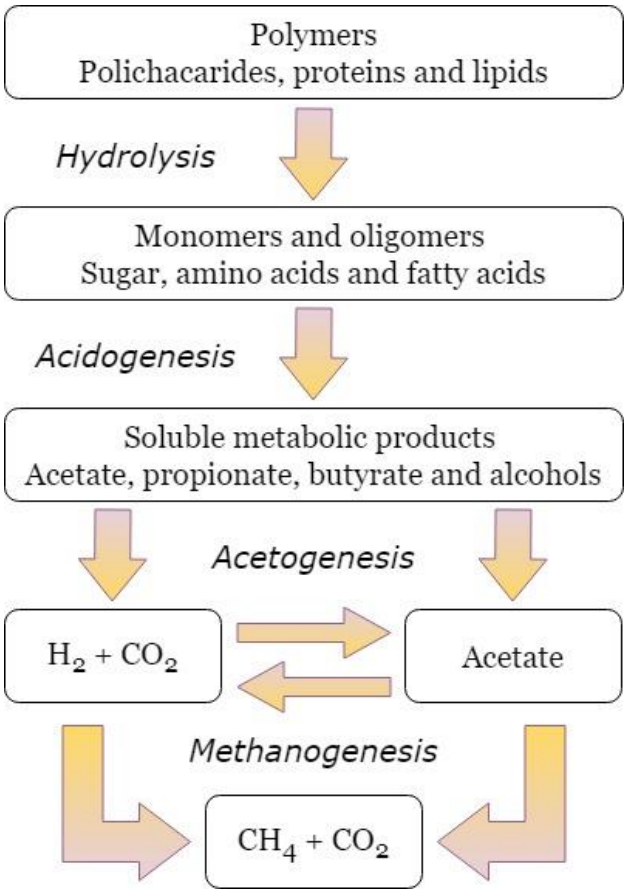

Figure 1. Scheme of biogas production.

The degradation of particulate organic matter follows a complex reaction network, during anaerobic degradation, particulate biopolymers (carbohydrates, proteins and lipids) are firstly hydrolyzed to organic monomers and oligomers, which can be utilized either as substrates by fermentative organisms (amino acids, sugars) or by anaerobic oxidizers (fatty acids). The carbonic products from these reactions are either acetate and hydrogen (H_2) or intermediate compounds, such as propionate and butyrate, which may later be converted to acetate and H_2. CH_4 is mostly

produced from acetate or H_2 and CO_2 or formate (Nozhevnikova et al., 2020; Ryckebosch et al., 2011). The nature of the raw materials and the operational conditions used during AD determined the chemical composition of the biogas (Möller and Müller, 2012; Persson, 2003; Tambone et al., 2010). Raw biogas consists mainly in CH_4 (40-75%) and CO_2 (15-60%) and other trace amounts. The impurities can affect the fuel quality and can cause problems to the devices for biogas utilization, e.g., large concentrations of O_2 can entail explosion hazards while high levels of H_2S in combination with condensate water cause corrosion. Likewise, NH_3 and halogenated hydrocarbons generate corrosive products during combustion which can severely damage engines and downstream pipelines. Moreover, the presence of impurities can also lead to undesired emissions during utilization (Chaemchuen et al., 2016; Deng et al., 2020; Persson et al., 2006). In **Table 1** it can be observed all the possible impacts that the trace components could cause (Ryckebosch et al., 2011).

Table 1. Possible impacts of trace components in biogas

Impurity	Possible Impact
Water	Corrosion in compressors, gas storage tanks and engines due to reaction with H_2S, NH_3 and CO_2 to form acids. Accumulation of water in pipes. Condensation and/or freezing due to high pressure.
Dust	Clogging due to deposition in compressors, gas storage tanks.
H_2S	Corrosion in compressors, gas storage tanks and engines. Toxic concentrations of H_2S (>5 cm_3/m^3) remain in the biogas. SO_2 and SO_3 are formed due to combustion, which are more toxic than H_2S and cause corrosion with water.
CO_2	Low calorific value.
Siloxanes	Formation of SiO_2 and microcrystalline quartz due to combustion; deposition at spark plugs, valves and cylinder heads abrading the surface.
Hydrocarbons	Corrosion in engines due to combustion.
NH_3	Corrosion when dissolved in water.
O_2/air	Explosive mixtures due to high concentrations of O_2 in biogas.
Cl-	Corrosion in combustion engines.
F-	Corrosion in combustion engines.

The main problems are related with corrosion and the low calorific value due to the large proportion of CO_2. For the above, it is necessary first to remove the harmful

trace components that are not CO_2 "cleaning" step (i.e. Ammonia, H_2 sulphide, water vapor, etc.) and then, the "upgrading" process to remove CO_2. The upgrading process, in which CO_2 is removed, is also needed to adjust the calorific value and relative density of biogas in order to meet the specifications of Wobbe Index, which is used to compare the combustion energy output of different composition fuel gases in an appliance (fire, cooker etc.). After conditioning, the final product is referred to as "biomethane", typically containing 95-97% of CH_4 and 1-3% of CO_2 (Baccioli et al., 2018; Sun et al., 2016). Biomethane can be used as an alternative for natural gas, but the type of end use sets in quality demands (Wellinger and Lindberg, 2005).

1.2 Nanomaterials promoting biogas production during anaerobic digestion

Nanoparticles (**NPs**) have one or more dimensions of the order of 100 nm ($1nm=10^{-9}$ m) or less, these have attracted great attention due to their unique physicochemical properties such as structure, surface area, solubility and catalytic characteristic that have enabled their application in different areas (Daniel and Astruc, 2004; Li et al., 2011; Sajid and Płotka-Wasylka, 2020). Their size and their relatively large surface-to-area ratio when compared to the same volume that is made from larger particles can result in a higher magnitude of reactivity or interaction with adjacent surfaces, hence enhancing the properties of the carrying fluid with a lower amount of the same material (Alsaba et al., 2020). The innovative and revolutionary nature of nanotechnology is attributed to quantum mechanics principles. Therefore the behavior of the material is now under the control of quantum laws rather than classical physics (Mohan Bhagyaraj and Oluwafemi, 2018). This fact gives the nanomaterial new properties that may be more favorable than those of the bulk material version.

Several studies have focused on the effects of the addition of different nanomaterials on the biogas production and biomethane production. These nanomaterials include metal oxides, zero-valent metals and carbon based materials (Ganzoury and Allam, 2015). Some of them have much potential for improving biogas and CH_4 production. In general, it has been found that the addition of some NPs in the AD process can

present a negative/positive or null effect on the production of biogas and CH_4, this depending on the type of nanoparticle, the concentration added and size.

1.2.1 Carbon based Nanoadditives

Currently, adding low-cost conductive materials (e.g. biochar; activated carbon, nanoscale iron and others) to anaerobic treatment is a promising technology. Carbon based nanoadditives have been applied to improve the AD efficiency and CH_4 yield. The main advantage with the use of these materials is that they play a higher conductivity role in promoting the direct interspecies electron transfer (**DIET**) (Chen et al., 2014a, 2014b; Lin et al., 2017; Tian et al., 2017; Zhang et al., 2017). DIET is an inherent mechanism for electrons exchange between different species of microorganisms, in which free electrons flow from one cell to another without being shuttled by reduced molecules such as molecular H_2 or formate (Dubé and Guiot, 2015). Conductive materials could act as either substitute of *e-pili* or electron conduit to promote DIET. However, there may be instances in which electrical contacts are made between electron transport proteins associated with the outer membranes of the partners (Lovley, 2017). Alternatively, DIET partners can plug into carbon materials, such as granular activated carbon, carbon cloth and biochar, for long-range electron exchange without the need for *e-pili* (Chen et al., 2014b, 2014a; F. Liu et al., 2012). Thereby, DIET is promoted by the addition of conductive materials. In addition, the conductive materials have high surface area and microporous structure, which could supply reaction sites for microorganisms and adsorb hazardous pollutants (Wei et al., 2018). **Table 2** shows different studies where conductive carbon based nanoadditives have been used in AD processes.

Table 2. Studies of carbon based nanoadditives in anaerobic digestion process.

Nanoadditive	Concentration and size	Effect	System & conditions	Comments	Reference
Fullerene	0.321 mg/ kg biomass	No effect	T: Ambient °C Substrate: Glucose, Ethanol and Methanol (75 µL)	No significant difference was shown	Nyberg et al., 2008

Single walled nanotubes	1000 mg/L	No effect	UASB T: 35°C HTR: 12 h COD: 10.28 COD/m^3 d Substrate: Sucrose	No effect on CH_4. Excretion of more extracellular polymer substance (EPS), which reduced its cytotoxicity	Li et al., 2014
Multi-wall carbon nanotubes (MWCNTs)	1500 mg/L MWCNTs	Positive	T: 36°C HTR: 12 h COD: 3.2 kg m^{-3} d^{-1} Substrate: Sucrose 2000 mg/L pH: 6.9	Enhancement of 43.9% of CH_4. EPS excretion, which reduced its cytotoxicity	Ambuchi et al., 2016
Graphene	30 and 120 mg/L	Positive	T: 35°C 100 rpm Substrate: Glucose 2000 mg-COD/L	Enhancement of 17% and 51.4% of CH_4 with 30 and 120 mg/L, respectivetly	Tian et al., 2017
Graphene	1 g/L	Positive	T: 35°C Analyzed every 2 d Substrate: Ethanol 2.5 mL pH: 7.5	CH_4 yield was enhanced 25% and increased the ethanol production rate 20%. Microbial structures of electro-active bacteria and archaea were revealed	Lin et al., 2017
Graphene oxide (GO)	5 mg/L 50 mg/L 100 mg/L 500 mg/L 500 nm- 5µm. Thickness of 0.8-1.2 nm	Negative	T: 37°C pH: Was not keep	CH_4 was reduced: [5mg/L]:13.1%; [50 mg/L]:10.6%; [100 mg/L]:2.7%; [500 mg/L]:17.1%. Archaea and bacteria community changed little after GO addition.	Zhang et al., 2017

As a highly-conductive nanomaterial, graphene has received heightened attention for biotechnological applications (ElMekawy et al., 2017; Perreault et al., 2015). Several studies have reported that supplementation graphene to anaerobic digester

promotes CH_4 production rate increases the population of electroactive microorganism (e.g., *Geobacter* and *Methanosarcina* species) (Lin et al., 2017; Tian et al., 2017). For instance, Lin et al. (2017) added three different concentrations of graphene (0.5, 1.0 and 2.0 g/L) in an AD degrading cellulose. They found that the addition of 1 g/L resulted in the highest biomethane yield (695±9.1 mL/g) and production rate (95.7±7.6 mL/g/d), corresponding to an enhancement of 25% in biomethane yield and 19.5% in production rate. The degradation rate of ethanol was simultaneously enhanced and the electrogenic bacteria of *Geobacter* and *Pseudomonas* along with archaea *Methanobacterium* and *Methanospirillum* might participate in DIET responsible for enhanced AD performance (Lin et al., 2017). At the same time, this study hypothesized that materials with high conductivity play a significant role in promoting the DIET, which was proved by the addition of activated charcoal (a material with a lower electrical conductivity). Moreover, the better performance with graphene was due to its micro size, which is much smaller, resulting in a higher specific surface area and a better interaction with microbes (Lin et al., 2017). Despite the positive results, the concentration of graphene added is high ompared with other studies, in the range of g/L. Other studies have added graphene at lower concentrations. Tian et al., (2017) found that the addition of 30 and 120 mg/L of graphene increased CH_4 production by 17% and 51%, respectivetly, in AD process. On the other hand, Zhang et al. (2017) studied the effects of graphene oxide (**GO**) on the performance, microbial community dynamics and antibiotic resistance genes reduction during AD of swine manure. Results showed that accumulative CH_4 production was reduced by 13.1%, 10.6%, 2.7% and 17.1 % at GO concentration of 5 mg/L, 50 mg/L, 100 mg/L and 500 mg/L, respectively. Thus, CH_4 reduction was not dose-dependent; the maximum reduction was at 5 mg/L and 500 mg/L, while the least CH_4 reduction was 100 mg/L. The unique physicochemical properties of graphene, such as exceptionally high electric conductivity, large surface area and good mechanical strength, may provide a solution to improve the stability and efficiency of AD.

Other conductive carbon materials such as fullerene, single and multi-wall carbon nanotubes have been also used as nanoadditives in AD. For example, Nyberg et al.,

(2008) studied the exposure of fullerene to an anaerobic digester sludge. They not found a significant difference with/without the addition of fullerene with the different substrates used. Therefore, a no significant effect over the CH_4 production rate. Such conclusion was based on the absence of toxicity indicated by no change in methanogenesis relative to untreated reference samples (Nyberg et al., 2008). Likewise, Li et al., (2014) reported a null effect on CH_4 production with the addition of 1000 mg/L of single walled nanotubes; Notwithstanding they observed more excretion of extracellular polymer substance (**EPS**). Otherwise, the addition of 1500 mg/L of multi-wall carbon nanotubes (**MWCNTs**) induced a 43.9% higher CH_4 production compared with the control. In addition, the study also revealed more EPS excretion and its interaction with the nanotubes which helped to reduce its cytotoxicity (Ambuchi et al., 2016). Overall, the addition of carbon based nanomaterials not only depends on their conductive properties to stimulate the AD process by DIET, but also on other factors such as its chemical nature, its shape, concentration among others.

1.2.2 Iron Nanoadditives

Many research have focused on improving the methanogenic activity and thus enhance the CH_4 production in AD. Among them, Fe^{2+} has being used as an electron-donor to reduce the oxidation-reduction potential and thus offer a more suitable microenvironment for methanogens (Chakraborty et al., 2010; Feng et al., 2014; Y. Zhang et al., 2011). For instance, it has been found that zero valent podwer can increase by 43.5% the CH_4 produciton in organic matter AD (Feng et al., 2014). In recent years, iron has been added at nanoscale to further potentiate the effects on CH_4 production. Iron has been added at nanoscale at different forms (e.g. zero valent, oxidized, magnetite, composites, etc.). Iron nanoadditives in AD processes are presented in **Table 3**. Zero valent iron, a low cost and metallic chemical, can be freely obtained from machinery factory. It has been proven to be able to enhance methanogenesis (Karri et al., 2005). Zero valent iron has proved to be an effective enhancer in biogas production and at the same time has presented a negative impact, this due to the concentration added. For instance, Su et al., (2013) reported

an improvement in biogas production of 30.4% and in CH_4 production of 40.4% with 0.1% wt added and a size of 20 nm. On the other hand, Gonzalez-Estrella et al., (2013) found that 1500 mg/L of Fe° NPs decreased the methanogenic activity by 85% and decreased the hydrogenotrophic methanogenesis by 91%. Yang et al., (2013) found a negative and a positive effect, with 1 and 10 nM of Fe°, biogas production decreased 20% and 70%, respectively, while with 30 nM of Fe°, CH_4 production increased 10%. Therefore, the addition of Fe° does not depend on concentration. On the other hand, iron has been added as magnetite. Casals et al. (2014) reported an increment in biogas production of 180% and an increment of 234% in CH_4 production when magnetite (Fe_3O_4) NPs (100 mg/L, 7 nm) were added. This is the largest improvement in biogas production to date, and approaches the theoretical limits of organic matter into biogas conversion. They introduce a novel concept of dosing ions by size and surface-state; where the NPs acts as the carrier and the released ion as the active compound. The NPs first disperse and then progressively dissolve over an extended period of time to yield the dietary supply of iron for the microorganisms in the reactor. Fe_3O_4 is an iron oxide of mixed oxidation state [Fe(II), Fe(III)] that contributes largely to geomagnetism and plays a significant role in diagenesis in marine and freshwater sediments. It ranks as the third or fourth most diverse mineral product formed biochemically by living organisms and it forms naturally in variety of human tissues (Kirschvink et al., 1992). Magnetite has also been added at no nanometric scale. For instance, 5 g/L of Fe_3O_4 powder (0.1 mm) has been shown as an additive to improve tetracycline degradation (antibiotic contaminant) and CH_4 production (Zhao et al., 2020). Such study showed the advantage of degrading pollutants simultaneously with use of Fe_3O_4. Likewise, the addition of 200 mg/L magnetic carbon (20-50 nm) allowed an enhancement of 58% in CH_4 production and at the same time they reached a pyrene removal rate of 77% (Li et al., 2020). The main advantaje of the addition of iron in magnetic based material is that the nanomaterial can be almost completely recovered and thus could be used in other cycles. The role that magnetite NPs make to enhance the CH_4 production has been reported by Zhong et al., (2020). They stated that Fe_3O_4 NPs addition to AD process accelerate the electrons transfer from acids oxidizers to syntrophic

methanogenes, further stimulate acids oxidizers to decompose acetate to H_2/CO_2, and finally facilitate more CH_4 production (Zhong et al., 2020).

Iron has also been added in composite form. For instance, Hassaneen et al., (2020) tested three nanocomposite formulations, Zinc ferrite (ZnFe), ZnFe with 10% carbon nanotubes, and zinc ferrite with 10% C76 fullerene, on lab scale biodigesters containing organic slurry. The maximum CH_4 enhancement was obtained for ZnFe (185%), followed by ZnFe with carbon nanotubes (ZFCNTs) (162%) and ZnFe with fullerene (ZFC76) (145%) at concentrations of 500 mg/L. They related the improvement to the synergistic effect of zinc and iron. Zinc is implied for methyl coenzyme-M activation of CH_4 formation, and catalyzes formate utilization, and iron is required for the activity of every single enzyme in methanogenic reactions. The main disadvantage of these nanoparticles is that they can be swept away by the current of the medium. Therefore, the addition of Fe NPs in magnetite form can present the main advantage of being recovered almost completely.

Table 3. Studies of iron nanoadditives in anaerobic digestion process.

Nanoadditive	Concentration and size	Effect	System & conditions	Comments	Reference
Fe^0	0.1 wt% 20 nm	Positive	T: 37°C Waste activated sludge pH: 8.6	Biogas production increased 30.4% CH_4 production increased 40.4%	Su et al., 2013
Fe^0	1500 mg/L	Negative	T: 30±2°C COD: 1 g COD L^{-1} Substrate: Sodium acetate pH: 7.2	Decreased methanogenic activity 85% Decreased hydrogenotrophic methanogenesis 91%	Gonzalez-Estrella et al., 2013
Fe^0	1, 10, 30 nM	Negative and Positive	T: 37°C COD: 1000 COD L^{-1} Substrate: Glucose pH: Was not kept	1 and 10 nM decreased 20% and 70% biogas production 30 nM increased 10% CH_4 production.	Yang et al., 2013
Fe^0	0.1% w/w 160 nm	Positive	T: 37°C	CH_4 increased 25.2%	Suanon et al., 2017

			Substrate: sewage sludge pH: 7	Effects on CH_4 yield, and pharmaceutical and personal care removal was investigated.	
FeO	750 mg/L 30nm	Positive	T: 36°C COD: 3.2 kg m^{-3} d^{-1} Substrate: Sucrose 2000 mg/L pH: 6.9	Enhancement of 38.1% of biogas production rate.	Ambuchi et al., 2016
Fe_2O_3	1500 mg/L; 10-100 nm	No effect and decreased hydrogenotrophic methanogenesis	T: 30±2°C COD: 1 g COD L-1 Substrate: Sodium acetate pH: 7.2	Acetoclastic methanogenesis had no effect. Hydrogenotrophic Methanogenesis was improved 82%.	Gonzalez-Estrella et al., 2013
Fe_3O_4	100 mg/L 7 nm	Positive	T: 37°C Substrate: Cellulose 1.7 g pH: 8	Biogas production increased 180% CH_4 production increased 234%	Casals et al., 2014
Fe **Fe_3O_4**	20 mg/L 7-9 nm	Positive	T: 37°C Substrate: Slurry pH: 6.13	1.4 times biogas volume with Fe 1.6 times biogas volume with Fe_3O_4	Abdelsalam et al., 2017
Fe_3O_4	10 mg/L	Positive	T: 37°C Substrate: Microalga biomass pH: 5.6-6.6	28% increase of biogas	Zaidi et al., 2018
Fe_3O_4	0.01, 0.04 and 0.12% w/w 20-30 nm	Positive	T: 37°C Substrate: sugar beets pH: 7	CH_4 production increased 19.77% (0.04% Fe_3O_4) Biogas production increased 15.09%. (0.04% Fe_3O_4)	Beiki and Keramati, 2019
Fe_3O_4	200 mg/L 40-60 nm	Positive	Anaerobic semi-continuous tank reactor (ASTR). T: 35°C	ASTR with Fe_3O_4 NPs improved COD removal efficiency and CH_4 production of 86.1% and 1350 mL/day as	Zhong et al., 2020

			HTR: 10 days Substrate: synthetic wastewater pH: 7	compared with control (55.0% and 670 mL/day).	
Zinc ferrite (ZnFe), ZnFe with 10% carbon nanotubes (ZFCNTs), ZnFe with 10% C76 fullerene (ZFC76)	500 mg/L ZnFe: 8-9 nm. ZFCNTs: ZnFe particles 5-6 nm anchored to the surface of nanotubes with wall thickness of 45 nm. ZFC76: core diameter of 14 nm coated with a uniform shell of ZnFe of 5 nm.	Positive	T: 40°C Substrate: cattle manures pH: 7.35	The maximum CH_4 enhancement was obtained for ZnFe (185%), followed by ZFCNTs (162%) and (ZFC76) (145%).	Hassaneen et al., 2020
Magnetic carbon (FeS)	200 mg/L 20-50 nm 100 m^2/g	Positive	T: 38°C Substrate: x pH: 6.6-7.5	CH_4 enhancement was 58%. The pyrene removal rates reached 77.5%. Reduced the accumulation of short-chain fatty acids and avoided acidification during the 25 days.	Li et al., 2020

1.2.3 Ag, Al, Au, Ce, Cu Nanoadditives

Table 4 shows studies of Ag, Al, Ce and Cu as nanoadditives in anaerobic digestion processes. In general, Ag, Au, CuO, Al_2O, CeO_2 have presented a either a negative or null effect in the AD process. However, it has been reported that the biogas production could increase in the last days of the experiment (Luna-delRisco et al., 2011). This can be explained by the anaerobic microorganisms that can became familiar to the toxic effect of the added materials.

Table 4. Studies of Ag, Al, Ce and Cu as nanoadditives in anaerobic digestion process.

Nanoadditive	Concentration and size	Effect	System & conditions	Comments	Reference
Ag **Au**	Ag: 170 mg/L Au: 100 mg/L 20, 30 nm	No effect	T: 37 and 55°C Substrate: Cellulose 1 g pH: 8	No significant difference	García et al., 2012
Ag^0 **Cu0**	1500 mg/L	Ag: No effect Cu: Negative	T: 30±2°C COD: 1 g COD L^{-1} Substrate: Sodium acetate pH: 7.2	Ag^0 did not show a significant effect. Cu^0 completely inhibited methanogenesis.	Gonzalez-Estrella et al., 2013
CuO	15 mg/L 5µm-30nm	Negative	T: 36°C Substrate: Cattle manure pH: 6.9	Biogas production increased in the las days of the experiment.	Luna-delRisco et al., 2011
CuO	1.4 mg/L 37nm	Negative	UASB reactor T: 30±2°C HTR: 12 h COD: 1.5 g COD L^{-1} Substrate: VFAs pH: 7.8	Decrease 15% CH_4 production. CuO inhibited acetoclastic activities instead of hydrogenotrophic.	Otero-González et al., 2014
Al_2O_3 **CeO_2** **CuO**	1500 mg/L; 10-100 nm	Al_2O_3 CeO_2 CuO No effect	T: 30±2°C COD: 1 g COD L^{-1} Substrate: Sodium acetate pH: 7.2	Al_2O_3 had no effect. CeO_2 decreased methanogenic activity (80%) CuO decreased methanogenic activity (87%) Al_2O_3 decreased Hydrogenotrophic methanogenesis (82%) CeO_2 decreased Hydrogenotrophic methanogenesis (82%) CuO had no effect.	Gonzalez-Estrella et al., 2013

1.2.4 Ti, Si, Mn, Zn Nanoadditives

Table 5 shows studies of Ti, Si, Mn and Zn as nanoadditives in anaerobic digestion process.

As can be seen in the Table, most studies have presented a negative or null effect in the biogas and CH_4 production. Only, García et al., (2012) found that the addition of 1120 mg/L (7.5 nm) of TiO_2 increased the biogas production by 10%.

Table 5. Studies of Ti, Si, Mn and Zn as nanoadditives in anaerobic digestion process.

Nanoadditive	Concentration and size	Effect	System & conditions	Comments	Reference
ZnO	15 mg/L ZnO: 15 µm, 50-70 nm	Negative	T: 36 °C Substrate: Cattle manure pH: 6.9	Biogas production increased in the las days of the experiment.	Luna-delRisco et al., 2011
Mn_2O_3 **TiO_2** **SiO_2** **ZnO**	1500 mg/L; 10-100 nm	Negative	T: 30±2°C COD: 1 g COD L^{-1} Substrate: Sodium acetate pH: 7.2	Mn_2O_3 and ZnO decreased their methanogenic activity (50-53%) TiO_2 and SiO_2 had no effect methanogenic activity. Mn_2O_3 and ZnO decreased their hydrogenotrophic activity (60-75%). TiO_2 and SiO_2 had no effect hydrogenotrophic activity.	Gonzalez-Estrella et al., 2013
TiO_2	1120 mg/L 7.5 nm		T: 37 and 55°C Substrate: Cellulose 1 g pH: 8	Biogas production increased (10%)	García et al., 2012
TiO_2	0.01, 0.04 and 0.12% w/w 10-15 nm	No effect	T: 37°C Substrate: sugar beets pH: 7	No effect	Beiki and Keramati, 2019

1.2.5 Other Nanoadditives

In literature other nanoadditives have been added to anaerobic processes. For instance, Lo et al., (2012) used micro/nano ash and flying ash from a municipal solid waste incinerator. They found a significant increase in the production of biogas. The highest biogas production was 193 mL/g of biogas, 3.5 times higher than the control. This was attributed to compounds contained in the ashes (Al_2O_3, $CaCO_3$, $Ca(OH)_2$, SiO_2, Ca_3SiO_5, $CaMg(CO_3)_2$, Ca_2SiO_4, PbO and ZnS) and due to the nature of the agglomeration of nanosubstances, which provided more space for microorganisms to gowth.

Table 6. Studies of other nanoadditives in anaerobic digestion process

Nanoadditive	Concentration and size	Effect	System & conditions	Comments	Reference
Micro/ nano bottom ash.	Micro/nano bottom ash: 0.6, 12, 36, 60 and 120 g/g VSS.	Positive	T: 35°C pH: was not kept	Increase in the production of biogas with 36 g/g VSS. Provided more habitats for microorganisms.	Lo et al., 2012
Flying ash	Flying ash: 0.12, 3, 6, 18 and 30 g/g VSS		Ashes obtained from a municipal solid waste incinerator		

3. Biogas upgrading

In general, the upgrading of biogas to biomethane can be accomplished by physicochemical separation and disposing of all gaseous compounds other than CH_4 by different methods such as gas/gas or liquid/gas separation by membrane separation, vacuum or pressure swing adsorption, as well as by using cryogenic separation as comprehensively reviewed elsewhere (Ryckebosch et al., 2011; Yang et al., 2014). Several studies are reported in order to solve this issue. Among them, biological CH_4 production using methanogenic *archaea* (**Equation 1**), is a promising technology for CO_2 neutral energy production and storage. During this process H_2 and CO_2 are converted into CH_4 and H_2O. Such route can be carried out in an AD (*in situ*), or in a separate reactor (*ex situ*).

$$CO_2 + 4 \cdot H_2 + archaea \leftrightarrow CH_4 + 2 \cdot H_2O \quad (1)$$

The responsible *archaea* for this biotransformation are part of the microbial consortium preset in any biogas plant and interact closely with syntrophic bacteria that convert organic acid and alcohols into acetate, CO_2 and H_2. The main drawback in the *in situ* process is related to the increase of the H_2 partial pressure (PH_2) in the biogas reactor, which leads to an inhibition of *VFAs* (propionate and butyrate) degradation and thus, a break down or process disturbance (Siriwongrungson et al., 2007). Its efficiency depends on the close syntrophic relationship between microorganisms. The complete hydrogenotrophic biometanisation is only feasible if all the H_2 can be forced quantitatively into the liquid phase (Simon & Rittmann 2015). On the other hand, higher volumetric CH_4 production rates have been reached in the *ex situ* process. However, a problem still remains with the mass transfer of gas phase of H_2 to the liquid phase. Notwithstanding, *ex situ* process have the advantage that individual process control can be applied. It is important to mention the use of H_2 since, availability and cost are limiting factors in its use and 4 moles of H_2 are needed per mole of CO_2. An attractive way of producing the H_2 needed for biological biogas upgrading process is through water electrolysis from exploiting surplus wind mill, since wind is one of the most promising renewable energy sources (Sherif et al., 2005). For instance, commercial wind power has been produced in Denmark since the 1970s, and wind power currently accounts for nearly 20% of the Danish electricity supply (Manson, 2008). Nowadays, this surplus of energy is used to produce H_2 by water electrolysis and then to biological biogas upgrading.

3.1 Nanoadditives in biogas upgrading

As mention above, the limiting step in biogas upgrading is the low mass transfer of H_2 from gas phase to liquid phase, so, it would be wise to add NPs that present an affinity to H_2 sorption by increasing the diffusion rate. Carbon based materials are interesting candidates for the storage of H_2 due to their low density, suitability for large scale production, wide range of structural shapes, chemical stability, their ability to be modified on the surface, wide range of preparation, carbonization and activation conditions (Srinivas et al., 2010). Moreover, it has been reported that the

storage capacity of H_2 is enhanced by the doping of metallic NPs (Ag, B, Ca, Fe, K, Li, Ni, Pd, Pt, Ru, Ti, TiO_2 and V) onto those nanostructures (Campesi et al., 2008; Ferre-Vilaplana, 2008; Hwang et al., 2009; Kim et al., 2005; Lee et al., 2010; Reyhani et al., 2011, 2009; Wang et al., 2009; Zacharia et al., 2005).

So far, few studies have attempted the addition of NPs to the biological process of biogas upgrading.

4. Syngas production and syngas fermentation

Gasification is the thermochemical process of converting carbonaceous materials, such as coal, petroleum or biomass, in the presence of a controlled amount of oxidant (air/O_2), into a gas mixture consisting mainly of CO, H_2, CH_4, CO_2, and N_2 (syngas). Biomass and other carbonaceous materials can be gasified to produce syngas with high concentrations of CO and H_2. Feedstock materials include wood, energy crops, grain wastes, manufacturing or municipal wastes, natural gas, petroleum and chemical wastes, lignin, coal and tires.

The produced syngas is then fermented into alcohols or other biochemicals. Compared with the biochemical conversion process, the gasification–syngas fermentation pathway has several advantages such as (1) the capability of using all components of biomass including lignin; (2) feedstock composition independence; (3) elimination of complex pretreatment and high enzyme costs; (4) independence of H_2:CO:CO_2 ratio in syngas fermentation (Munasinghe and Khanal, 2010). Syngas fermentation, however, is still limited by several factors such as low efficient gas–liquid mass transfer, inhibitory compounds in syngas (ethylene, ethane, acetylene, tar, sulfur, and ash), and high medium cost (Bredwell et al., 1999; Klasson et al., 1993; Worden et al., 1997).

The production of acetic acid and ethanol from syngas, CO, H_2 and CO_2, follows a sequenced set of elementary chemical reactions as seen in **Figure 2** (Latif et al., 2014; Liew et al., 2013; Phillips et al., 1994). Each reaction proceeds with an associated enzyme in a specific location within a cell, either free in the cytoplasm, tethered to the surface of the cell membrane or embedded in the membrane. Each cell acts independently, but the combined action of all cells sets conditions in the

fermentation bulk liquid. The simple inorganic chemical substrates, CO, H_2 and CO_2, are transformed, step, by step, first to acetyl-CoA and then to organic products, such as acetic acid and ethanol. Some acetyl-CoA is diverted to form complex organic cell components, carbohydrates, proteins and lipids. However, the majority of gas consumed provides energy for cell function, resulting in the accumulation of acetic acid and ethanol.

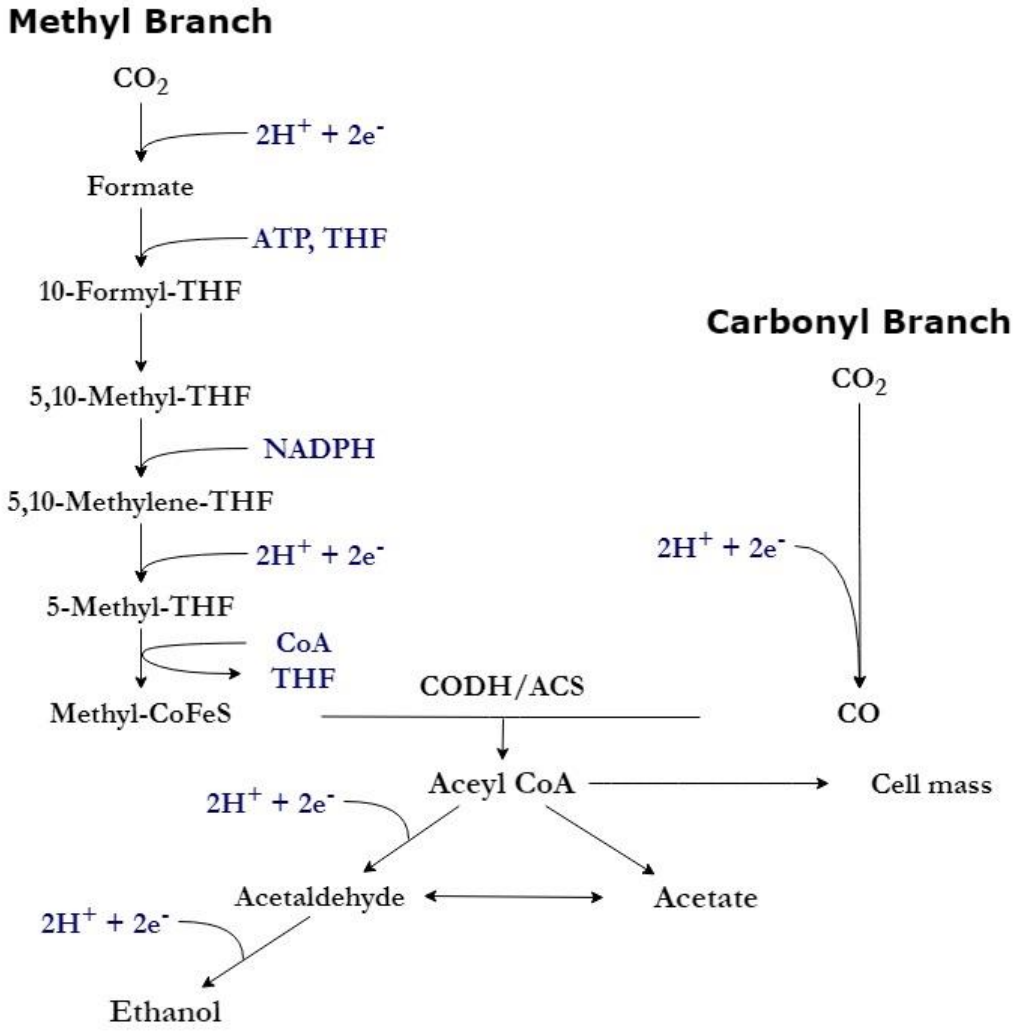

Figure 2. The Wood–Ljungdahl pathway for the production of ethanol and acetic acid.

4.1 Nanoadditives for syngas fermentation

Few studies have studied the addition of nanomaterials for syngas fermentation. For instance, Zhu et al., (2010) used MCM41 NPs with and without mercaptopropyl

functional groups for syngas fermentation using *Rhososporillum rubrum*. However, they only reported that such nanomaterial enhanced the CO-water mass transfer in the microorganism-free reactor, which may improve the syngas fermentation process. On the other hand, Kim and Lee, (2016), examined the effect of two types of nanoparticles (Methyl-functionalized silica and methyl-functionalized cobalt ferrite–silica ($CoFe_2O_4$@SiO_2–CH_3)) on the enhancement of bioethanol production in syngas fermentation by *Clostridium ljungdahlii*. $CoFe_2O_4$@SiO_2–CH_3 nanoparticles were more efficient for the productivity of syngas fermentation due to improved syngas mass transfer. The biomass, ethanol, and acetic acid production compared to a control were increased by 227.6%, 213.5%, and 59.6%, respectively by addition of $CoFe_2O_4$@SiO_2–CH_3 nanoparticles.

Sanusi et al., (2019) investigated the impact of 9 metallic oxide NPs (Cu, Mn, Ni, Fe, Fe3O4, Fe-Ag, Zn, Co and Ag) on ethanol production by *Saccharomices cerevisiae* BY4743. They found that ethanol decreased at concentrations above 0.02 wt% for all the NPs. The best ethanol production was at 0.01 wt% Fe_3O_4 producing 5.03 g/L (control 4.5 g/L). They demonstrated that metallic oxide NPs act as biocatalyst to enhance substrate conversion efficiency and ethanol yield.

Overall, these studies have been carried out for pure cultures and mainly for ethanol production. Further investigations would be focused in mixed cultures rather than pure, since the mixed culture fermentation presents several advantages (i.e. consume less power, more stable to environmental changes and works under non-sterile conditions) (Kleerebezem and van Loosdrecht, 2007). Likewise, more research is needed to enhance the production of different biofuels such as volatile fatty acids such as acetate, alcohols such as butanol and ethanol and medium chain fatty acids such as caproate.

5. Inhibitor compounds from lignocellulosic biomass

Lignocellulose biomass is one of the most abundant renewable resources available on the planet. Biomass pretreatment for depolymerizing lignocellulosics to fermentable sugars has been studied for nearly 200 years. Researches have aimed at high sugar production with minimal degradation to inhibitory compounds. The

different pretreatment methods are categorized in biological pretreatment methods such as fungi, bacteria, archaeal, etc. (Kumar and Sharma, 2017), physical pretreatment methods including milling, ultrasonic, microwave, pyrolysis and mechanical extrusion, etc. (McMillan, 1994), chemical pretreatment methods such as liquid hot water, weak and strong acid hydrolysis, alkaline hydrolysis, organosolv, oxidation delignification, ozonolysis, etc., and physicochemical pretreatment methods such as steam explosion, ammonia fiber explosion, etc. (Bhutto et al., 2017; Kumar and Sharma, 2017; McMillan, 1994). Recently, new methods such as application of ionic liquid (Gu et al., 2013), sub and super critical fluids (Daza Serna et al., 2016; Narayana Swamy, 2010), microwave-assisted methods (Ethaib et al., 2015) have been proposed, as well (Gu, 2013; Morais et al., 2015; Zheng and Rehmann, 2014). The previous methods suffer from various drawbacks such as low sugar yield compare to degraded products, harsh operational conditions, elevated processing cost, environmental concerns, loss of sugar during pretreatment methods and so on, while the new methods could provide more sugar yield at lower operating cost (Morais et al., 2015). Nonetheless, to date, single pretreatment method has not been established yet for delignification without sugar degradation. Therefore, the tendency is to apply successive treatment to remove the generated by-products other than sugars (i.e. furans, aliphatic acids, and phenolic compounds). Such compounds can decrease the activity of several enzymes, break down the DNA and inhibit protein and RNA synthesis in microorganisms (Jung et al., 2014, 2013; Liu et al., 2004; Palmqvist and Hahn-Hägerdal, 2000a, 2000b; Taherzadeh et al., 2000). In order to decrease the amount of toxic compounds in wood hydrolysates, several detoxification methods have been studied such as overliming, ion exchange, membranes, enzymatic hydrolysis, microorganisms and adsorption using polymeric sorbents or activated carbon (Grzenia et al., 2010; Ludwig et al., 2013; Myoung et al., 2010; K. Zhang et al., 2011). The main drawback of detoxification processes is the simultaneous removal of fermentable sugars resulting in a decrease of final products (Almeida et al., 2009; Deng and Aita, 2018; Li et al., 2013; Myoung et al., 2010).

5.1 Nanomaterials for detoxification of Inhibitor compounds present in lignocellulosic biomass

During the last decade, the implementation of nanoscale materials has emerged as an attractive alternative in several applications. Graphene-based materials have been successfully applied to remove organic pollutants like dyes, polycyclic aromatic hydrocarbons and gasoline (Gupta et al., 2012; Xu et al., 2012). Different structures of graphene such as sponges, beads, fibres, membranes and crumpled nanosheets have been studied to remove a wide range of organic substances from water and air (Yousefi et al., 2019). For instance, graphene aerogel has been used to separate oil and organic solvent from water (Ren et al., 2019). Likewise, the reduction degree of graphene oxide for tuning the adsorption of phenolic compounds, finding that the adsorption capacities increase with the increment of the reduction degree (X. Wang et al., 2014a). The hydrophobic behavior of the reduced form of graphene oxide enhances the adsorption of hydrophobic molecules and has been utilized to fabricate super-hydrophobic and super-oleophilic materials (Kemp et al., 2013).

So far, no research has attempted to remove furfural or another type of microbial growth inhibitor from wood hydrolysate using graphene nanomaterials.

6. Phytotoxicity/ecotoxicity effect of nanoparticles

It is important to highlight that with time, microorganisms can adapt to survive in the presence of nanomaterials. For instance, Luna-delRisco et al. (2011) indicated that the anaerobic bacteria became familiar to the toxic effect of the added materials at the end of the experiment.

On the other hand, Ahmed and Rodrigues (2013) studied the toxic effects of GO in samples of activated sludge from a wastewater treatment plant. The results showed that toxic effects of GO on microbial communities were dose dependent, especially in concentrations between 50 and 300 mg/L. Bacterial metabolic activity, bacterial viability, and biological removal of nutrients, such as organics, nitrogen and phosphorus, were significantly impacted by the presence of GO in the activated sludge. Liu et al., (2011) reported that antimicrobial actions of graphene based materials were attributed to membrane and oxidative stress. They compared the

antibacterial activity of Gt, GtO, GO, and rGO toward a bacterial model (Escherichia coli) under similar concentration (0.005-0.08 g/L) and incubation conditions. GO showed the highest antibacterial activity, sequentially followed by rGO, Gt, and GtO. They proposed that initial cell deposition on graphene-based materials cause membrane stress by direct contact with the sharp nanosheets, and the ensuing superoxide anion-independent oxidation. In general, graphene materials, which contain a higher density of functional groups, and are smaller in size, have more chances to interact with bacterial cells, resulting in cell deposition. The toxicity will not only depend on the size, concentration and type of graphene, but on the type of biological system and the microorganism present.

7. Molecular biology and chemical test of bioprocesses with nanoadditives

As nanotechnology matures from research discovery to large-volume manufacturing, releases will be inevitable. In this sense, the analysis of microbial communities can provide information about the effects that those materials can make to the environment and, at the same time the better understanding of a stable specialized consortium can lead to new insight into the performance and stability of processes subjected to nanoadditives. So far, few studies have carried out the microbial analysis of anaerobic systems exposed to nanoadditives, none in biogas enrichment and any in culture mix syngas fermentation. The studies that have reported microbial molecular analysis in anaerobic systems subjected to nanoadditives are presented in **Table 7**. Among the molecular techniques that have been used are, gradient gel electrophoresis (DGGE), DNA or rRNA pyrosequencing, and Fluorescence in situ hybridization (FISH). For instance, Nyberg et al., (2008) studied the biosolids from anaerobic wastewater treatment sludge that was exposed to fullerene (C_{60}). Changes in community structure were monitored by DGGE using primer sets of rRNA genes of Bacteria, *Archea*, and *Eukarya*. They did not find community shifts over an exposure period of few months with C_{60} addition. This conclusion was based on the absence of toxicity which was indicated by no change in methanogenesis. Likewise, Ambuchi et al., (2016) studied the role of iron oxide NPs and multi-wall nanotubes for biogas enhancement; By DNA pyrosequencing,

the revealed the predominance of bacteria *Anaerolineaceae* and *Longilinea*; which role in biodegradation of the substrate could have been boosted by the addition of the nanomaterials. The *Archaea* predominance of the genus level of *Methanosaeta* and *Methanobacterium* enhanced methanation process, and the presence of *Geobacter* contributed to DIET. FISH analysis helped to see changes in *Archaea* population. On the other hand, Kökdemir Ünşar and Perendeci, (2018) found that the reduction in CH_4 with 500 mg of magnetite NPs/g total solid (TS) was not due to the reduction of H_2 and CO_2 utilizing microorganisms but due to the reduction of acetic acid utilizing microorganisms such as *Methanosaeta spp*.

Interestingly, Li et al., (2020) analyzed the microbial community structure during sludge anaerobic digestion by adding 200 mg/L of bio-nano magnetic carbon (FeS) to enhance biomethane production and pyrene degradation. They found a biomethane enhancement as high as 58% and a pyrene removal rate as high as 77%. The analysis of microbial community structure by 16SrRNA pyrosequencing revealed that methanogens (e.g., *Methanosarcina* and *Methanosaeta*) and extracellular electron-transfer bacteria (e.g., *Pseudomonas*, *Cloastridia*, and *Synergistetes*) were enriched in the reactors added with bio-nano FeS or magnetic carbon; indicating that the addition of FeS or magnetic carbon may promote the activity and growth of microorganisms and improve the efficiency of CH_4 production and pyrene degradation by enhancing DIET.

The importance of studying of the composition of the microbial communities provides a better understanding of the complex interactions between microbial community structure, biodegradation functions and nanoadditives.

Table 7. Molecular biology studies from anaerobic processes provided with nanoadditives.

Nanoadditive	Concentration and size	Exposure period	Effect AD	Analytical technique	Findings	Reference
Fullerene	8200 mg/L	months	x	DGGE	No community shifts.	Nyberg et al., 2008
Iron Oxide NPs and MWCNTs	Iron Oxide NPs: 750 mg/L	96 hours	Positive	ADN pyrosequencing	Enrichment of methanoge	Ambuchi et al., 2016

	MWCNTs: 1500 mg/L No size reported.				ns and extracellular electron-transfer bacteria.	
Fe_2O_3 NPs	5, 50, 150, 250 and 500 mg/total solid. 30-60 nm	50 days	Positive	FISH	Inhibition depended on exposure time and dosage.	Kökdemir Ünşar and Perendeci, 2018
Magnetite and granular activated carbon (GAC)	27 g/L granule magnetite (8-12 mm). 27 GAC (8-12 mm). 13.5 g/L magnetite and 13.5 g/L GAC for combined experiment	56 days	Positive	16S rRNA pyrosequencing	Clostridium species were enriched in the magnetite digester. GAC digester presented a syntrophic metabolism.	Peng et al., 2018
Magnetic carbon (FeS)	200 mg/L 20-50 nm 100 m^2/g	25 days	Positive	rRNA pyrosequencing	Reactors with FeS were enriched with methanogens and extracellular electron-transfer bacteria.	Li et al., 2020

8. Impact and fate of the sludge with nanoparticles in the environment

With the rapid development of nanotechnology, NPs produced by industries for numerous applications can end in the environment including water, soils and sediments. Althoug NPs have always occurred in nature, the latest developments in the use and production of manufactured NPs have raised concerns over their potential release and impact on the environment. The manufactured nanoparticles include, metals, metal oxides and alloys, carbon based materials, silicates and

quantum dots as well as polymer composites (Colvin, 2003; Maynard et al., 2006; Roco, 2005). The environmental concern comes from the intrinsic hazards related to the nanomaterials and the environmental exposure, and of course the concentrations at which these materials will be present in the environment (Wagner et al., 2014).

NPs can enter the environment along their life cycle and three emission scenarios are generally considered: (1) release during production of raw material and nano-enabled products; (2) release during use; and (3) release after disposal of NP-containing products (waste handling) (Gottschalk et al., 2013, 2009; Tolaymat et al., 2017). The complex interaction between environmental matrices and NPs is important. Abiotic and biotic pathways influence transformation, altering bioavaibility and the aging process (Glenn and Klaine, 2013). Different parameters such as pH, ionic strength, hardness, and O_2^- limiting conditions change aggregation kinetics (Levard et al., 2011). Another important parameters are the natural organic matter present, which can alter the stability of the NPs through electrostatic and steric interactions (Chowdhury et al., 2012) and the adsorption of molecules in surrounding environmental matrices, which can lead to macromolecular transformations (Van Hoecke et al., 2011). Likewise, if the NPs are functionalized by surface coatings, this can lead to alter environmental pathways (Jarvie and King, 2010).

Particularly for sparingly soluble or insoluble NP that may accumulate in certain environmental compartments (e.g. sediments) over time, investigations covering multiple years of (repeated) exposure and assessment are suggested to properly assess their potential long-term implications in aquatic and terrestrial ecosystems. This aspect directly links to the acknowledgement of NP-induced alterations in horizontal and vertical trophic interactions with food webs

All above, more research is needed to understand the fate and impact that the different NPs can produce in the environment. An alternative to minimize the impact of nanomaterials to the environment would be the use and development of materials that can be easily recovered such as the case of magnetic nanoparticles. Nevertheless, these materials would also need studies related with exposure assessment.

9. References

Abdelsalam, E., Samer, M., Attia, Y.A., Abdel-Hadi, M.A., Hassan, H.E., Badr, Y., 2017. Influence of zero valent iron nanoparticles and magnetic iron oxide nanoparticles on biogas and methane production from anaerobic digestion of manure. Energy 120, 842–853. https://doi.org/https://doi.org/10.1016/j.energy.2016.11.137

Ahmed, F., Rodrigues, D.F., 2013. Investigation of acute effects of graphene oxide on wastewater microbial community: a case study. J. Hazard. Mater. 256–257, 33–39. https://doi.org/10.1016/j.jhazmat.2013.03.064

Almeida, J.R.M., Bertilsson, M., Gorwa-Grauslund, M.F., Gorsich, S., Lidén, G., 2009. Metabolic effects of furaldehydes and impacts on biotechnological processes. Appl. Microbiol. Biotechnol. 82, 625–638. https://doi.org/10.1007/s00253-009-1875-1

Alsaba, M.T., Al Dushaishi, M.F., Abbas, A.K., 2020. A comprehensive review of nanoparticles applications in the oil and gas industry. J. Pet. Explor. Prod. Technol. 10, 1389–1399. https://doi.org/10.1007/s13202-019-00825-z

Ambuchi, J.J., Zhang, Z., Feng, Y., 2016. Biogas Enhancement Using Iron Oxide Nanoparticles and Multi-Wall Carbon Nanotubes. Int. J. Chem. Mol. Nucl. Mater. Metall. Eng. 10, 1305–1311.

Baccioli, A., Antonelli, M., Frigo, S., Desideri, U., Pasini, G., 2018. Small scale bio-LNG plant: Comparison of different biogas upgrading techniques. Appl. Energy 217, 328–335. https://doi.org/https://doi.org/10.1016/j.apenergy.2018.02.149

Beiki, H., Keramati, M., 2019. Improvement of Methane Production from Sugar Beet Wastes Using TiO2 and Fe3O4 Nanoparticles and Chitosan Micropowder Additives. Appl. Biochem. Biotechnol. 189, 13–25. https://doi.org/10.1007/s12010-019-02987-2

Bhutto, A.W., Qureshi, K., Harijan, K., Abro, R., Abbas, T., Bazmi, A.A., Karim, S., Yu, G., 2017. Insight into progress in pre-treatment of lignocellulosic biomass. Energy 122, 724–745. https://doi.org/https://doi.org/10.1016/j.energy.2017.01.005

Bredwell, M.D., Srivastava, P., Worden, R.M., 1999. Reactor Design Issues for

Synthesis-Gas Fermentations. Biotechnol. Prog. 15, 834–844. https://doi.org/https://doi.org/10.1021/bp990108m

Campesi, R., Cuevas, F., Gadiou, R., Leroy, E., Hirscher, M., Vix-Guterl, C., Latroche, M., 2008. Hydrogen storage properties of Pd nanoparticle/carbon template composites. Carbon N. Y. 46, 206–214. https://doi.org/https://doi.org/10.1016/j.carbon.2007.11.006

Casals, E., Barrena, R., García, A., González, E., Delgado, L., Busquets-Fité, M., Font, X., Arbiol, J., Glatzel, P., Kvashnina, K., Sánchez, A., Puntes, V., 2014. Programmed iron oxide nanoparticles disintegration in anaerobic digesters boosts biogas production. Small 10, 2801–2808. https://doi.org/10.1002/smll.201303703

Chaemchuen, S., Zhou, K., Verpoort, F., 2016. From Biogas to Biofuel: Materials Used for Biogas Cleaning to Biomethane. ChemBioEng Rev. 3, 250–265. https://doi.org/https://doi.org/10.1002/cben.201600016

Chakraborty, N., Chatterjee, M., Sarkar, G.M., Lahiri, S.C., 2010. Inhibitory Effects of the Divalent Metal Ions on Biomethanation by Isolated Mesophilic Methanogen in AC21 Medium in Presence or Absence of Juices from Water Hyacinth. BioEnergy Res. 3, 314–320. https://doi.org/10.1007/s12155-010-9083-5

Chen, S., Rotaru, A.E., Liu, F., Philips, J., Woodard, T.L., Nevin, K.P., Lovley, D.R., 2014a. Carbon cloth stimulates direct interspecies electron transfer in syntrophic co-cultures. Bioresour. Technol. 173, 82–86. https://doi.org/10.1016/j.biortech.2014.09.009

Chen, S., Rotaru, A.E., Shrestha, P.M., Malvankar, N.S., Liu, F., Fan, W., Nevin, K.P., Lovley, D.R., 2014b. Promoting interspecies electron transfer with biochar. Sci. Rep. 4. https://doi.org/10.1038/srep05019

Chowdhury, I., Cwiertny, D.M., Walker, S.L., 2012. Combined Factors Influencing the Aggregation and Deposition of nano-TiO2 in the Presence of Humic Acid and Bacteria. Environ. Sci. Technol. 46, 6968–6976. https://doi.org/10.1021/es2034747

Colvin, V.L., 2003. The potential environmental impact of engineered

nanomaterials. Nat. Biotechnol. 21, 1166–1170. https://doi.org/10.1038/nbt875

Daniel, M.C.M., Astruc, D., 2004. Gold Nanoparticles: Assembly, Supramolecular Chemistry, Quantum-Size Related Properties and Applications toward Biology, Catalysis and Nanotechnology. Chem. Rev. 104, 293–346. https://doi.org/10.1021/cr030698

Daza Serna, L. V, Orrego Alzate, C.E., Cardona Alzate, C.A., 2016. Supercritical fluids as a green technology for the pretreatment of lignocellulosic biomass. Bioresour. Technol. 199, 113–120. https://doi.org/https://doi.org/10.1016/j.biortech.2015.09.078

Deng, F., Aita, G.M., 2018. Detoxification of dilute ammonia pretreated energy cane bagasse enzymatic hydrolysate by soluble polyelectrolyte flocculants. Ind. Crops Prod. 112, 681–690. https://doi.org/https://doi.org/10.1016/j.indcrop.2017.12.061

Deng, L., Liu, Y., Wang, W., 2020. Biogas Cleaning and Upgrading BT - Biogas Technology, in: Deng, L., Liu, Y., Wang, W. (Eds.), . Springer Singapore, Singapore, pp. 201–243. https://doi.org/10.1007/978-981-15-4940-3_6

Dubé, C.-D., Guiot, S.R., 2015. Direct Interspecies Electron Transfer in Anaerobic Digestion: A Review, in: Guebitz, G.M., Bauer, A., Bochmann, G., Gronauer, A., Weiss, S. (Eds.), Biogas Science and Technology. Springer International Publishing, Cham, pp. 101–115. https://doi.org/10.1007/978-3-319-21993-6_4

ElMekawy, A., Hegab, H.M., Losic, D., Saint, C.P., Pant, D., 2017. Applications of graphene in microbial fuel cells: The gap between promise and reality. Renew. Sustain. Energy Rev. 72, 1389–1403. https://doi.org/https://doi.org/10.1016/j.rser.2016.10.044

Ethaib, S., Omar, R., Kamal, S., Biak, D.R.., 2015. Microwave-assisted pretreatment of lignocellulosic biomass: a review. J. Eng.

Fehrenbach, H., Giegrich, J., Reinhardt, G., Sayer, U., Gretz, M., Lanje, K., Schmitz, J., 2008. Kritieren einer nachhaltigen Bioenergienutzung im globalen Maβstab.

Feng, Y., Zhang, Y., Quan, X., Chen, S., 2014. Enhanced anaerobic digestion of waste activated sludge digestion by the addition of zero valent iron. Water

Res. 52, 242–250. https://doi.org/10.1016/j.watres.2013.10.072

Ferre-Vilaplana, A., 2008. Storage of hydrogen adsorbed on alkali metal doped single-layer all-carbon materials. J. Phys. Chem. C 112, 3998–4004. https://doi.org/10.1021/jp0768874

Ganzoury, M.A., Allam, N.K., 2015. Impact of nanotechnology on biogas production: a mini-review. Renew. Sustain. Energy Rev. 50, 1392–1404. https://doi.org/10.1016/j.rser.2015.05.073

García, A., Delgado, L., Torà, J.A., Casals, E., González, E., Puntes, V., Font, X., Carrera, J., Sánchez, A., 2012. Effect of cerium dioxide, titanium dioxide, silver, and gold nanoparticles on the activity of microbial communities intended in wastewater treatment. J. Hazard. Mater. 199–200, 64–72. https://doi.org/10.1016/j.jhazmat.2011.10.057

Glenn, J.B., Klaine, S.J., 2013. Abiotic and Biotic Factors That Influence the Bioavailability of Gold Nanoparticles to Aquatic Macrophytes. Environ. Sci. Technol. 47, 10223–10230. https://doi.org/10.1021/es4020508

Gonzalez-Estrella, J., Sierra-Alvarez, R., Field, J.A., 2013. Toxicity assessment of inorganic nanoparticles to acetoclastic and hydrogenotrophic methanogenic activity in anaerobic granular sludge. J. Hazard. Mater. 260, 278–285. https://doi.org/10.1016/j.jhazmat.2013.05.029

Gottschalk, F., Sonderer, T., Scholz, R.W., Nowack, B., 2009. Modeled Environmental Concentrations of Engineered Nanomaterials (TiO2, ZnO, Ag, CNT, Fullerenes) for Different Regions. Environ. Sci. Technol. 43, 9216–9222. https://doi.org/10.1021/es9015553

Gottschalk, F., Sun, T., Nowack, B., 2013. Environmental concentrations of engineered nanomaterials: Review of modeling and analytical studies. Environ. Pollut. 181, 287–300. https://doi.org/https://doi.org/10.1016/j.envpol.2013.06.003

Grzenia, D.L., Schell, D.J., Wickramsinghe, S.R., 2010. Detoxification of biomass hydrolysates by reactive membrane extraction. J. Memb. Sci. 348, 6–12. https://doi.org/10.1016/j.memsci.2009.10.035

Gu, T., 2013. Pretreatment of Lignocellulosic Biomass Using Supercritical Carbon

Dioxide as a Green Solvent BT - Green Biomass Pretreatment for Biofuels Production, in: Gu, T. (Ed.), . Springer Netherlands, Dordrecht, pp. 107–125. https://doi.org/10.1007/978-94-007-6052-3_5

Gu, T., Held, M.A., Faik, A., 2013. Supercritical CO2 and ionic liquids for the pretreatment of lignocellulosic biomass in bioethanol production. Environ. Technol. 34, 1735–1749. https://doi.org/10.1080/09593330.2013.809777

Gupta, S. Sen, Sreeprasad, T.S., Maliyekkal, S.M., Das, S.K., Pradeep, T., 2012. Graphene from Sugar and its Application in Water Purification. ACS Appl. Mater. Interfaces 4, 4156–4163. https://doi.org/10.1021/am300889u

Hassaneen, F.Y., Abdallah, M.S., Ahmed, N., Taha, M.M., Abd ElAziz, S.M.M., El-Mokhtar, M.A., Badary, M.S., Allam, N.K., 2020. Innovative nanocomposite formulations for enhancing biogas and biofertilizers production from anaerobic digestion of organic waste. Bioresour. Technol. 309, 123350. https://doi.org/10.1016/j.biortech.2020.123350

Hwang, S.-W., Rather, S., Naik, M., Soo, C.S., Nahm, K.-S., 2009. Hydrogen uptake of multiwalled carbon nanotubes decorated with Pt–Pd alloy using thermal vapour deposition method. J. Alloys Compd. 480, L20–L24. https://doi.org/https://doi.org/10.1016/j.jallcom.2009.01.136

Jarvie, H.P., King, S.M., 2010. Just scratching the surface? New techniques show how surface functionality of nanoparticles influences their environmental fate. Nano Today 5, 248–250. https://doi.org/https://doi.org/10.1016/j.nantod.2010.06.001

Jönsson, O., Polman, E., Jensen, J.., Eklund, R., Schyl, H., Ivanrsson, S., 2003. Sustainable gas enters the European gas distribution system. Danish gas Technol. Cent.

Jung, Y.H., Kim, I.J., Kim, H.K., Kim, K.H., 2013. Dilute acid pretreatment of lignocellulose for whole slurry ethanol fermentation. Bioresour. Technol. 132, 109–114. https://doi.org/https://doi.org/10.1016/j.biortech.2012.12.151

Jung, Y.H., Park, H.M., Kim, I.J., Park, Y., Seo, J., Kim, K.H., 2014. One-pot pretreatment, saccharification and ethanol fermentation of lignocellulose based on acid–base mixture pretreatment 55318–55327.

https://doi.org/10.1039/c4ra10092a

Karri, S., Sierra-Alvarez, R., Field, J.A., 2005. Zero valent iron as an electron-donor for methanogenesis and sulfate reduction in anaerobic sludge. Biotechnol. Bioeng. 92, 810–819. https://doi.org/https://doi.org/10.1002/bit.20623

Kemp, K.C., Seema, H., Saleh, M., Le, N.H., Mahesh, K., Chandra, V., Kim, K.S., 2013. Environmental applications using graphene composites: Water remediation and gas adsorption. Nanoscale 5, 3149–3171. https://doi.org/10.1039/c3nr33708a

Kim, H.-S., Lee, H., Han, K.-S., Kim, J.-H., Song, M.-S., Park, M.-S., Lee, J.-Y., Kang, J.-K., 2005. Hydrogen storage in Ni nanoparticle-dispersed multiwalled carbon nanotubes. J. Phys. Chem. B 109, 8983–8986. https://doi.org/10.1021/jp044727b

Kim, Y.K., Lee, H., 2016. Use of magnetic nanoparticles to enhance bioethanol production in syngas fermentation. Bioresour. Technol. 204, 139–144. https://doi.org/10.1016/j.biortech.2016.01.001

Kirschvink, J.L., Kobayashi-Kirschvink, A., Woodford, B.J., 1992. Magnetite biomineralization in the human brain. Proc. Natl. Acad. Sci. U. S. A. 89, 7683–7. https://doi.org/10.1073/PNAS.89.16.7683

Klasson, K.T., Ackerson, M.D., Clausen, E.C., Gaddy, J.L., 1993. Biological conversion of coal and coal-derived synthesis gas. Fuel 72, 1673–1678. https://doi.org/https://doi.org/10.1016/0016-2361(93)90354-5

Kleerebezem, R., van Loosdrecht, M.C.M., 2007. Mixed culture biotechnology for bioenergy production. Curr. Opin. Biotechnol. 18, 207–212. https://doi.org/https://doi.org/10.1016/j.copbio.2007.05.001

Kökdemir Ünşar, E., Perendeci, N.A., 2018. What kind of effects do Fe2O3 and Al2O3 nanoparticles have on anaerobic digestion, inhibition or enhancement? Chemosphere 211, 726–735. https://doi.org/https://doi.org/10.1016/j.chemosphere.2018.08.014

Koniuszewska, I., Korzeniewska, E., Harnisz, M., Czatzkowska, M., 2020. Intensification of biogas production using various technologies: A review. Int. J. Energy Res. 44, 6240–6258. https://doi.org/https://doi.org/10.1002/er.5338

Kumar, A.K., Sharma, S., 2017. Recent updates on different methods of pretreatment of lignocellulosic feedstocks: a review. Bioresour. Bioprocess. 4, 7. https://doi.org/10.1186/s40643-017-0137-9

Latif, H., Zeidan, A.A., Nielsen, A.T., Zengler, K., 2014. Trash to treasure: production of biofuels and commodity chemicals via syngas fermenting microorganisms. Curr. Opin. Biotechnol. 27, 79–87. https://doi.org/https://doi.org/10.1016/j.copbio.2013.12.001

Lee, H., Ihm, J., Cohen, M.L., Louie, S.G., 2010. Calcium-decorated graphene-based nanostructures for hydrogen storage. Nano Lett. 10, 793–798. https://doi.org/10.1021/nl902822s

Letcher, T.M., 2019. 1 - Why do we have global warming?, in: Letcher, T.M.B.T.-M.G.W. (Ed.), . Academic Press, pp. 3–15. https://doi.org/https://doi.org/10.1016/B978-0-12-814104-5.00001-6

Levard, C., Reinsch, B.C., Michel, F.M., Oumahi, C., Lowry, G. V, Brown, G.E., 2011. Sulfidation Processes of PVP-Coated Silver Nanoparticles in Aqueous Solution: Impact on Dissolution Rate. Environ. Sci. Technol. 45, 5260–5266. https://doi.org/10.1021/es2007758

Li, L.-L., Tong, Z.-H., Fang, C.-Y., Chu, J., yu H, Q., 2014. Response of anaerobic granular sludge to single-wall carbon nanotube exposure. Water Res. 1–8. https://doi.org/10.1016/j.watres.2014.11.042

Li, L., Zhang, X., Zhu, P., Yong, X., Wang, Y., An, W., Jia, H., Zhou, J., 2020. Enhancing biomethane production and pyrene biodegradation by addition of bio-nano FeS or magnetic carbon during sludge anaerobic digestion. Environ. Technol. (United Kingdom) 0, 1–53. https://doi.org/10.1080/09593330.2020.1733674

Li, X., Xu, H., Chen, Z.S., Chen, G., 2011. Biosynthesis of nanoparticles by microorganisms and their applications. J. Nanomater. 2011. https://doi.org/10.1155/2011/270974

Li, Y., Shao, J., Wang, X., Yang, H., Chen, Y., Deng, Y., Zhang, S., Chen, H., 2013. Upgrading of bio-oil: Removal of the fermentation inhibitor (furfural) from the model compounds of bio-oil using pyrolytic char. Energy and Fuels 27,

5975–5981. https://doi.org/10.1021/ef401375q

Liew, F.M., Köpke, M., Simpson, S.D., 2013. Gas fermentation for commercial biofuels production. In Liquid, Gaseous and Solid Biofuels—Conversion Techniques.

Lin, R., Cheng, J., Zhang, J., Zhou, J., Cen, K., Murphy, J.D., 2017. Boosting biomethane yield and production rate with graphene: the potential of direct interspecies electron transfer in anaerobic digestion. Bioresour. Technol. 239, 345–352. https://doi.org/10.1016/j.biortech.2017.05.017

Liu, F., Rotaru, A.E., Shrestha, P.M., Malvankar, N.S., Nevin, K.P., Lovley, D.R., 2012. Promoting direct interspecies electron transfer with activated carbon. Energy Environ. Sci. 5, 8982–8989. https://doi.org/10.1039/c2ee22459c

Liu, S., Zeng, T.H., Hofmann, M., Burcombe, E., Wei, J., Jiang, R., Kong, J., Chen, Y., 2011. Antibacterial activity of graphite, graphite oxide, graphene oxide, and reduced graphene oxide: membrane and oxidative stress. ACS Nano 5, 6971–6980. https://doi.org/10.1021/nn202451x

Liu, Z.L., Slininger, P.J., Dien, B.S., Berhow, M.A., Kurtzman, C.P., Gorsich, S.W., 2004. Adaptive response of yeasts to furfural and 5-hydroxymethylfurfural and new chemical evidence for HMF conversion to 2,5-bis-hydroxymethylfuran. J. Ind. Microbiol. Biotechnol. 31, 345–352. https://doi.org/10.1007/s10295-004-0148-3

Lo, H.M., Chiu, H.Y., Lo, S.W., Lo, F.C., 2012. Effects of micro-nano and non micro-nano MSWI ashes addition on MSW anaerobic digestion. Bioresour. Technol. 114, 90–94. https://doi.org/10.1016/j.biortech.2012.03.002

Lovley, D.R., 2017. Syntrophy Goes Electric: Direct Interspecies Electron Transfer. Annu. Rev. Microbiol. 71, 643–664. https://doi.org/10.1146/annurev-micro-030117-020420

Ludwig, D., Amann, M., Hirth, T., Rupp, S., Zibek, S., 2013. Bioresource Technology Development and optimization of single and combined detoxification processes to improve the fermentability of lignocellulose hydrolyzates. Bioresour. Technol. 133, 455–461. https://doi.org/10.1016/j.biortech.2013.01.053

Luna-delRisco, M., Orupõld, K., Dubourguier, H.C., 2011. Particle-size effect of CuO and ZnO on biogas and methane production during anaerobic digestion. J. Hazard. Mater. 189, 603–608. https://doi.org/10.1016/j.jhazmat.2011.02.085

Manson, V., 2008. Wind power in Denmark.

Maynard, A.D., Aitken, R.J., Butz, T., Colvin, V., Donaldson, K., Oberdörster, G., Philbert, M.A., Ryan, J., Seaton, A., Stone, V., Tinkle, S.S., Tran, L., Walker, N.J., Warheit, D.B., 2006. Safe handling of nanotechnology. Nature 444, 267–269. https://doi.org/10.1038/444267a

McMillan, J.., 1994. Pretreatment of lignocellulosic biomass.

Mohan Bhagyaraj, S., Oluwafemi, O.S., 2018. Nanotechnology: The Science of the Invisible, Synthesis of Inorganic Nanomaterials. Elsevier Ltd. https://doi.org/10.1016/b978-0-08-101975-7.00001-4

Möller, K., Müller, T., 2012. Effects of anaerobic digestion on digestate nutrient availability and crop growth: A review. Eng. Life Sci. 12, 242–257. https://doi.org/https://doi.org/10.1002/elsc.201100085

Morais, A.R.C., da Costa Lopes, A.M., Bogel-Łukasik, R., 2015. Carbon Dioxide in Biomass Processing: Contributions to the Green Biorefinery Concept. Chem. Rev. 115, 3–27. https://doi.org/10.1021/cr500330z

Munasinghe, P.C., Khanal, S.K., 2010. Biomass-derived syngas fermentation into biofuels: Opportunities and challenges. Bioresour. Technol. 101, 5013–5022. https://doi.org/https://doi.org/10.1016/j.biortech.2009.12.098

Myoung, J., Venditti, R.A., Jameel, H., Kenealy, W.R., 2010. Detoxification of woody hydrolyzates with activated carbon for bioconversion to ethanol by the thermophilic anaerobic bacterium Thermoanaerobacterium saccharolyticum. Biomass and Bioenergy 35, 626–636. https://doi.org/10.1016/j.biombioe.2010.10.021

Narayana Swamy, N., 2010. Supercritical Carbon Dioxide Pretreatment of Various Lignocellulosic Biomasses. Ohio University, Ohio University.

Nozhevnikova, A.N., Russkova, Y.I., Litti, Y. V., Parshina, S.N., Zhuravleva, E.A., Nikitina, A.A., 2020. Syntrophy and Interspecies Electron Transfer in Methanogenic Microbial Communities. Microbiol. (Russian Fed. 89, 129–147.

https://doi.org/10.1134/S0026261720020101

Nyberg, L., Turco, R.F., Nies, L., 2008. Assessing the impact of nanomaterials on anaerobic microbial communities. Environ. Sci. Technol. 42, 1938–1943. https://doi.org/10.1021/es072018g

O'Connor, S., Ehimen, E., Pillai, S.C., Black, A., Tormey, D., Bartlett, J., 2021. Biogas production from small-scale anaerobic digestion plants on European farms. Renew. Sustain. Energy Rev. 139, 110580. https://doi.org/https://doi.org/10.1016/j.rser.2020.110580

Otero-González, L., Field, J.A., Sierra-Alvarez, R., 2014. Inhibition of anaerobic wastewater treatment after long-term exposure to low levels of CuO nanoparticles. Water Res. 58, 160–168. https://doi.org/10.1016/j.watres.2014.03.067

Palmqvist, E., Hahn-Hägerdal, B., 2000a. Fermentation of lignocellulosic hydrolysates. I: inhibition and detoxification. Bioresour. Technol. 74, 17–24. https://doi.org/https://doi.org/10.1016/S0960-8524(99)00160-1

Palmqvist, E., Hahn-Hägerdal, B., 2000b. Fermentation of lignocellulosic hydrolysates. II: inhibitors and mechanisms of inhibition. Bioresour. Technol. 74, 25–33. https://doi.org/https://doi.org/10.1016/S0960-8524(99)00161-3

Peng, H., Zhang, Y., Tan, D., Zhao, Z., Zhao, H., Quan, X., 2018. Roles of magnetite and granular activated carbon in improvement of anaerobic sludge digestion. Bioresour. Technol. 249, 666–672. https://doi.org/10.1016/j.biortech.2017.10.047

Perreault, F., de Faria, A., Elimelech, M., 2015. Environmental applications of graphene-based nanomaterials. Chem. Soc. Rev. 44, 5861–5896. https://doi.org/10.1039/C5CS00021A

Persson, M., 2003. Utvärdering av uppgraderingstekniker för biogas. Malmö, Sweden.

Persson, M., Jönsson, O., Wellinger, A., 2006. Biogas Upgrading to Vehicle Fuel Standards and Grid Injection.

Phillips, J.R., Clausen, E.C., Gaddy, J.L., 1994. Synthesis gas as substrate for the biological production of fuels and chemicals. Appl. Biochem. Biotechnol. 45,

145–157. https://doi.org/10.1007/BF02941794

Ren, R.P., Wang, Z., Ren, J., Lv, Y.K., 2019. Highly compressible polyimide/graphene aerogel for efficient oil/water separation. J. Mater. Sci. 54, 5918–5926. https://doi.org/10.1007/s10853-018-03238-1

Reyhani, A., Mortazavi, S.Z., Mirershadi, S., Moshfegh, A.Z., Parvin, P., Golikand, A.N., 2011. Hydrogen storage in decorated multiwalled carbon nanotubes by Ca, Co, Fe, Ni, and Pd nanoparticles under ambient conditions. J. Phys. Chem. C 115, 6994–7001. https://doi.org/10.1021/jp108797p

Reyhani, A., Mortazavi, S.Z., Moshfegh, A.Z., Golikand, A.N., Amiri, M., 2009. Enhanced electrochemical hydrogen storage by catalytic Fe-doped multi-walled carbon nanotubes synthesized by thermal chemical vapor deposition. J. Power Sources 188, 404–410. https://doi.org/https://doi.org/10.1016/j.jpowsour.2008.11.131

Roco, M.C., 2005. International Perspective on Government Nanotechnology Funding in 2005. J. Nanoparticle Res. 7, 707–712. https://doi.org/10.1007/s11051-005-3141-5

Ryckebosch, E., Drouillon, M., Vervaeren, H., 2011. Techniques for transformation of biogas to biomethane. Biomass and Bioenergy 35, 1633–1645. https://doi.org/10.1016/j.biombioe.2011.02.033

Sajid, M., Płotka-Wasylka, J., 2020. Nanoparticles: Synthesis, characteristics, and applications in analytical and other sciences. Microchem. J. 154, 104623. https://doi.org/https://doi.org/10.1016/j.microc.2020.104623

Sanusi, I.A., Faloye, F.D., Gueguim Kana, E.B., 2019. Impact of Various Metallic Oxide Nanoparticles on Ethanol Production by Saccharomyces cerevisiae BY4743: Screening, Kinetic Study and Validation on Potato Waste. Catal. Letters 149, 2015–2031. https://doi.org/10.1007/s10562-019-02796-6

Sherif, S.A., Barbir, F., Veziroglu, T.N., 2005. Wind energy and the hydrogen economy-review of the technology. Sol. Energy 78, 647–660. https://doi.org/10.1016/j.solener.2005.01.002

Siegl, S., Laaber, M., Holubar, P., 2012. Green electricity from biomass, part II: Environmental impacts considering avoided burdens from replacing the

conventional provision of additional functions. Waste and Biomass Valorization 3, 1–21. https://doi.org/10.1007/s12649-011-9091-5

Siegl, S., Laaber, M., Holubar, P., 2011. Green electricity from biomass, Part I: Environmental impacts of direct life cycle emissions. Waste and Biomass Valorization 2, 267–284. https://doi.org/10.1007/s12649-011-9077-3

Simon, K., Rittmann, M.., 2015. A critical assessment of microbiological biogas to biomethane upgrading systems, in: Biogas Science and Technology. pp. 117–135.

Siriwongrungson, V., Zeng, R.J., Angelidaki, I., 2007. Homoacetogenesis as the alternative pathway for H2 sink during thermophilic anaerobic degradation of butyrate under suppressed methanogenesis. Water Res. 41, 4204–4210. https://doi.org/10.1016/j.watres.2007.05.037

Srinivas, G., Zhu, Y., Piner, R., Skipper, N., Ellerby, M., Ruoff, R., 2010. Synthesis of graphene-like nanosheets and their hydrogen adsorption capacity. Carbon N. Y. 48, 630–635. https://doi.org/10.1016/j.carbon.2009.10.003

Stadistics International Energy Agency, 2016. CO2 Emissions from fuel combustion-highlights.

Su, L., Shi, X., Guo, G., Zhao, A., Zhao, Y., 2013. Stabilization of sewage sludge in the presence of nanoscale zero-valent iron (nZVI): Abatement of odor and improvement of biogas production. J. Mater. Cycles Waste Manag. 15, 461–468. https://doi.org/10.1007/s10163-013-0150-9

Suanon, F., Sun, Q., Li, M., Cai, X., Zhang, Y., Yan, Y., Yu, C.P., 2017. Application of nanoscale zero valent iron and iron powder during sludge anaerobic digestion: Impact on methane yield and pharmaceutical and personal care products degradation. J. Hazard. Mater. 321, 47–53. https://doi.org/10.1016/j.jhazmat.2016.08.076

Sun, S., Ge, Z., Zhao, Y., Hu, C., Zhang, H., Ping, L., 2016. Performance of CO2 concentrations on nutrient removal and biogas upgrading by integrating microalgal strains cultivation with activated sludge. Energy 97, 229–237. https://doi.org/https://doi.org/10.1016/j.energy.2015.12.126

Taherzadeh, M.J., Gustafsson, L., Niklasson, C., Lidén, G., 2000. Physiological

effects of 5-hydroxymethylfurfural on Saccharomyces cerevisiae. Appl. Microbiol. Biotechnol. 53, 701–708. https://doi.org/10.1007/s002530000328

Tambone, F., Scaglia, B., D'Imporzano, G., Schievano, A., Orzi, V., Salati, S., Adani, F., 2010. Assessing amendment and fertilizing properties of digestates from anaerobic digestion through a comparative study with digested sludge and compost. Chemosphere 81, 577–583. https://doi.org/https://doi.org/10.1016/j.chemosphere.2010.08.034

Tian, T., Qiao, S., Li, X., Zhang, M., Zhou, J., 2017. Nano-graphene induced positive effects on methanogenesis in anaerobic digestion. Bioresour. Technol. 224, 41–47. https://doi.org/10.1016/j.biortech.2016.10.058

Tolaymat, T., El Badawy, A., Genaidy, A., Abdelraheem, W., Sequeira, R., 2017. Analysis of metallic and metal oxide nanomaterial environmental emissions. J. Clean. Prod. 143, 401–412. https://doi.org/https://doi.org/10.1016/j.jclepro.2016.12.094

Van Hoecke, K., De Schamphelaere, K.A.C., Ramirez–Garcia, S., Van der Meeren, P., Smagghe, G., Janssen, C.R., 2011. Influence of alumina coating on characteristics and effects of SiO2 nanoparticles in algal growth inhibition assays at various pH and organic matter contents. Environ. Int. 37, 1118–1125. https://doi.org/https://doi.org/10.1016/j.envint.2011.02.009

Wagner, S., Gondikas, A., Neubauer, E., Hofmann, T., von der Kammer, F., 2014. Spot the Difference: Engineered and Natural Nanoparticles in the Environment—Release, Behavior, and Fate. Angew. Chemie Int. Ed. 53, 12398–12419. https://doi.org/https://doi.org/10.1002/anie.201405050

Wang, L., Lee, K., Sun, Y.Y., Lucking, M., Chen, Z., Zhao, J.J., Zhang, S.B., 2009. Graphene oxide as an ideal substrate for hydrogen storage. ACS Nano 3, 2995–3000. https://doi.org/10.1021/nn900667s

Wang, X., Huang, S., Zhu, L., Tian, X., Li, S., Tang, H., 2014. Correlation between the adsorption ability and reduction degree of graphene oxide and tuning of adsorption of phenolic compounds. Carbon N. Y. 69, 101–112. https://doi.org/https://doi.org/10.1016/j.carbon.2013.11.070

Wei, W., Cai, Z., Fu, J., Xie, G.-J., Li, A., Zhou, X., Ni, B.-J., Wang, D., Wang, Q.,

2018. Zero valent iron enhances methane production from primary sludge in anaerobic digestion. Chem. Eng. J. 351, 1159–1165. https://doi.org/https://doi.org/10.1016/j.cej.2018.06.160

Wellinger, A., Lindberg, A., 2005. Biogas upgrading and utilisation [WWW Document]. IEA Bioenergy, task 24 energy from Biol. bionversion Org. waste.

Worden, R.M., Bredwell, M.D., Grethlein, A.J., 1997. Engineering Issues in Synthesis-Gas Fermentations, in: Fuels and Chemicals from Biomass, ACS Symposium Series. American Chemical Society, pp. 18–320. https://doi.org/doi:10.1021/bk-1997-0666.ch018

Xu, J., Wang, L., Zhu, Y., 2012. Decontamination of Bisphenol A from Aqueous Solution by Graphene Adsorption. Langmuir 28, 8418–8425. https://doi.org/10.1021/la301476p

Yang, L., Ge, X., Wan, C., Yu, F., Li, Y., 2014. Progress and perspectives in converting biogas to transportation fuels. Renew. Sustain. Energy Rev. 40, 1133–1152. https://doi.org/10.1016/j.rser.2014.08.008

Yang, Y., Guo, J., Hu, Z., 2013. Impact of nano zero valent iron (NZVI) on methanogenic activity and population dynamics in anaerobic digestion. Water Res. 47, 6790–6800. https://doi.org/10.1016/j.watres.2013.09.012

Yoro, K.O., Daramola, M.O., 2020. Chapter 1 - CO2 emission sources, greenhouse gases, and the global warming effect, in: Rahimpour, M.R., Farsi, M., Makarem, M.A.B.T.-A. in C.C. (Eds.), . Woodhead Publishing, pp. 3–28. https://doi.org/https://doi.org/10.1016/B978-0-12-819657-1.00001-3

Yousefi, N., Lu, X., Elimelech, M., Tufenkji, N., 2019. Environmental performance of graphene-based 3D macrostructures. Nat. Nanotechnol. 14, 107–119. https://doi.org/10.1038/s41565-018-0325-6

Zacharia, R., Kim, K.Y., Fazle Kibria, A.K.M., Nahm, K.S., 2005. Enhancement of hydrogen storage capacity of carbon nanotubes via spill-over from vanadium and palladium nanoparticles. Chem. Phys. Lett. 412, 369–375. https://doi.org/https://doi.org/10.1016/j.cplett.2005.07.020

Zaidi, A.A., RuiZhe, F., Shi, Y., Khan, S.Z., Mushtaq, K., 2018. Nanoparticles augmentation on biogas yield from microalgal biomass anaerobic digestion.

Int. J. Hydrogen Energy 43, 14202–14213. https://doi.org/https://doi.org/10.1016/j.ijhydene.2018.05.132

Zanganeh, K.E., Shafeen, A., 2007. A novel process integration, optimization and design approach for large-scale implementation of oxy-fired coal power plants with CO2 capture. Int. J. Greenh. Gas Control 1, 47–54. https://doi.org/10.1016/S1750-5836(07)00035-7

Zhang, J., Wang, Z., Wang, Y., Zhong, H., Sui, Q., 2017. Effects of graphene oxide on the performance, microbial community dynamics and antibiotic resistance genes reduction during anaerobic digestion of swine manure. Bioresour. Technol. 245, 850–859. https://doi.org/dx.doi.org/10.1016/j.biortech.2017.08.217

Zhang, K., Agrawal, M., Harper, J., Chen, R., Koros, W.J., 2011. Removal of the Fermentation Inhibitor, Furfural, Using Activated Carbon in Cellulosic-Ethanol Production 14055–14060. https://doi.org/10.1021/ie2013983

Zhang, Q., Hu, J., Lee, D.-J., 2016. Biogas from anaerobic digestion processes: Research updates. Renew. Energy 98, 108–119. https://doi.org/https://doi.org/10.1016/j.renene.2016.02.029

Zhang, Y., An, X., Quan, X., 2011. Enhancement of sludge granulation in a zero valence iron packed anaerobic reactor with a hydraulic circulation. Process Biochem. 46, 471–476. https://doi.org/https://doi.org/10.1016/j.procbio.2010.09.021

Zhao, Z., Zhang, G., Zhang, Y., Dou, M., Li, Y., 2020. Fe3O4 accelerates tetracycline degradation during anaerobic digestion: Synergistic role of adsorption and microbial metabolism. Water Res. 185. https://doi.org/10.1016/j.watres.2020.116225

Zheng, J., Rehmann, L., 2014. Extrusion Pretreatment of Lignocellulosic Biomass: A Review. Int. J. Mol. Sci. . https://doi.org/10.3390/ijms151018967

Zhong, D., Li, J., Ma, W., Qian, F., 2020. Clarifying the synergetic effect of magnetite nanoparticles in the methane production process. Environ. Sci. Pollut. Res. 27, 17054–17062. https://doi.org/10.1007/s11356-020-07828-y

Zhu, H., Shanks, B.H., Choi, D.W., Heindel, T.J., 2010. Effect of functionalized

MCM41 nanoparticles on syngas fermentation. Biomass and Bioenergy 34, 1624–1627. https://doi.org/10.1016/j.biombioe.2010.06.008

Justification of the thesis work

Great attention has been paid to develop non-fossil fuel energy sources to reduce carbon emissions and create a sustainable energy systems for the future. Among this efforts is the biogas production originated from agricultural residues and organic wastes. Biogas plays an important role as a versatile source of renewable energy, but must be treated for its later use. The purified and enriched version of biogas can be used for replacement of fossil fuels in power and heat production, and it can be used also as gaseous vehicle fuel. To remove the CO_2 from its composition the biological conversion of CO_2 to CH_4 by methanogenic *archaea* is an attractive option. However, the main limiting factor is the mass transfer of the gaseous H_2 in the liquid phase resulting in a low production rate of CH_4.

On the other hand, syngas can be produced from biomass gasification and also it is a byproduct of several industrial processes. It is carrier of a high amount of energy and carbon that cannot be stored (due to high content of H_2 and CO) unless it is processed. One alternative is the production of other metabolites by syngas fermentation, such as volatile fatty acids or alcohols. Such compounds can present higher economic values due to their wider range of applications in the chemical industry.

Overall, biogas upgrading and syngas fermentation is limited by the slow gas–liquid mass transfer, which results in low productivity on the end-products.

Currently, the implementation of nanoscale materials has emerged as an alternative to improve different biotechnological processes. It has been found that magnetite nanoparticles dissolve slowly, boosting the microbial activity and thus increased the end-products. Also, recent studies have reported that the capacity of H_2 sorption is enhanced by doping metal nanoparticles (Ag, Ni, Pd, Ca, Fe, K, TiO_2…) to carbon nanostructures (i.e. multilayer nanotubes, activated amorphous carbon, graphene...). In addition, graphene-based materials are promising candidates due to their unique characteristics, such as their high chemical stability, conductivity (promote DIET), low density, large-scale production suitability, wide range of synthesis approaches and structural shapes. Moreover, graphene based materials have been successfully applied to remove organic pollutants.

To the best of our knowledge, few studies have attempted the addition of reduced graphene in the biological processes of biogas upgrading and syngas fermentation. On the other hand, the detoxification of lignocellulosic hydrolysates is a topic of interest due to this biomass is an abundant and renewable feedstock for biofuels, biochemicals and biomaterials. The main drawback in the adsorption of inhibitory fermentation compounds is the high loss of sugar. Thus the exploration of other adsorbent to detoxification is necessary.

All above, in this thesis project we explore the use of magnetite, reduced graphene oxide and reduced graphene adorned with magnetite nanoparticles to: 1) improve slow gas–liquid mass transfer, 2) stimulate the microorganism with the use of Fe^{2+} released from magnetite, 3) take advantage of the conductive characteristics of nanomaterials to improve electron transfer, 4) use the hydrophobic properties of nanomaterials to absorb substrates or compounds of interest. All to enhance biological processes to produce energy (i.e. biogas enrichment, syngas fermentation and valorization of compounds removed from the detoxification of hydrolysates).

Hypothesis

The addition of graphene materials in the form of reduce graphene oxide (rGO) and magnetite adorned/decorated with rGO to biological processes like biogas enrichment and syngas fermentation will help to improve microbial activity and mass transport processes. The improvements come from the high surface area, microporous structure, conductivity and hydrophobicity of the materials added. Mass transfer of the gaseous substrates (CO_2, H_2, CO) to the liquid phase will be improved due to the hydrophobic behavior of the reduced form of graphene oxide.Thus, the nacomposite will be able to adsorb high amounts of hydrophobic gases. Likewise, the hydrophobic nature of reduced graphene adorned with magnetite nanoparticles will be an attractive adsorbent for inhibitory compounds present in wood hydrolysates.The conductive nature of graphene materials will enhance the bioenergy processes due to their capacity to exchange electrons via DIET processes. The leaching Fe^{2+} from the materials will boost the metabolic activity of microorganisms. Magnetite addition under anaerobic conditions will increase ferric

hydroxide precipitates, which will be reduced to Fe^{2+} becoming soluble (bioavailable to microorganisms).

General objective

Study the effects of the implementation of magnetite nanoparticles, reduced graphene oxide and reduced graphene oxide adorned with magnetite nanoparticles in bioenergy related processes, i.e. biological process of biogas upgrading, syngas fermentation and detoxification of wood hydrolysates.

Specific objectives

1. Acclimate and obtain a consortium of hydrogenotrophic methanogens microorganisms that consume biogas.
2. Carry out the biological purification of biogas by means of the enriched consortium of hydrogenotrophic microorganisms.
3. Acclimate and obtain a consortium that consumes syngas (H_2, CO and CO_2).
4. Carry out the syngas fermentation by means of the enriched sludge that consume syngas.
5. Characterize samples of the experiment at different stages (before and after the biological processes).
6. Explore the use of reduced graphene oxide adorned with magnetite nanoparticles as an adsorbent of inhibitors compounds present in wood hydrolysates.
7. Understand the mechanism of the interaction between the nanomaterials and the microorganisms.

Chapter II: Reduced graphene oxide decorated with magnetite nanoparticles enhance biomethane enrichment

Itzel Covarrubias-García, Guillermo Quijano, Aitor Aizpuru, José Luis Sánchez-García, José Luis Rodríguez-López, Sonia Arriaga. Reduced graphene oxide decorated with magnetite nanoparticles enhance biomethane enrichment. *Journal of Hazardous Materials*, Volume 397, 2020, 122760, ISSN 0304-3894.
https://doi.org/10.1016/j.jhazmat.2020.122760
https://www.sciencedirect.com/science/article/pii/S0304389420307494

Graphical Abstract

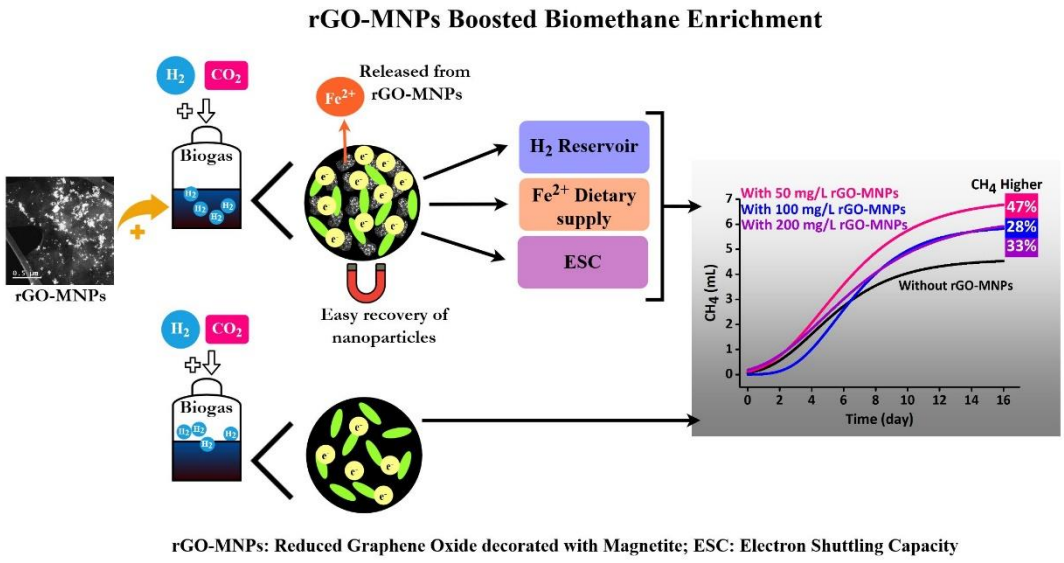

rGO-MNPs: Reduced Graphene Oxide decorated with Magnetite; ESC: Electron Shuttling Capacity

Abstract

The addition of magnetite nanoparticles (MNPs), reduced graphene oxide (rGO), and reduced graphene oxide decorated with magnetite nanoparticles (rGO-MNPs) was evaluated during biomethane enrichment process. rGO-MNPs presented the highest beneficial impact on the hydrogenotrophic assays with an improvement of 47% in CH_4 production. The improvement was linked to the increase of the electron shuttling capacity (ESC) by rGO-MNPs addition which boosted the hydrogenotrophic activity of microorganisms and that the rGO and rGO-MNPs served as reservoirs of hydrogen, which improved H_2 transport from the gas to the liquid phase and to the iron ions released acted as a dietary supply for microorganisms. Raman and XRD

confirmed a greater disorder and lower crystallinity of rGO-MNPs after the hydrogenotrophic assays, with a lower effect at a nanoparticle concentration of 50 mg/L. Moreover, FTIR analysis indicated that rGO-MNPs were oxidized during the hydrogenotrophic tests. This study highlights the advantages of adding rGO-MNPs as a magnetic nanocomposite. Furthermore, rGO-MNPs can be easily recovered, minimizing their release to the environment.

Keywords: biogas enrichment; electron shuttling capacity-ESC; graphene; hydrogenotrophic process; magnetite.

1. Introduction

Industrial biogas is produced in sewage treatment plants, landfills, industrial processing sites, and digestion plants treating agricultural organic waste, under both mesophilic (35°C) and thermophilic (55°C) conditions (Jönsson et al., 2003). Raw biogas (mostly composed of CH_4 40-75% and CO_2 15-60%) can be upgraded into biomethane, which is a fuel gas typically containing CH_4 concentrations ≥ 95% and constitutes a renewable alternative to natural gas (Ryckebosch et al., 2011). In general, biogas upgrading to biomethane can be accomplished by physicochemical treatments such as gas/gas or liquid/gas separation by membranes, vacuum or pressure swing adsorption, and cryogenic separation (Ryckebosch et al., 2011; Yang et al., 2014). Biogas enrichment can also be achieved by hydrogenotrophic processes performed by methanogenic archaea according to the theoretical stoichiometry presented in **Equation 1** (Madigan et al., 2012).

$$CO_2 + 4H_2 \rightarrow CH_4 + 2H_2O \quad (1)$$

ΔG= -130.1 kJ/mol

H_2 needed for biological biogas enrichment process can be obtained through water electrolysis from exploiting surplus wind mill, since wind is one of the most promising renewable energy sources (Sherif et al., 2005). Since storage costs of H_2 are consequently high, H_2 can be converted to CH_4 by the action of hydrogenotrophic methanogens. Hydrogenotrophic processes can be carried out directly in the biogas producing system (e.g. a digester) by injecting a H_2 stream (*in situ*), or in a separate

reactor (*ex situ*) (Simon and Rittmann, 2015). The main drawback encountered in the *in situ* process is the increase of the H_2 partial pressure in the reactor, which might inhibit the degradation of volatile fatty acids (e.g. propionate and butyrate), leading to hindered anaerobic digestion processes (Siriwongrungson et al., 2007). On the other hand, higher volumetric CH_4 production rates have been reached in the *ex situ* process (Simon and Rittmann, 2015). Easier processes control (H_2-to-biogas flow ratios, temperature, pH, etc.) constitutes a key advantage of the ex situ configuration (Simon and Rittmann, 2015). However, in general terms, biogas enrichment by means of hydrogenotrophic processes is intrinsically limited by the H_2 mass transfer from the gas to the liquid (Bensmann et al., 2014; Luo and Angelidaki, 2012; Simon and Rittmann, 2015).

Currently, the implementation of nanoscale materials has emerged as an attractive alternative to stimulate microbial activity during CH_4 and biogas production (Ganzoury and Allam, 2015). It has been reported that addition of nanomaterials can present a positive effect on the production of CH_4 and biogas, depending on the type, concentration, and size of the nanoparticles (Ambuchi et al., 2016; Casals et al., 2014; Ganzoury and Allam, 2015; Lin et al., 2017; Lo et al., 2012; Su et al., 2013; Yang et al., 2013). For instance, it was found that magnetite nanoparticles (100 mg/L, 7 nm) boosted microbial activity and increased biogas production by up to 180% (Casals et al., 2014). Likewise, the addition of 1000 mg/L of graphene enhanced the CH_4 yield by 25%, and the production rate by 19.5%, due to the stimulation of direct interspecies electron transfer (Lin et al., 2017). Recently, biomethanation of gaseous CO_2 was found to depend on nanoscale zero valent iron concentration, as a result of H_2 production during the iron corrosion process (Dong et al., 2019). So far, only few studies have evaluated the effect of nanoparticles on *ex situ* hydrogenotrophic biogas enrichment process.

Since the limiting step of the hydrogenotrophic processes is the H_2 mass transfer from the gas to the liquid phase, the addition of nanoparticles with a high H_2 affinity is particularly relevant. Nanostructured and nanoscale materials can strongly influence the thermodynamics and kinetics of H_2 sorption by increasing the diffusion rate, as well as by decreasing the required diffusion length (Niemann et al., 2008).

Carbon based materials are promising candidates for the storage of H_2 due to their low density, high chemical stability, large-scale production suitability, wide range of synthesis approaches and structural shapes, and property adaptability (Srinivas et al., 2010). Moreover, it has been reported that the H_2 storage capacity of carbon-based nanomaterials is enhanced by doping metallic nanoparticles (Ag, B, Ca, Fe, K, Li, Ni, Pd, Pt, Ru, Ti, TiO_2 and V) onto those nanostructures (Campesi et al., 2008; Ferre-Vilaplana, 2008; Hwang et al., 2009; Kim et al., 2005; Lee et al., 2010; Reyhani et al., 2011, 2009; Wang et al., 2009; Zacharia et al., 2005).

In the present study, magnetite nanoparticles (MNPs), reduced graphene oxide (rGO), and rGO decorated with magnetite nanoparticles (rGO-MNPs) were used as additives to study their effects on the performance of *ex situ* hydrogenotrophic process of biomethane enrichment.

2. Materials and Methods

2.1 Synthesis of magnetite nanoparticles (MNPs)

MNPs synthesis was carried out by co-precipitation of Fe(II) and Fe(III). In brief, a 100 mL solution of Fe(II) and Fe(III) chloride (2:1) in Milli-Q water was added into a five-neck flask reaction vessel. The solution was kept under N_2 atmosphere at room temperature and was vigorously stirred with the N_2 flux. Then, 70 mL of NaOH (0.2 N) was dropwise added. After 15 min reaction, the precipitated MNPs were washed with Milli-Q water and separated by decantation with a magnet. Finally, the MNPs were dried at 60°C overnight.

2.2 Synthesis of graphene oxide (GO) and reduced graphene oxide (rGO)

GO suspension was prepared by the modified Hummer's method (Esfandiar et al., 2011). In brief, 0.5 g of natural graphite powder microcrystal grade (2-15 μm, Alfa Aesar) and 0.5 g $NaNO_3$ were added to 23 mL of H_2SO_4. Then, the mixture was stirred in an ice bath for 10 min. After that, 3.0 g of $KMnO_4$ was slowly added to the suspension while it warmed up to room temperature. The suspension was stirred continuously in a water bath for 2 h at 35°C. Then the prepared suspension was diluted with 40 mL of Milli-Q water. During the dilution, the temperature of the

suspension was maintained at less than 60°C. Finally, 100 mL Milli-Q water with 3 mL H_2O_2 (30%) was added. The residual acids and salts of the suspension were removed by filtering through an anodic membrane filter of 0.22 µm pore size. The filtered powder was dispersed in Milli-Q water to obtain an aqueous graphene oxide suspension with yellow-brownish color. Then, the aqueous suspension was centrifuged at 2000 rpm for 15 min, and 8000 rpm for 10 min, to remove any unexfoliated graphitic plated and tiny graphite particles, respectively. Powder was dried at 60°C overnight. Graphene oxide nanosheets were obtained by ultrasonication of the filtered graphite oxide suspension for 1 h.

The rGO was prepared as follows: 0.8 g of GO was added to 80 mL of ethylene glycol. The mixture was maintained at 110°C for 15 min. Then, rGO suspension was filtered and dried at 60°C.

2.3 Preparation of reduced graphene oxide decorated with magnetite nanoparticles (rGO-MNPs) composites

The rGO-MNPs composite was synthesized as follows: 0.1 g of rGO was dispersed in 10 mL of Milli-Q water and 0.01 g of MNPs (relation of 10 % (w/w) of rGO) in 6 mL of Milli-Q water. Solution with rGO was mounted on a stand inside a sonicator, and, drop by drop, the magnetite solution was added. Finally, after completion of the reaction, the product was washed and dried at 60°C.

2.4 Sorption experiment with nanomaterial

Sorption tests were carried out to analyze if the mass transfer of H_2 from the gas phase to the liquid phase was increased by the presence of nanoparticles. The assay consisted in measuring the profile of H_2 concentration in headspace along the time in batch tests with 20 mL of mineral medium salt under incubation condition of 37°C and 150 rpm.

The sorption capacity (Q) was calculated using **Equation 2**.

$$Q = \frac{(C_0 - C_f) * V_h}{C_n * V_m} \quad (2)$$

C_0 and C_f are the initial and final concentrations of H_2 in the headspace. C_n is the concentration of the nanoparticles in the mineral medium salt, and V_h and V_m are the volume of the headspace and the volume of mineral salt medium with the nanoparticles, respectively.

2.5 Mineral salt medium

The composition of the mineral salt medium used was: (0.25 g) K_2HPO_4; (0.28 g) NH_4Cl; (0.83 g) $MgCl_2.6H2O$; (0.01 g) $CaCl_2$; (2.5 g) $NaHCO_3$; and (0.1 g) of yeast extract. No trace elements (micronutrients) were added.

2.6 Enriched sludge

The enriched sludge with hydrogenotrophic microorganisms was performed in 120 mL serological flasks sealed with rubber stoppers and aluminum rings (working volume of 80 mL). Flasks contained 32 mL of mineral medium and 48 mL of inoculum coming from an anaerobic reactor treating tequila *vinasse*. The headspace was flushed with N_2, and the excess N_2 was released to balance the system to ambient pressure with a needle connected to a solution with deionized water. Then, the headspace was replaced daily with 32 mL of H_2 and 8 mL CO_2 (H_2/CO_2 ratio of 4:1) for at least two months before starting the hydrogenotrophic assays. Cultures were incubated at 37°C and stirred at 150 rpm.

2.7 Hydrogenotrophic assays with and without synthesized nanomaterial

Control experiments were performed in 60 mL serological flasks, sealed with rubber stoppers and aluminum rings that contained 1.6 mL of the enriched sludge in 18.4 mL of mineral medium with a final concentration of 3 g/L of volatile suspended solids (working volume 20 mL). The flasks were incubated under the same conditions as the enriched sludge (37°C, 150 rpm, and 32 mL of H_2 and 8 mL CO_2). The following controls were carried out: (1) enriched sludge with reactive gases (H_2 and CO_2) and without nanomaterials, (2) enriched sludge without reactive gases and without nanomaterials, (3) enriched sludge without gases and with nanomaterials. Controls without reactive gases had an inert N_2 headspace.

For the assays including nanomaterial, the same procedure was carried out, supplementing the mineral medium with nanoparticles. The homogeneous nanoparticle suspension was obtained by sonication of MNPs, rGO, and rGO-MNPs in mineral medium during 30, 6, and 6 min, respectively. Three final concentrations of each nanoparticles were tested (50, 100, and 200 mg/L). The hydrogenotrophic tests lasted 16 days.

2.8 Gompertz model

The integrated Gompertz sigmoidal model was used to analyze the production of CH_4. In this logistic model the CH_4 production (S_c) may be expressed as a function of time according to **Equation 3** (Acuña et al., 1999).

$$S_c = a\ exp\{-\beta\ e^{-kt}\} \quad (3)$$

Where S_c= (S_0 – S), α (mL CH_4) is the maximum CH_4 production (at t→∞), β is the parameter related to the initial conditions when [t= 0, then S = S_0 = α exp (-β)], and k (day^{-1}) is the CH_4 production rate. The values of α, β, and k were obtained from Eq. 3 fitting to experimental data using a nonlinear regression program (OriginPro2016). The maximum CH_4 production rate in the experiments, V_{max}, was calculated from the model parameters as V_{max}= 0.368αk and expressed in mL CH_4 day^{-1} (Acuña et al., 1999).

2.9 Statistical analysis

Statistical analysis was performed using OriginPro2016 software. Paired sample T-Test at 0.05 significance level was used for each hydrogenotrophic treatment and its respective control.

2.10 Characterization of the nanomaterial

Scanning electron microscopy (SEM) images of rGO-MNPs composite were obtained with a scanning electron microscope FIB Dual Beam Helios Nanolab 600. Samples were sonicated in isopropanol and a drop of each sample was set into a carbon-coated copper grid and dried at room temperature for 24 h. Scanning transmission electron microscopy (STEM) was also used for rGO-MNPs and MNPs

and prepared with the same methodology used for SEM images. Raman, X-ray powder diffraction (DRX) and Fourier-transform infrared (FTIR) spectroscopy characterizations were also performed for rGO-MNPs before and after the hydrogenotrophic assays, since it was the material that best enhanced CH_4 production. Particles after hydrogenotrophic assays were recovered with a magnet on days 10 and 16, for the three tested concentrations. They were then dried in an atmosphere of N_2, at 60°C, for 24 h. FTIR scans of dried powders were performed by attenuated total reflection (ATR) in a Thermo-Nicolet brand equipment (Nexus 470 FT-IR E.S.P.), with a resolution of 4 cm^{-1} for 120 cycles. In every case, the spectra of the samples were recorded and divided by the background single beam spectrum before converting to transmittance spectra. The X-ray diffraction patterns were obtained in a diffractometer XRD Bruker D8 Advance with an X-ray generator of Cu (K_λ = 0.15414 nm) and a NaI detector with a scan rate of 0.02° min^{-1}, 2θ range of 5° to 80°. For Raman analysis, the samples were deposited on double-sided tape without using any solvent in a spectrophotometer InVía MICRORAMAN: RENISHAW at room temperature (514 nm, at 1% power).

2.11 Analytical methods

Acid digestion was carried out to measure the amount of iron deposited on rGO. In brief, 0.0025 g of sample was added in a microwave digestion system reactor (MILESTON) with 20 mL of an acid solution of HNO_3: H_2SO_4 (5:1), then closed at 2 Pa and heated to 150°C for 1 h. After digestion, solutions were made up to 50 mL with Milli-Q water and subsequently analyzed by inductively coupled plasma spectroscopy (ICP).

H_2, CO_2 and CH_4 concentrations were measured in a Thermo Scientific Trace 1300 GC with a thermal conductivity detector (TCD). The operation temperatures were 230, 200, and 220°C for the injector, column, and detector, respectively. N_2 was used as the carrier gas at a flow rate of 2.5 mL min^{-1}. Gas phase measurements were carried out by injecting 100 µL of headspace samples from the flasks in triplicate. The partial pressure of the batch assays was measured with an EXTECH instrument differential pressure manometer (Model # 407910). Alkalinity in hydrogenotrophic

tests was determined according to standard methods (APHA, 1998). The pH of the medium was monitored throughout the different biological tests in a Thermo Scientific ORION VERSTAR PRO potentiometer.

The dissolved iron content of supernatant was determined by ferrozine assay. Ferrozine reacts with divalent iron forming stable magenta complex species soluble in water (Stookey, 1970). The absorbance of the complex obtained was measured at 562 nm in a spectrophotometer (Cary 60, Agilent Technologies). The calibration curve was performed by dissolving the Mohr's salt under anoxic conditions. The electron shuttling capacity (ESC) of rGO and rGO-MNPs was determined according to methodologies previously reported (Lovley et al., 1996; Valenzuela, Edgardo et al., 2017). Conductive nanomaterials can shuttle electrons between them and the microorganisms due to their redox properties, which may enhance the capacity of microorganisms to reduce electron acceptors, such as insoluble Fe(III) oxide, organic matter or H_2. This electron transfer is measured indirectly by the total amount of Fe^{3+} reduced to Fe^{2+}. Briefly, representative slurry samples with nanomaterial were taken from experiments with a disposable syringe, while bottles were being manually shaken inside an anaerobic chamber. Each sample was mixed with an equal volume of HCl 0.5 M and allowed to stand for 30 min, while the same volume of sample was reacted with ferric citrate 20 mM for 3 h. Then, samples were mildly resuspended in a vortex, and 200 μL were left repose with the same volume of HCl solution for 30 min. Afterwards, each sample was centrifuged for 10 min at 10,000 g and 200 μL of supernatant were recovered and reacted with ferrozine reagent. The ferrozine solution was buffered with HEPES 50 mM and allowed to stand 10 min before measurement of optical density at 562 nm in the spectrophotometer. All solutions employed in this determination were bubbled with N2 for 30 min to ensure the absence of dissolved oxygen.

3. Results and Discussion

3.1 SEM and STEM micrographs of MNPs and rGO-MNPs

Composite rGO-MNPs presented a homogeneous distribution of MNPs over the surface of rGO (**Figure S1**). The dominant coverage of MNPs over the flakes of rGO

could be attributed to the fact that MNPs are entrapped inside the rGO sheets rather than being simply mixed up or blended with rGO. To corroborate this observation, STEM images were obtained for the synthesized MNPs and the composite rGO-MNPs (**Figure 1**a and 2b). Figure 1a depicts the synthesized MNPs with an average size of 8.3±3.6 nm. Figure 1b clearly shows that the MNPs are well dispersed over the surface of rGO. The red circle indicates that flakes of rGO present internalization of MNPs between the rGO sheets, as previously discussed. ICP analysis of rGO-MNPs indicated an iron content of 8.6±0.9 % (w/w). This result suggests a good deposition of MNPs over the surface of rGO flakes, since 10 % (w/w) of MNPs was added for the preparation of rGO-MNPs. The SEM micrographs obtained present a resemblance in morphology to a previous study, with a good distribution of magnetite over the surface of graphene and where the MNPs were entrapped inside the rGO sheets (Chandra et al., 2010; Hou et al., 2011).

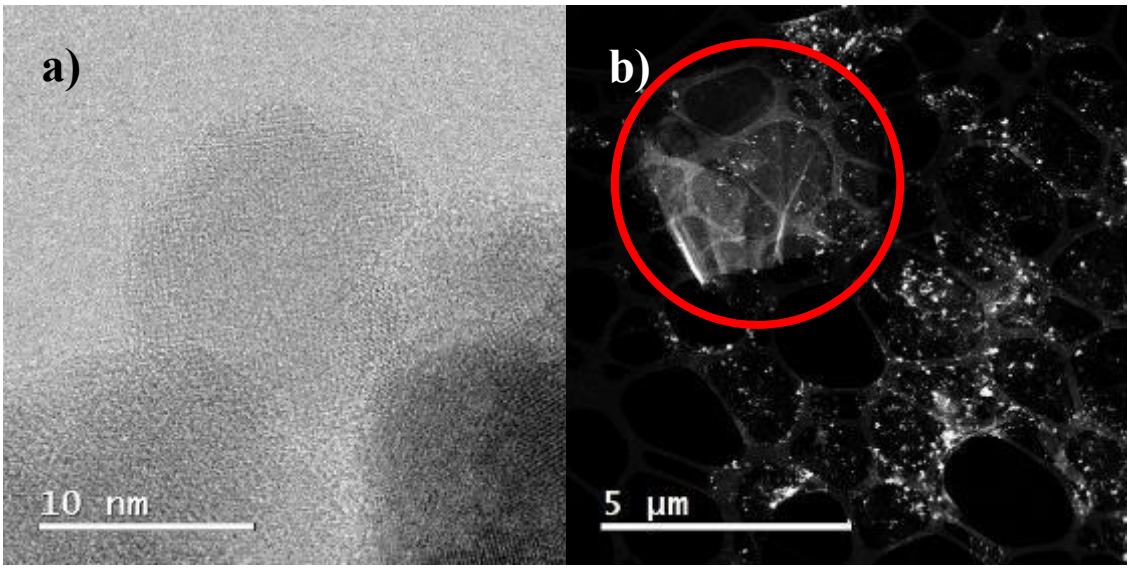

Figure 1. (a) STEM of MNPs with an average diameter of 8.3±3.6 nm, (b) STEM of rGO-MNPs, the red circle shows a zone where MNPs are clearly internalized inside the rGO-MNPs flakes.

3.2 Hydrogen sorption assays with nanomaterial

The initial measurement of H_2 in the headspace of the control assay (mineral medium without any nanomaterial) was 32.81±0.58 mL of H_2, while the final value of H_2 was 32.25±0.77 mL (**Figure S2**); these values indicated a low solubility of H_2, since H_2 is a poorly soluble gas. Table 1 presents the initial and the final concentrations of H_2 in

the headspace and the sorption capacity (Q) of the mineral solution with nanomaterial. MNPs showed a Q of 190.80, 104.30, 59.60 and 28.30 mg $H_2/g_{sorbent}$ for 25, 50, 100 and 200 mg/L, respectively. These values were lower than Q values of rGO and rGO-MNPs with concentrations of 25, 50 and 100 mg/L tested. Regarding the low adsorption of H_2 by MNPs, it has been reported that MNPs display a great tendency for intrinsic agglomeration due to inter-particle magnetic dipolar interaction, London attractive and van der Walls forces. Thus, a support material like graphene would be an alternative for avoiding the agglomeration and improve their stability (Krishna et al., 2016).

For all nanomaterials (MNPs, rGO and rGO-MNPs), higher Q values were achieved at 25 mg/L. The higher Q obtained were 1116.63 and 572.97 mg $H_2/g_{sorbent}$ for 25 and 50 mg/L of rGO. At 100 mg/L for rGO and rGO-MNPs similar values of Q were obtained (225.07 and 193.26 mg $H_2/g_{sorbent}$, respectively).

As can be seen in **Table 1**, among all tested nanomaterials, rGO achieved the better H_2 adsorption, leading to the lower final H_2 concentrations in the headspace, with C_f values of 0.058, 0.057, 0.061 and 0.062 mg/mL, for rGO concentrations of 25, 50, 100 and 200 mg/L, respectively.

Table 1. Sorption capacity (Q) of mineral medium with nanoparticles.

	Nanoparticle Concentration	**C_0**	**C_f**	**Q**
	mg/L	**mg/mL**	**mg/mL**	**mg $H_2/g\ sor_{bent}$**
Control	0	0.073	0.072	*
MNPs	25	0.072	0.069	190.80
	50	0.071	0.068	104.30
	100	0.071	0.068	59.60
	200	0.071	0.068	28.30
rGO	25	0.072	0.058	1116.63
	50	0.072	0.057	572.97
	100	0.072	0.061	225.07
	200	0.072	0.062	99.64
rGO-MNPs	25	0.072	0.066	475.92
	50	0.073	0.065	326.96
	100	0.072	0.063	193.26
	200	0.073	0.061	119.99

*** Non significant**

The higher C_f values achieved for H_2 at higher amounts of adsorbent could be attributed to agglomeration. Actually, it has been previously reported that aggregation via π-π stacking can be a great disadvantage of reduced graphene materials, which hinders their application (J. Liu et al., 2012). Thus, at nanoparticle concentrations of 100 and 200 mg/L, the nanomaterial may have agglomerated, making the H_2 sorption sites less available. On the other hand, rGO-MNPs was the second best nanomaterial regarding H_2 adsorption, reaching C_f values of 0.066, 0.065, 0.063 and 0.061 mg/L for 25, 50, 100 and 200 mg/L. The lower C_f of rGO-MNPs at higher amounts of adsorbent seems to indicate that the stabilization and functionalization of rGO via MNPs decoration allowed to avoid undesirable aggregation. The lower adsorption capacity of rGO-MNPs compared with rGO is likely due to the decrease in the amount of surface area of rGO by decoration of MNPs, which led to a decrease in the reactive adsorption sites of rGO.

Overall, this analysis disclosed that rGO and rGO-MNPs functioned as a reservoir of H_2 from the gas to the liquid phase, helping to improve the process, since it has been reported that even if the biogas enrichment process occurs in a separated reactor (*ex situ*), the problem of interphase mass transfer of H_2 is a limiting step (Bassani et al., 2015; Luo and Angelidaki, 2012). rGO and rGO-MNPs can act as transfer vectors, then, H_2 could be released continuously for microbial consumption and at the same time a new pseudo-equilibrium of adsorption/desorption of H_2 could take place until H_2 is totally consumed.

3.3 Hydrogenotrophic tests of enriched sludge provided with nanomaterial

Control test experiments of hydrogenotrophic assays are presented in **Table 2**.

Table 2. Methane production of hydrogenotrophic test controls (averages and std=standard deviation).

Control	Concentration	MNPs		rGO		rGO- MNPs	
	mg/L	mL CH_4	± std	mL CH_4	± std	mL CH_4	± std
	50	1.61	0.55	1.35	0.40	1.58	0.76
	100	1.98	0.29	1.42	0.48	1.63	0.82

Sludge without reactive gases and with nanomaterial	200	1.83	0.64	1.66	0.68	1.73	0.90
Sludge without reactive gases and without nanomaterials	0	1.29	0.33	1.27	0.42	1.55	0.74
Sludge with reactive gases and without nanomaterial	0	4.56	2.01	4.22	1.82	3.57	1.82

Controls without addition of reactive gases and the addition of nanomaterial did not present a significant difference in CH_4 production in all treatments. On the other hand, the volume of CH_4 produced in the controls without gases and without the addition of nanomaterial were 1.9% to 34.8% lower, compared with the controls without the addition of gases and with the addition of the three nanomaterial at the three concentrations. The controls with reactive gases and without the addition of nanomaterial were 106.4% to 212.6% higher than all controls, which corroborates the hydrogenotrophic activity of the microorganisms.

The results obtained in the batch assays supplemented with nanomaterial at the three concentrations (50, 100 and 200 mg/L) are shown in **Figure 2**.

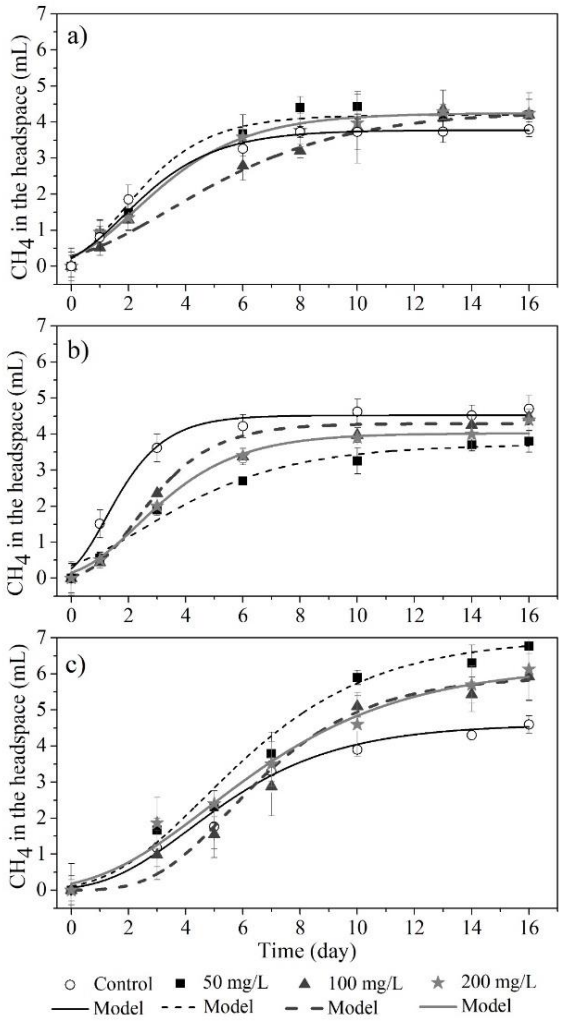

Figure 2. Hydrogenotrophic tests of enriched sludge provided with nanoparticles; a) MNPs, b) rGO and c) rGO-MNPs.

It can be observed that the controls with reactive gases and without nanomaterial presented a small variation in each panel of Figure 2. Nevertheless, the mean value of CH_4 production at the end was very similar (4.36±0.5 mL).

The overall trend of CH_4 production did not show improvement with regards to the control without MNPs (Figure 2a). Volume of CH_4 of the control (without MNPs) at the end of the experiment was 3.81±0.2 mL, compared to 4.22±0.43, 4.21±0.61, and 4.23±0.11 mL in presence of 50, 100, and 200 mg/L of MNPs, respectively. Over the duration of the experiment, paired sample T-Test analysis indicated no significant difference with the control (p=0.053, 0.609 and 0.218, for the three concentrations of MNPs tested). On the other hand, hydrogenotrophic tests provided with rGO

(Figure 2b) indicated that the tested concentrations (50, 100 and 200 mg/L) did not boost the production of CH_4; on the contrary, they seemed to have an inhibitory effect until day 10. From day 10 on, CH_4 production behaved similarly to the control till the end of the experiment. The volume of CH_4 produced without rGO was 4.72±0.36 mL, while in presence of rGO, 3.80±0.31, 4.47±0.11 and 4.39±0.32 mL of CH_4 were obtained for nanomaterial concentrations of 50, 100 and 200 mg/L, respectively. The same observation was corroborated with a paired T-Test, indicating that the three concentrations were significantly different from the control (p=4.971E-4, 0.008 and 0.006, for 50, 100 and 200 mg/L of rGO, respectively). In relation to the results obtained with the composite rGO-MNPs, the three concentrations achieved a higher CH_4 production (Figure 2c) compared with the control. The produced volume of CH_4 at the end of the experiment was 4.6±0.24 mL for the control assay without composite, while 6.77 ± 0.09 mL, 5.92±0.65 mL and 6.13±0.88 mL of CH_4 were produced in presence of rGO-MNPs, corresponding to an improvement of 47.20%, 28.34% and 31.31% at the end of the experiment, compared to the control, for nanomaterial concentrations of 50, 100 and 200 mg/L, respectively. Paired T-Test analysis, considering the overall assay, supports the CH_4 production enhancement for two concentrations, 50 and 200 mg/L, with p=0.014 and p=0.009, respectively (for 100 mg/L, p=0.221). The experimental data of the hydrogenotrophic tests, at the three nanomaterial concentrations, were successfully fitted to the Gompertz model with correlation coefficients r2> 0.96. A V_{max} value of 0.78 mL CH_4/day was calculated for the control in the experiments with MNPs. This value was lower than 0.92 mL/day and 0.46 mL/day, when 50 and 100 mg/L of MNPs were added, respectively. A similar V_{max} value of 0.72 mL CH_4/day was calculated for 200 mg/L of MNPs. Regarding rGO, it was observed that V_{max} for the control was higher than the values recorded with the three concentrations of rGO added, which indicated an inhibitory effect of this nanomaterial with a lower effect at 100 mg/L (V_{max}=1.04 mL/day) than at 50 mg/L (V_{max}=0.46mL/day) and 200 mg/L (V_{max}=0.75 mL/day). Therefore, the inhibition mediated by rGO was not dose dependent. Finally, comparing the results of Vmax of rGO-MNPs, the improvement in CH_4 production can be further corroborated, since Vmax recorded when the composite was added

was 32.76%, 41.38% and 5.17% higher than that observed in the control test (for 50, 100 and 200 mg/L of nanomaterial, respectively). Also, a paired sample T-Test was carried out with the parameters obtained from the model (control against treatments). Such comparison is shown in **Table 3** (asterisk).

Table 3. Parameters obtained after fitting the hydrogenotrophic tests to the Gompertz model.

Experiment		**α**	**β**	**k**	**Vmax**	**r^2**
		(mL)		day^{-1}	(mL/day)	
MNPs	Control	3.77±0.09	1.81±0.25	0.56±0.09	0.78	0.98
	50 mg/L	4.19±0.02*	1.79±0.21	0.60±0.14	0.92	0.99
	100 mg/L	4.31±0.40*	3.47±0.55*	0.29±0.05*	0.46	0.98
	200 mg/L	4.24±0.05*	2.24±0.19*	0.46±0.05*	0.72	0.99
rGO	Control	4.52±0.10	1.20±0.14	0.86±0.14	1.43	0.98
	50 mg/L	3.71±0.19*	2.46±0.33*	0.34±0.05*	0.46	0.96
	100 mg/L	4.29±0.15*	222±0.07*	0.66±0.03*	1.04	0.99
	200 mg/L	4.02±0.08*	2.31±0.10*	0.51±0.06*	0.75	0.99
rGO-MNPs	Control	4.60±0.13	4.12±0.32	0.34±0.05	0.58	0.97
	50 mg/L	6.99±0.17*	4.66±0.33*	0.30±0.04	0.77	0.98
	100 mg/L	5.99±0.36*	5.49±0.41*	0.37±0.08	0.82	0.98
	200 mg/L	6.23±0.43*	4.78±0.41*	0.26±0.05*	0.61	0.98

*Values significantly different from the control.

Maximum CH_4 production (α) was significantly different from the control in each treatment of the three nanomaterial tested.

To the best of our knowledge, very few studies have attempted the addition of nanoparticles in the ex situ hydrogenotrophic process. Thus, the results herein presented are compared with some studies where nanoparticles were added in anaerobic digestion processes for biogas production. The effect of MNPs addition in anaerobic batch assays has been reported previously, indicating an improvement in biogas and CH_4 production of 180% and 234%, respectively, at 100 mg/L MNPs (7 nm) (Casals et al., 2014). It was found that small iron oxide nanoparticles under non-saturation conditions slowly dissolve and boost bacterial activity in the anaerobic digester, introducing a novel concept of dosing ions by size and surface-state, nanoparticles act as the carrier and the released iron ions as the active compound. NPs were first dispersed and then progressively dissolved over an extended period

of time to yield the dietary supply of iron for the microorganisms in the reactor (Casals et al., 2014). However, in the present study the addition of MNPs did not have a significant effect on CH_4 production. This could be attributed to the lack of a stabilizing agent like Tetramethylammonium hydroxide which was used in the study above mentioned. Such agent was added in that experiment in order to obtain a stable colloidal solution of magnetite nanoparticles. Another study reported the magnetite particle aggregation and the decrease in their reactivity when using humic substances to remove biologically Cr (VI) from solution (Sundman et al., 2020). Thereby, agglomeration/aggregation of nanoparticles is a crucial factor in a real application scenario.

The inhibitory effect of rGO attained in the present study could be attributed to the concentrations added. Comparing with related materials, a study assessed the effects of GO on the performance, microbial community and antibiotic resistance, during the anaerobic digestion of swine manure showing that the CH_4 production was not dose-dependent. CH_4 production was reduced by 13.1%, 10.6%, 2.7% and 17.1% at GO concentrations of 5 mg/L, 50 mg/L, 100 mg/L and 500 mg/L, respectively. The maximum reduction was at 5 mg/L and 500 mg/L, while the least CH_4 reduction was obtained at 100 mg/L (Zhang et al., 2017). In another study, toxic effects of GO on wastewater microbial communities have been dose dependent for concentrations between 50 and 300 mg/L (Ahmed and Rodrigues, 2013). Thus, in the present study, a lower concentration of rGO could probably be more effective. However, it is worth noting that many factors can influence efficiency, since toxicity depends on the concentration, the size and type of graphene, the grade of reduction or oxidation, and the type of microorganisms present in the biological system. Furthermore, it is important to highlight that over the time, microorganisms can adapt to survive in the presence of the nanoparticles, as indicated in a study where the anaerobic bacteria became familiar to the toxic effect of the added material at the end of the experiment (Luna-delRisco et al., 2011) which happened in the hydrogenotrophic tests with rGO at three concentrations, 50, 100 and 200 mg/L from day 10 till the end of the experiment. The rGO decorated with MNPs could have caused a lower inhibitory effect as antimicrobial actions of graphene-based materials

are attributed to membrane and oxidative stress by direct contact with the sharp nanosheets, and the ensuing superoxide anion-independent oxidation (Liu et al., 2011). Furthermore, MNPs present unique characteristics, including magnetic, electric, catalytic, biocompatibility and low toxicity properties (He and Gao, 2010; Thanikaivelan et al., 2012; Wei et al., 2013), which seem appropriate for the decoration of graphene materials. **Table S1** displays different references on nanomaterial used in anaerobic digestion systems. In general, it has been found that the addition of nanomaterials can present a negative, positive or null effect on the production of CH_4 and biogas in anaerobic digestion processes, this due to the toxicity they may present depending on the type of nanoparticle (chemical and physical structure), the concentration added, and the size.

At the same time, it has been reported that the storage capacity of H2 is enhanced by the doping of metallic nanoparticles (Ag, B, Ca, Fe, K, Li, Ni, Pd, Pt, Ru, Ti, TiO_2 and V) to carbon nanostructures (Campesi et al., 2008; Ferre-Vilaplana, 2008; Hwang et al., 2009; Kim et al., 2005; Lee et al., 2010; Reyhani et al., 2011, 2009; Wang et al., 2009; Zacharia et al., 2005). Thus, in the present work, the synergistic combination of rGO-MNPs improved the biological biogas enrichment process *ex situ*.

3.4 Electron shuttling capacity in hydrogenotrophic tests provided with rGO and composite rGO-MNPs

ESC is the measuring of the total electron accepting capacity of the conductive materials. ESC of rGO and rGO-MNPs was obtained by the methodology described in Section 2.11. **Figure 3** shows, on the left axis, the ESC of rGO and rGO-MNPs at the three concentrations, i.e., 50, 100, and 200 mg/L and, in the right axis, the CH_4 production.

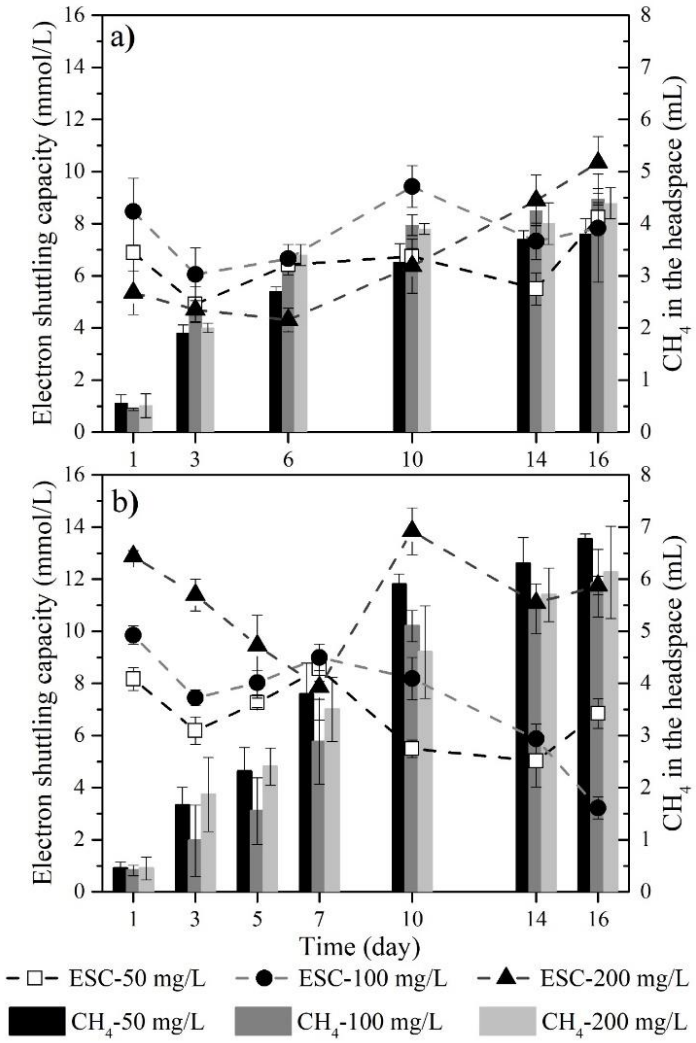

Figure 3. Electron shuttling capacity (ESC) of hydrogenotrophic tests provided with nanoparticles; a) rGO and b) composite rGO-MNPs, for 50, 100 and 200 mg/L, respectively.

For rGO (Figure 3a), ESC did not present a clear time trend for concentrations of 50 and 100 mg/L, whereas at a concentration of 200 mg/L, ESC increased from day 6 onwards, reaching a final value of 10.34±1.01 mmol/L. Such an increase in ESC is related to the day that CH_4 production reached steady-state. On the other hand, peaks with the highest ESC values were observed on day 7 (8.56±0.48 mmol/L), 7 (9.0±0.5 mmol/L), and 10 (13.84±0.9 mm/L), for concentrations of rGO-MNPs of 50, 100, and 200 mg/L, respectively. From those days onwards ESC clearly diminished. As shown in Figure 3b, rGO-MNPs presented higher ESC than rGO alone,

confirming that MNPs improve the redox properties of rGO, promoting a better electron transfer.

The material that presented the highest ESC was rGO-MNPs nanocomposite at 200 mg/L (7.86±1.27 to 13.84±0.9), followed by rGO-MNPs at 100 mg/L (3.22±0.43 to 9.0±0.5) and rGO-MNPs at 50 mg/L (5.02±1.01 to 8.56±0.48). This is consistent as the ESC of conductive materials is function of the concentration of the material, the higher the concentration of material, the higher ESC. Even though the ESC of the rGO-MNPs was higher at 200 mg/L, CH_4 production was not the highest as the overall process is not only function of the ESC and the sorption capacity of H_2 by the materials. Other processes inherent of microorganisms are present in the system known like direct interspecies electron transfer (DIET) and mediated interspecies electron transfer (MIET) which are triggered by conductive materials and permit to enhance microbial activity (Chen et al., 2014b, 2014a; F. Liu et al., 2012; Lovley, 2017). DIET is an inherent mechanism for electron exchange between different species of microorganisms, in which free electrons flow from one cell to another without being shuttled by reduced molecules such as molecular H_2 or formate (Dubé and Guiot, 2015). Electrically conductive *pili* (*e-pili*) are an important electrical conduit for DIET. However, there may be instances in which electrical contacts are made between electron transport proteins associated with the outer membranes of the partners. Alternatively, DIET partners can plug into carbon materials, such as granular activated carbon, carbon cloth and biochar, for long-range electron exchange without the need for e-*pili* (Chen et al., 2014b, 2014a; F. Liu et al., 2012). Thereby, DIET is promoted by the addition of conductive materials such as the ones used in this study (Lovley, 2017).

Other studies have quantified the electron shuttling capacity (ESC) for humic substances, indicating that some microorganisms in soils and sediments are able to use humic substances as an electron acceptor for the anaerobic oxidation of organic compounds and H_2. This electron transport yields energy to support growth (Lovley et al., 1996). In this context, since graphene presents similarities with humic substances and possesses quinone functional groups with redox properties,

Furthermore, the important role of conductive iron oxides has been previously

reported in co-cultures (Kato et al., 2012; Liu et al., 2015). Kato et al (2012) reported that *Geobacter sulfurrenducens* shared electrons with *Thiobacillu*s though electric currents in the presence of magnetite in the process of acetate oxidation and nitrate reduction (Kato et al., 2012). At the same time Liu et al (2015) reported that magnetite can compensate the lack of electron transfer functions of *Geobacter sulfurreducens* and *G. metallireducens* (Liu et al., 2015). Another study also reported that magnetite served as electron conduits in enrichment cultures with butyrate (Li et al., 2015).

In literature, in an effort to better understand the electron transfer interactions between conductive materials (i.e; biochar, humic substances, activated carbon, etc.) and microorganisms, different inherent electron properties of the added materials have been described, calculated and measured, such as redox properties. **Table 4** presents different studies that have reported ESC values of different materials.

Table 4. Electron shuttling capacity values of different materials reported in literature.

Material	**Concentration (g/L)**	**ESC (Fe^{2+}) mmol/L**	**Reference**
Biochar	0.5 and 1	0.2 to 0.25	(Kappler et al., 2014)
Biochar	5 and 10	1 to 2	(Kappler et al., 2014)
Sediment solid phase humic substance	50	0.8 to 5	(Roden et al., 2010)
Humic acid fraction	x	5-7.5	(Bai et al., 2020)
Water-extractable organic matter	x	5	(Bai et al., 2020)
Fulvic acids	x	7.5 to 10	(Bai et al., 2020)
rGO	0.05	4.9±0.7 to 8.2±0.6	*
rGO	0.1	6.0±1.0 to 9.4±0.8	*
rGO	0.2	4.3±0.4 to 10.3±1.1	*
rGO-MNPs	0.05	5.0±1.0 to 8.5±0.5	*
rGO-MNPs	0.1	3.2±0.4 to 8.2±0.8	*
rGO-MNPs	0.2	7.8±1.3 to 13.8±0.9	*

*Present study

Kappler et al. (2014) obtained the ESC of biochar. They found that biochar concentrations of 5 and 10 g/L stimulate both the rate and the exent of microbial

reduction of Fe(III) oxydydroxide mineral ferrihydrite by *Shewanella oneidenis MR-1* (ESC of 1 to 2 mmol/L), while lower biochar concentrations, 0.5 and 1 g/L, presented a negative effect on ferrihydrite reduction (ESC of 0.2 to 0.25 mmol/L) , after 72 h (3 days) incubation (Kappler et al., 2014). In the present study, as previously stated, the ESC values of rGO and rGO-MNPs were function of the mass amount of material present in the system. Amounts of material ranged between 0.05 and 0.2 g/L, whereas in the studies presented in Table 4, higher amounts of 0.5-10 g/L were tested for biochar, humic substances, fulvic acids and organic matter. Even though the amount of conductive material used in the present study was at least 200 times lower than the studies carried out with biochar, the ESC was around 60 times greater than biochar, for rGO and rGO-MNPs (Kappler et al., 2014). The high ESC for rGO and rGO-MNPs obtained can be function of physical properties, such as the surface area and the conductivity of the material. For example, the biochar presented a surface area of 341 m^2/g (Kappler et al., 2014), while the theorerical value reported for graphene is 2630 m^2/g (Peigney et al., 2001), and typical experimental values range from 600 to 900 m^2/g and 600-700 m^2/g, for graphene and funtionalized graphene, respectively (McAllister et al., 2007). Thus, the surface area of the tested materials in this study were at least 2 times greater than the biochar. Also, the conductivity of biochar in Kappler's study is lower (49.75 mS/m) (Kappler et al., 2014) than the reduce graphene oxide (60mS/m) (Soni et al., 2018). On the other hand, Roden et al. (2010) confirmed that 50 g/L of Fe-stripped Talladega Wetland sediment greatly increased the rate of Fe(III) reduction, finding different ESC values in the presence of *S. putrefaciens* cells (0.8 to 3.5 mmol/L) and *G. sulfurreducens* cells (0.8 to 5 mmol/L) after 24 h (Roden et al., 2010). Bai et al., (2020) obtained the ESC values of extracted water-extractable organic matter, fulvic acids and humic acids fractions amended with a model quinone by the ferrozine assay. They reported values between 0.8 and 7.5 mmol/L, finding that a key factor of ESC is the concentration of aromatic groups of the extracted fractions (Bai et al., 2020).

3.5 Dissolved Fe^{2+} in hydrogenotrophic tests provided with MNPs and rGO-MNPs

An increase of Fe^{2+} was observed with CH_4 production for MNPs in Figure 4a (days 1 and 2), for concentrations of 50 mg/L and 100 mg/L. The rise of Fe^{2+} may be related with the iron released of the nanoparticle and due to the low initial activity of the microorganisms (low production of CH_4, low consumption of Fe^{2+}), since the most labile iron is released. From day 6 on, a stationary phase of CH_4 and Fe^{2+} appeared for 50 mg/L of MNPs until the end of the experiment, and for 100 mg/L of MNPs until day 10. From day 10 on, at 100 mg/L (days 13 and 16), an increase of Fe^{2+} was observed at a rate of 19.57 mg/L-day till the end of the experiment (Figure 4a). Fe^{2+} for 200 mg/L of MNPs was very similar along the assay and did not present a clear tendency with CH_4 production.

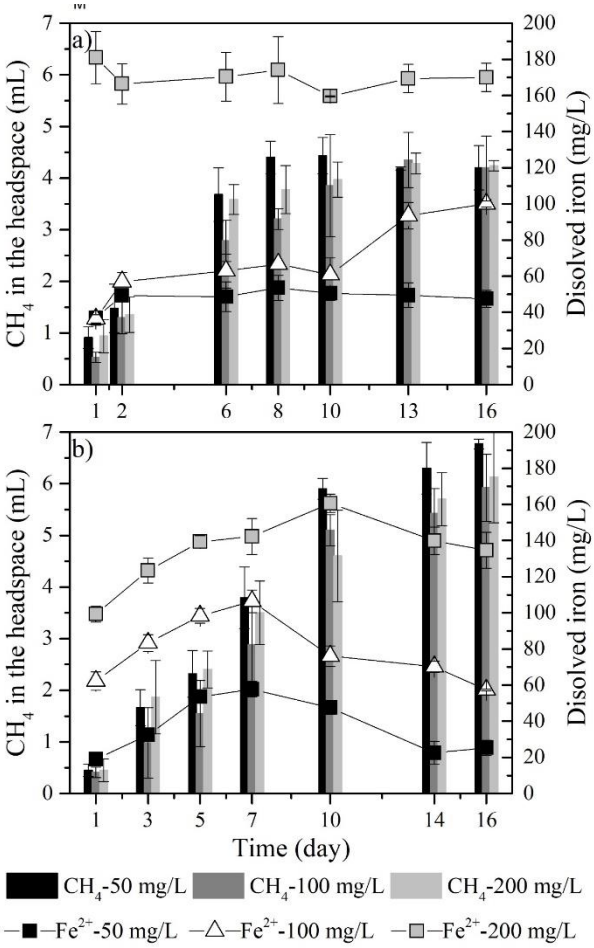

Figure 4. Dissolved iron (Fe^{2+}) from supernatant of the hydrogenotrophic tests provided with MNPs and composite rGO-MNPs. a) MNPs and b) nanocomposite rGO-MNPs, for 50, 100 and 200 mg/L, respectively.

On the other hand, same initial increase of Fe^{2+} as with MNPs (50 and 100 mg/L) was observed for rGO-MNPs in Figure 4b (days 1, 3, 5 and 7) for the three concentrations. After those days, the Fe^{2+} concentrations decreased, as the higher CH_4 production for rGO-MNPs (Fig 4b) could justify a higher consumption of Fe^{2+} by the microorganisms, and a decrease in concentration in solution. However, it may be because this catalyst contains much less iron than the catalyst composed of pure magnetite (MNPs). Therefore, Fe^{2+} triggered the CH_4 production for rGO-MNPs at the three concentrations tested when the highest CH_4 production began. At the same time, the peaks when more Fe^{2+} was observed (Figure 4b) matched with peaks with the highest ESC values on day 7 (8.56±0.48 mmol/L), 7 (9.0±0.5 mmol/L), and 10 (13.84±0.9 mm/L), for concentrations of rGO-MNPs of 50, 100, and 200 mg/L, respectively (Figure 3b). Thus, Fe^{2+} released in the media could be acting like a dietary supply for the microorganisms improving their microbial activity. At the same time, during the hydrogenotrophic process of CH_4 enrichment, while Fe ions from rGO-MNPs are being released, more sites from these nanomaterials are available to adsorb more H_2, this mechanism is conducted several times until H_2 is totally consumed, then, the overall rates of biomethane production were improved. The dietary effect of iron to stimulate anaerobic digestion systems has been previously studied (Abdelsalam et al., 2017; Casals et al., 2014; Patel et al., 1993; Ram et al., 1999; Zaidi et al., 2018). The reported concentration of trace metals (i.e; iron) required during anaerobic digestion differs significantly, depending on the substrate type, operating temperature, digestion operating mode, and type of methanogens (Thanh et al., 2016). For instance, Patel et al. (1993) found that the addition of $FeCl_3$ increased gas production more than 60% with high CH_4 content (Patel et al., 1993). In this context, Casals et al. (2014) hypothesized that maintaining optimal iron concentrations is a critical step to enhance CH_4 production in anaerobic digestion processes. Also, Abdelsalam et al. (2017) found that 20 mg/L Fe and 20 mg/L Fe_3O_4 nanoparticles biostimulated the methanogenic bacteria increasing by 1.4 and 1.66 times the biogas volume, respectively (Abdelsalam et al., 2017) and Zaidi et al. (2018) attained a cumulative increase of biogas of 28% with the addition of 10 mg/L of Fe_3O_4 nanoparticles in microalga biomass anaerobic digestion (Zaidi et al., 2018).

However, the media content of Fe^{2+} was not measured in any study. In another study, chloride salt of Fe^{2+} was added at 5 mM during anaerobic mineralization of organic matter. It was observed that Fe^{2+} stimulated biogas yield (5-10%) during the first 24-48 hours; afterwards, the gas production decreased and it was similar to that of the controls, which suggested that iron was consumed (Ram et al., 1999). Nevertheless, Fe^{2+} concentration was not determined during that study. Furthermore, this study found that Fe^{2+} considerably enhanced H_2 utilization at 37°C. Finally, the iron that was not used for microorganism could work also as electron conduct like graphene in the present study.

Moreover, MNPs over the surface of rGO (decorated nanocomposite) are more available to microorganisms, since they are well dispersed over the surface of rGO and do not agglomerate easily, which represents an advantage over MNPs alone. Another advantage could be the fact that the concentration of MNPs is lower in the nanocomposite than the nanoparticles alone; thus, the toxic effect could be lower.

It has been established that, whereas magnetite particles are smaller than microbial cells and thus attach to individual cells, multiple partner cells attach to conductive carbon materials, such as granular activated carbon, biochar and carbon cloth, facilitating DIET (Chen et al., 2014a, 2014b; F. Liu et al., 2012). The electrical contact between cytochromes associated with the outer cell surface and the conductive materials is sufficient (due to the ESC) to carry out processes via DIET, like in the case of rGO-MNPs. To the best of our knowledge, no studies about the promotion of interspecies electron transfer with graphene materials have been reported in literature.

The fact that MNPs alone did not present the triggering effect, and apparently no consumption of Fe^{2+} by microorganisms, but only release of Fe^{2+}, could be attributed to the fact that MNPs tend to agglomerate easily, which could be affecting their bioavailability for microorganisms. In the present study, MNPs did not enhance the CH_4 production, even if it has been previously reported that they can promote the electron capacity exchange in other systems (Kato et al., 2012; Li et al., 2015; Liu et al., 2015).

Finally, results of alkalinity and pH obtained for the hydrogenotrophic batch tests indicated that the Fe^{2+} released was not carried by chemical mean, since alkalinity and pH between the different materials and concentrations tested were not different (Table S2).

3.6 Characterization before and after hydrogenotrophic tests with rGO-MNPs

In Raman analysis (**Figure 5**), the common characteristic peaks of carbon materials can be observed at 1350 cm^{-1} associated with the D band peak, the G band peak at ~1600 cm^{-1} and the 2D peak at ~ 2700 cm^{-1}, all present in the rGO-MNPs before and after the hydrogenotrophic assays.

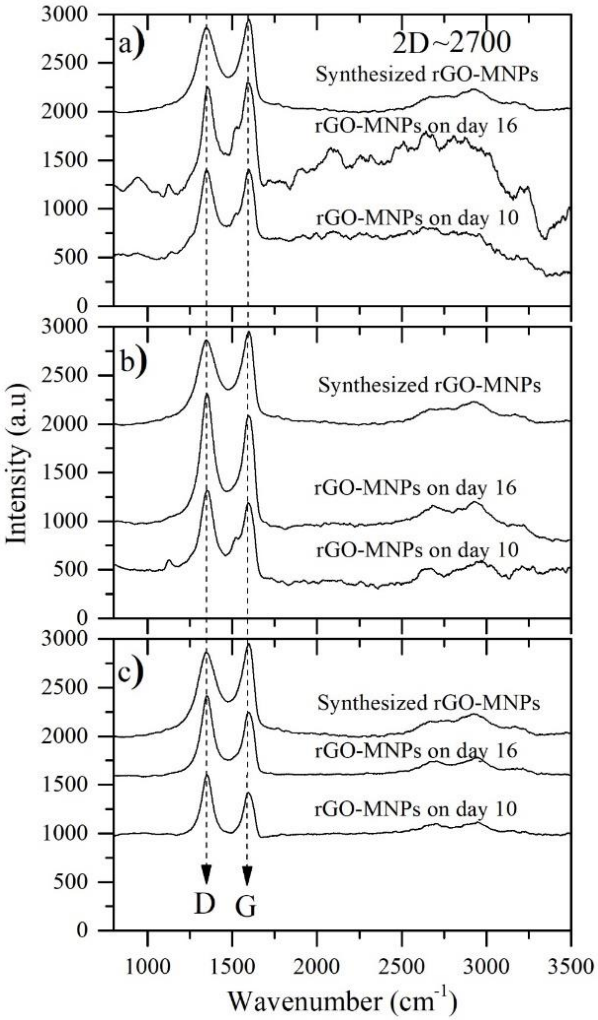

Figure 5. Raman spectra of composite rGO-MNPs and on day 10 and 16 after hydrogenotrophic assay. a) 50 mg/L, b) 100 mg/L and c) 200 mg/L.

Raman spectrum of rGO-MNPs before treatment (synthesized composite) in all the panels (a), (b) and (c) presented similar intensity of D and G bands, corresponding to an I_D/I_G ratio of 0.91. On the other hand, an I_D/I_G ratio of 0.99 and 0.94 was observed with 50 mg/L at day 10 and day 16, respectively. An I_D/I_G ratio of 1.21 was achieved with 100 mg/L at day 10 and day 16. Finally, with 200 mg/L, I_D/I_G ratios of 1.44 and 1.28 were observed for days 10 and 16. The above can be visually corroborated with Figure 5, where for 50 mg/L, there is no big difference between D and G peaks, and clearly the D peak looks higher than the G peak, for 100 and 200 mg/L, after the hydrogenotrophic assays. Literature indicated that the intensity of D and G bands is used to determine the degree of disorder or "quality" of the carbon materials. The D band is attributed to extremes, defects and disordered carbon, while the G band corresponds to the sp^2 carbon atoms with a well ordered structure (Kudin et al., 2008). Thus, rGO-MNPs acquired a greater disorder or lower crystallinity after the biological treatment; with a lower effect for 50 mg/L. Chouhan et al. (2016) reported a change in the ratio I_D/I_G from 0.23 to 0.11 with graphene oxide after the interaction with resistant bacteria *Trabulsiella guamensis*. This change in ratio indicated that the graphene oxide layers were structurally degraded through possible surface reduction due to their interaction with resistant bacteria (Chouhan et al., 2016a). On the other hand, an increase of I_D/I_G ratio from 0.7 to 1.2 was observed in the biotransformation of multi-walled carbon nanotubes mediated by resistant bacteria, linking this to an structural change of oxidation process (Chouhan et al., 2016b). In this sense, the results previously described of I_D/I_G ratios in the present study indicate that rGO-MNPs composite is being oxidized during the hydrogenotrophic process. This is also corroborated by FTIR analysis discussed below. As far as we know, no study has been reported on the structure modification of graphene materials by microorganism's action. The XRD analysis also revealed structural changes occurring during the hydrogenotrophic process (**Figure 6**). Sharp diffraction peaks can be observed in the XRD patterns of the MNPs (Figure 6a), an indication of their crystallinity. The crystal atomic planes from the diffraction peaks had been indexed as (220), (311), (400), (422), (511), (440), and (533). These matched the characteristic peaks for Fe_3O_4 (MNPs) in the standard PDF card in the

X-ray diffraction atlas (JCPDS card 19-0629) issued by the International Powder Union.

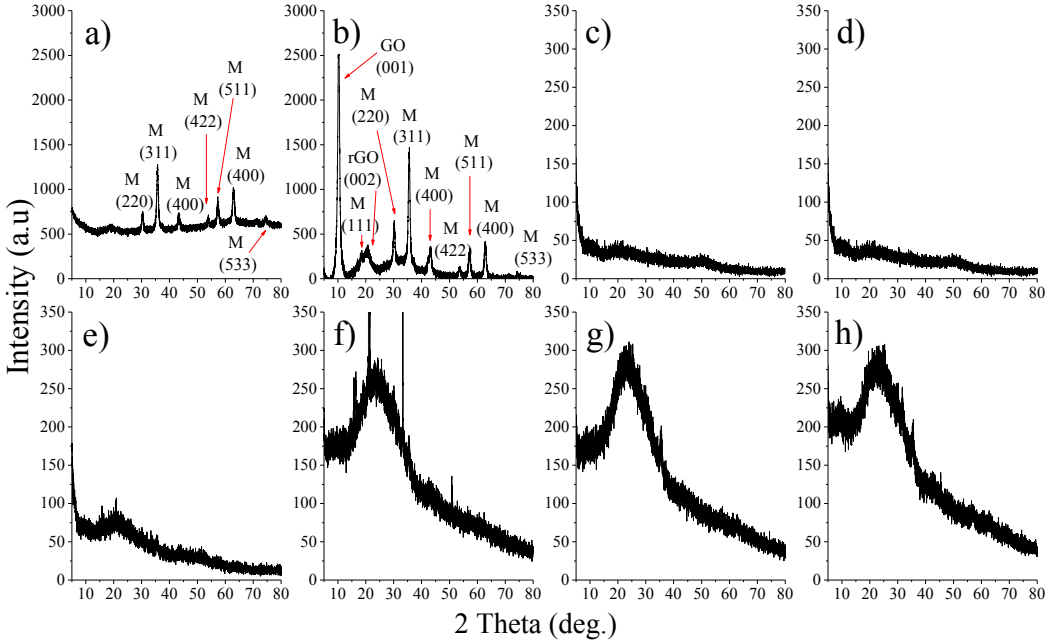

Figure 6. XRD patters of a) MNPs synthesized, b) rGO-MNPs synthesized, c) rGO-MNPs at 50 mg/L after hydrogenotrophic assay on day 10, d) rGO-MNPs at 50 mg/L after hydrogenotrophic assay on day 16, e) rGO-MNPs at 100 mg/L after hydrogenotrophic assay on day 10, f) rGO-MNPs at 100 mg/L after hydrogenotrophic assay on day 16, g) rGO-MNPs at 200 mg/L after hydrogenotrophic assay on day 10 and h) rGO-MNPs at 200 mg/L after hydrogenotrophic assay on day 16.

No extraneous peaks were observed, demonstrating that the prepared MNPs were Fe_3O_4 of high purity. These characteristic peaks were also observed in the synthesized rGO-MNPs (Figure 6b). As can be observed after biological treatment, XRD pattern became amorphous and lost its crystallinity, as observed in Figures 6 c-h. Furthermore, the signal of magnetite disappeared during the biological treatment, which could be attributed to the lower concentration of magnetite present in the nanocomposite and the fact that microorganisms may be using it. Casals et al. (2014) also presented XRD patterns of nanoparticles recovered after anaerobic digestion. They showed that XRD peaks progressively became smaller and broader, indicating the decrease in both size and number of nanoparticles. Results of XRD

and Raman in this study present main differences in the signal of graphene, since the concentration of magnetite is too low; thus, it can be stated that graphene lost its crystallinity during the biological process, becoming amorphous.

Figure S2 shows the collated FTIR spectra of the composite rGO-MNPs, before and after the biological biogas upgrading process, at days 10 and 16, for the three tested concentrations. The peak at 618 cm^{-1} corresponds to deformation vibrations of C-C-HO of aromatic aldehydes. In the zoom of Figure S2, the peak marked at 580 cm^{-1} is attributed to typical Fe-O stretching vibration of Fe_3O_4 nanoparticles, although this signal was only clearly observed in the recovered rGO-MNPS at 100 mg/L, at day 10. Comparing the synthesized composite before and after the biological treatment, it can be observed that the following peaks did not present a difference: at 1040 cm^{-1}, assigned to C-OH stretching vibrations of COOH groups (carboxylic acids) at 1218 cm^{-1}, ascribed to C-O stretching vibrations of the phenolic and carboxylic groups from the reduced GO sheets and the peak at 1400 cm^{-1} (C-HO). The signal at 1540 cm^{-1} corresponds to the asymmetric stretching of carboxyl groups, COO- that appeared more marked after the material was exposed to the microorganisms. The observation of this signal further indicated that carboxyl groups of GO sheets were deprotonated as previously reported (Lin et al., 2017; Nethravathi et al., 2009; Titelman et al., 2005). Such observation points toward rGO-MNPs were oxidized after the biological treatment, a result that agrees with the lower ESC at day 10 and at the end of the experiment.

4. Conclusions

Magnetite (MNPs) and reduced graphene oxide (rGO) at the three concentrations tested did not boost the CH_4 production in the hydrogenotrophic test. The synergistic combination of the reduced graphene oxide material decorated with magnetite (rGO-MNPs) boosted the CH_4 production by 47%, 28% and 33% relative to the control without nanomaterial for 50, 100 and 200 mg/L, respectively. The improving in CH_4 enrichment was linked to the sorption capacity of the nanomaterials, to the ESC provided from the addition of conductive materials like rGO-MNPs into the process, to the release of Fe^{2+} in the media which permitted to adsorb more H_2 and at the

same time served as a dietary supply to stimulate microbial activity.

Significant structural changes occurred in the rGO-MNP composite after hydrogenotrophic tests. Raman spectra and XRD patterns of the recovered rGO-MNPs suggested a loss of crystallinity, and FTIR and Raman indicated that the material was oxidized during biological treatment.

5. Supplementary data

Figure S1. SEM micrograph presents a homogeneous distribution of MNPs over the surface of rGO in the rGO-MNPs composite.

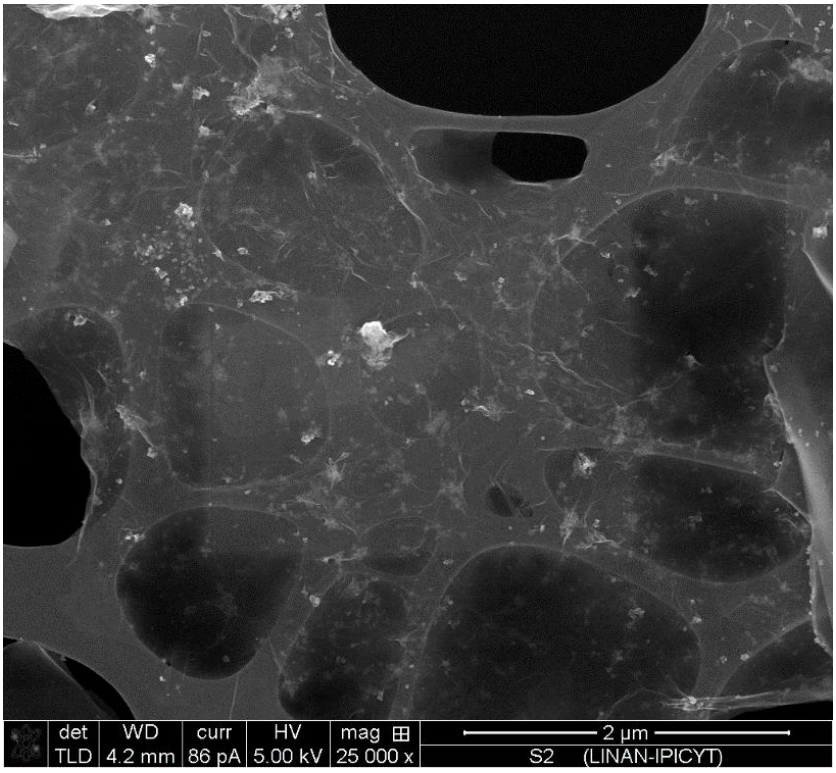

Figure S2. Sorption assay of H_2 in mineral medium with NPs at concentration of 25, 50, 100 and 200 mg/L.

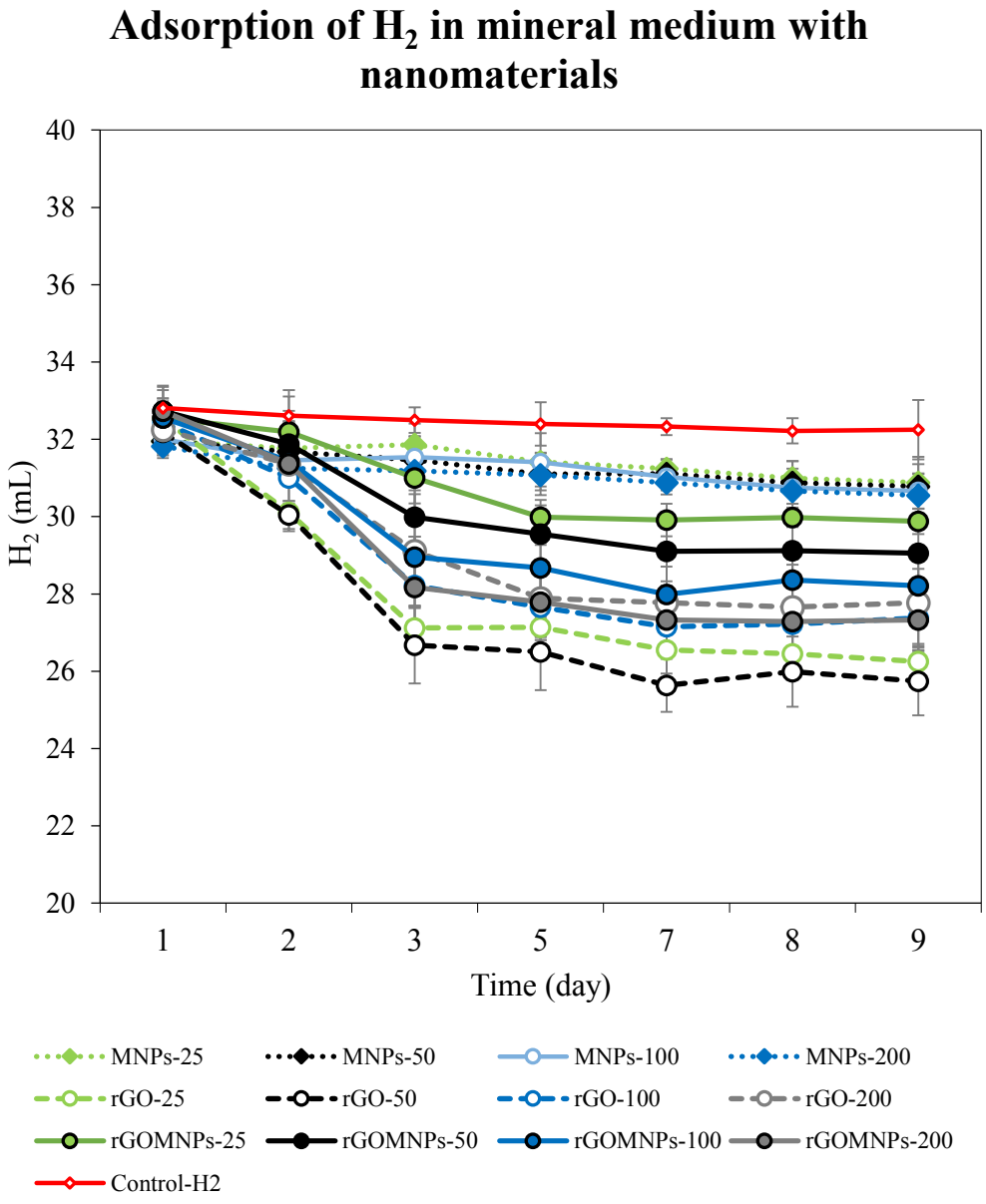

Figure S3. FTIR spectra of the composite rGO-MNPs, before and after the biological biogas upgrading process, at days 10 and 16, at the three tested concentrations.

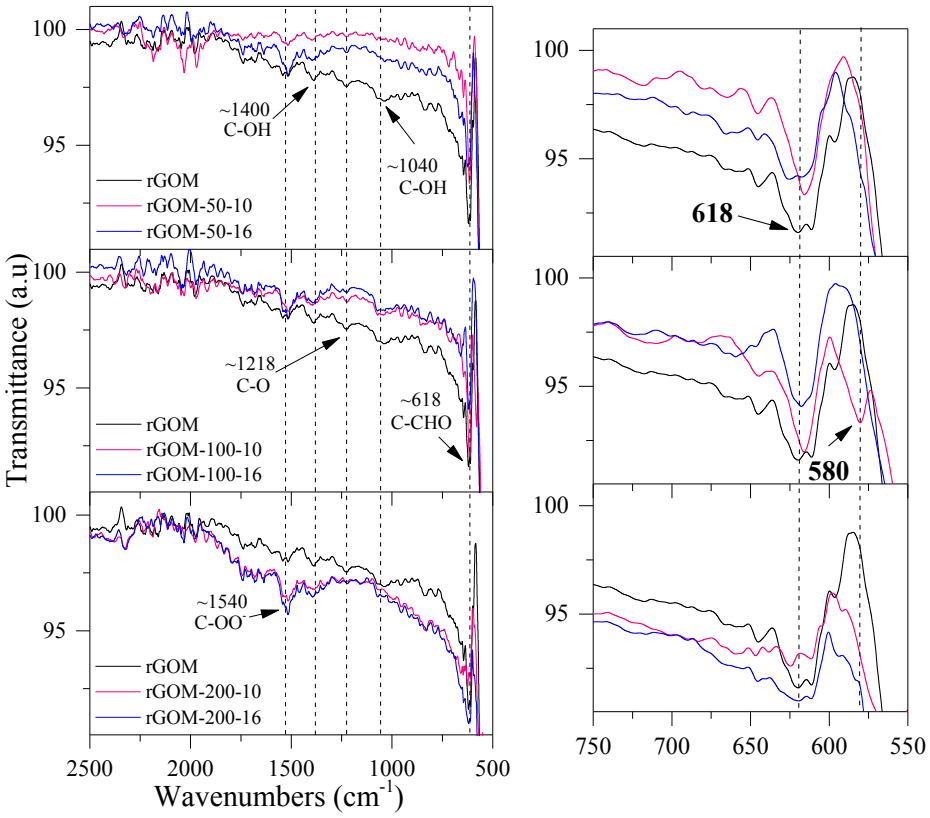

Table S1. Nanoadditives in anaerobic digestion processes.

Material	System & conditions	Comments	Concentration and size	Reference
Ag^0 Cu^0 Fe^0	T: 30±2°C COD: 1 g COD L^{-1} Substrate: Sodium acetate pH: 7.2	Cu^0 completely inhibited methanogenesis. Fe^0 decreased 85% methanogenic activity and decreased 91% hydrogenotrophic methanogenesis. Ag^0 did not show a significant effect.	1500 mg/L	(Gonzalez-Estrella et al., 2013)
Fe^0	T: 37°C COD: 1000 COD/L Substrate: Glucose pH: Was not kept	30 nM increased 10% CH_4 production. 1 and 10 nM decreased 20% and 70% biogas production	1, 10, 30 nM	(Yang et al., 2013)
Au Ag	T: 37 and 55°C Substrate: Cellulose 1 g pH: 8	No significant difference was shown	Au: 100 mg/L Ag: 170 mg/L 20, 30 nm	(García et al., 2012)

Graphene	T: 35°C Analyzed every 2 d Substrate: Ethanol 2.5 mL pH: 7.5	CH_4 was enhanced 25% and increased the ethanol production rate 20%. Microbial structures of electro-active bacteria and archaea were revealed	1 g/L	(Lin et al., 2017)
GO	T: 37°C pH: Was not keep	CH_4 was reduced: [5mg/L]:13.1%; [50 mg/L]:10.6%; [100 mg/L]:2.7%; [500 mg/L]:17.1%.	5 mg/L 50 mg/L 100 mg/L 500 mg/L 500 nm- 5µm. Thickness of 0.8-1.2 nm	(Zhang et al., 2017)

Table S2. Alkalinity and pH (averages with standard deviation) of the supernatant of the hydrogenotrophic tests provided with nanoparticles.

Structure	**MNPs**	**MNPs**	**MNPs**	**rGO**	**rGO**	**rGO**	**rGO-MNPs**	**rGO-MNPs**	**rGO-MNPs**
Concentration (mg/L)	50	100	200	50	100	200	50	100	200
Alkalinity $CaCO_3$ (mg/L)	1368.7 ±26.4	1273.2 ±94.3	1322.9 ±90.7	1395.7 ±61.3	1400± 88.5	1391.6 ±64.3	1416.7 ±75.6	1422.9 ±74.2	1387.5 ±138.8
pH	8.28 ±0.14	7.99 ±0.09	8.12 ±0.10	8.17 ±0.05	8.13 ±0.12	8.15 ±0.10	8.23 ±0.09	8.14 ±0.07	8.14 ±0.08

References

Abdelsalam, E., Samer, M., Attia, Y.A., Abdel-Hadi, M.A., Hassan, H.E., Badr, Y., 2017. Influence of zero valent iron nanoparticles and magnetic iron oxide nanoparticles on biogas and methane production from anaerobic digestion of manure. Energy 120, 842–853. https://doi.org/https://doi.org/10.1016/j.energy.2016.11.137

Acuña, M.E., Pérez, F., Auria, R., Revah, S., 1999. Microbiological and kinetic aspects of a biofilter for the removal of toluene from waste gases. Biotechnol. Bioeng. 63, 175–184. https://doi.org/10.1002/(SICS)1097-0290(19990420)63:2

Ahmed, F., Rodrigues, D.F., 2013. Investigation of acute effects of graphene oxide

on wastewater microbial community: a case study. J. Hazard. Mater. 256–257, 33–39. https://doi.org/10.1016/j.jhazmat.2013.03.064

Ambuchi, J.J., Zhang, Z., Feng, Y., 2016. Biogas Enhancement Using Iron Oxide Nanoparticles and Multi-Wall Carbon Nanotubes. Int. J. Chem. Mol. Nucl. Mater. Metall. Eng. 10, 1305–1311.

APHA, 1998. Standar methods for the examination of water of wastewater, in: Americam Public Health Association. Washington, DC, p. 578.

Bai, Y., Subdiaga, E., Haderlein, S.B., Knicker, H., Kappler, A., 2020. High-pH and anoxic conditions during soil organic matter extraction increases its electron-exchange capacity and ability to stimulate microbial Fe(III) reduction by electron shuttling. Biogeosciences 17, 683–698. https://doi.org/10.5194/bg-17-683-2020

Bassani, I., Kougias, P.G., Treu, L., Angelidaki, I., 2015. Biogas upgrading via hydrogenotrophic methanogenesis in two-stage continuous stirred tank reactors at mesophilic and thermophilic conditions. Am. Chem. Soc. 49, 1285–12593. https://doi.org/10.1021/acs.est.5b03451

Bensmann, A., Hanke-Rauschenbach, R., Heyer, R., Kohrs, F., Benndorf, D., Reichl, U., Sundmacher, K., 2014. Biological methanation of hydrogen within biogas plants: a model-based feasibility study. Appl. Energy 134, 413–425. https://doi.org/10.1016/j.apenergy.2014.08.047

Campesi, R., Cuevas, F., Gadiou, R., Leroy, E., Hirscher, M., Vix-Guterl, C., Latroche, M., 2008. Hydrogen storage properties of Pd nanoparticle/carbon template composites. Carbon N. Y. 46, 206–214. https://doi.org/https://doi.org/10.1016/j.carbon.2007.11.006

Casals, E., Barrena, R., García, A., González, E., Delgado, L., Busquets-Fité, M., Font, X., Arbiol, J., Glatzel, P., Kvashnina, K., Sánchez, A., Puntes, V., 2014. Programmed iron oxide nanoparticles disintegration in anaerobic digesters boosts biogas production. Small 10, 2801–2808. https://doi.org/10.1002/smll.201303703

Chandra, V., Park, J., Chun, Y., Lee, J.W., Hwang, I., Kim, K.S., 2010. Water-dispersible magnetite-reduced graphene oxide composites for arsenic

removal. ACS Nano 4, 3979–3986. https://doi.org/10.1021/nn1008897

Chen, S., Rotaru, A.E., Liu, F., Philips, J., Woodard, T.L., Nevin, K.P., Lovley, D.R., 2014a. Carbon cloth stimulates direct interspecies electron transfer in syntrophic co-cultures. Bioresour. Technol. 173, 82–86. https://doi.org/10.1016/j.biortech.2014.09.009

Chen, S., Rotaru, A.E., Shrestha, P.M., Malvankar, N.S., Liu, F., Fan, W., Nevin, K.P., Lovley, D.R., 2014b. Promoting interspecies electron transfer with biochar. Sci. Rep. 4. https://doi.org/10.1038/srep05019

Chouhan, R.S., Pandey, A., Qureshi, A., Ozguz, V., Niazi, J.H., 2016a. Nanomaterial resistant microorganism mediated reduction of graphene oxide. Colloids Surfaces B Biointerfaces 146, 39–46. https://doi.org/10.1016/j.colsurfb.2016.05.053

Chouhan, R.S., Qureshi, A., Yagci, B., Gülgün, M.A., Ozguz, V., Niazi, J.H., 2016b. Biotransformation of multi-walled carbon nanotubes mediated by nanomaterial resistant soil bacteria. Chem. Eng. J. 298, 1–9. https://doi.org/10.1016/j.cej.2016.04.019

Dong, D., Aleta, P., Zhao, X., Kyung, O., Kim, S., Woo, J., 2019. Effects of nanoscale zero valent iron (nZVI) concentration on the biochemical conversion of gaseous carbon dioxide (CO2) into methane (CH4). Bioresour. Technol. 275, 314–320. https://doi.org/10.1016/j.biortech.2018.12.075

Dubé, C.-D., Guiot, S.R., 2015. Direct Interspecies Electron Transfer in Anaerobic Digestion: A Review, in: Guebitz, G.M., Bauer, A., Bochmann, G., Gronauer, A., Weiss, S. (Eds.), Biogas Science and Technology. Springer International Publishing, Cham, pp. 101–115. https://doi.org/10.1007/978-3-319-21993-6_4

Esfandiar, A., Akhavan, O., Irajizad, A., 2011. Melatonin as a powerful bio-antioxidant for reduction of graphene oxide. J. Mater. Chem. 21, 10907. https://doi.org/10.1039/c1jm10151j

Ferre-Vilaplana, A., 2008. Storage of hydrogen adsorbed on alkali metal doped single-layer all-carbon materials. J. Phys. Chem. C 112, 3998–4004. https://doi.org/10.1021/jp0768874

Ganzoury, M.A., Allam, N.K., 2015. Impact of nanotechnology on biogas

production: a mini-review. Renew. Sustain. Energy Rev. 50, 1392–1404. https://doi.org/10.1016/j.rser.2015.05.073

García, A., Delgado, L., Torà, J.A., Casals, E., González, E., Puntes, V., Font, X., Carrera, J., Sánchez, A., 2012. Effect of cerium dioxide, titanium dioxide, silver, and gold nanoparticles on the activity of microbial communities intended in wastewater treatment. J. Hazard. Mater. 199–200, 64–72. https://doi.org/10.1016/j.jhazmat.2011.10.057

Gonzalez-Estrella, J., Sierra-Alvarez, R., Field, J.A., 2013. Toxicity assessment of inorganic nanoparticles to acetoclastic and hydrogenotrophic methanogenic activity in anaerobic granular sludge. J. Hazard. Mater. 260, 278–285. https://doi.org/10.1016/j.jhazmat.2013.05.029

He, H., Gao, C., 2010. Supraparamagnetic, Conductive, and Processable Multifunctional Graphene Nanosheets Coated with High-Density Fe3O4 Nanoparticles. ACS Appl. Mater. Interfaces 2, 3201–3210. https://doi.org/10.1021/am100673g

Hou, C., Zhang, Q., Zhu, M., Li, Y., Wang, H., 2011. One-step synthesis of magnetically-functionalized reduced graphite sheets and their use in hydrogels. Carbon N. Y. 49, 47–53. https://doi.org/10.1016/j.carbon.2010.08.040

Hwang, S.-W., Rather, S., Naik, M., Soo, C.S., Nahm, K.-S., 2009. Hydrogen uptake of multiwalled carbon nanotubes decorated with Pt–Pd alloy using thermal vapour deposition method. J. Alloys Compd. 480, L20–L24. https://doi.org/https://doi.org/10.1016/j.jallcom.2009.01.136

Jönsson, O., Polman, E., Jensen, J.., Eklund, R., Schyl, H., Ivanrsson, S., 2003. Sustainable gas enters the European gas distribution system. Danish gas Technol. Cent.

Kappler, A., Wuestner, M.L., Ruecker, A., Harter, J., Halama, M., Behrens, S., 2014. Biochar as an Electron Shuttle between Bacteria and Fe(III) Minerals. Environ. Sci. Technol. Lett. 1, 339–344. https://doi.org/10.1021/ez5002209

Kato, S., Hashimoto, K., Watanabe, K., 2012. Methanogenesis facilitated by electric syntrophy via (semi)conductive iron-oxide minerals. Environ. Microbiol.

14, 1646–1654. https://doi.org/10.1111/j.1462-2920.2011.02611.x

Kim, H.-S., Lee, H., Han, K.-S., Kim, J.-H., Song, M.-S., Park, M.-S., Lee, J.-Y., Kang, J.-K., 2005. Hydrogen storage in Ni nanoparticle-dispersed multiwalled carbon nanotubes. J. Phys. Chem. B 109, 8983–8986. https://doi.org/10.1021/jp044727b

Krishna, R., Dias, C., Ventura, J., Titus, E., 2016. Green and facile decoration of Fe3O4 nanoparticles on reduced graphene oxide. Mater. Today Proc. 3, 2807–2813. https://doi.org/10.1016/j.matpr.2016.06.030

Kudin, K.N., Ozbas, B., Schniepp, H.C., Prud'Homme, R.K., Aksay, I.A., Car, R., 2008. Raman spectra of graphite oxide and functionalized graphene sheets. Nano Lett. 8, 36–41. https://doi.org/10.1021/nl071822y

Lee, H., Ihm, J., Cohen, M.L., Louie, S.G., 2010. Calcium-decorated graphene-based nanostructures for hydrogen storage. Nano Lett. 10, 793–798. https://doi.org/10.1021/nl902822s

Li, H., Chang, J., Liu, P., Fu, L., Ding, D., Lu, Y., 2015. Direct interspecies electron transfer accelerates syntrophic oxidation of butyrate in paddy soil enrichments. Environ. Microbiol. 17, 1533–1547. https://doi.org/10.1111/1462-2920.12576

Lin, R., Cheng, J., Zhang, J., Zhou, J., Cen, K., Murphy, J.D., 2017. Boosting biomethane yield and production rate with graphene: the potential of direct interspecies electron transfer in anaerobic digestion. Bioresour. Technol. 239, 345–352. https://doi.org/10.1016/j.biortech.2017.05.017

Liu, F., Rotaru, A.E., Shrestha, P.M., Malvankar, N.S., Nevin, K.P., Lovley, D.R., 2015. Magnetite compensates for the lack of a pilin-associated c-type cytochrome in extracellular electron exchange. Environ. Microbiol. 17, 648–655. https://doi.org/10.1111/1462-2920.12485

Liu, F., Rotaru, A.E., Shrestha, P.M., Malvankar, N.S., Nevin, K.P., Lovley, D.R., 2012. Promoting direct interspecies electron transfer with activated carbon. Energy Environ. Sci. 5, 8982–8989. https://doi.org/10.1039/c2ee22459c

Liu, J., Tang, J., Gooding, J.J., 2012. Strategies for chemical modification of graphene and applications of chemically modified graphene. J. Mater. Chem. 22, 12435–12452. https://doi.org/10.1039/c2jm31218b

Liu, S., Zeng, T.H., Hofmann, M., Burcombe, E., Wei, J., Jiang, R., Kong, J., Chen, Y., 2011. Antibacterial activity of graphite, graphite oxide, graphene oxide, and reduced graphene oxide: membrane and oxidative stress. ACS Nano 5, 6971–6980. https://doi.org/10.1021/nn202451x

Lo, H.M., Chiu, H.Y., Lo, S.W., Lo, F.C., 2012. Effects of micro-nano and non micro-nano MSWI ashes addition on MSW anaerobic digestion. Bioresour. Technol. 114, 90–94. https://doi.org/10.1016/j.biortech.2012.03.002

Lovley, D.R., 2017. Syntrophy Goes Electric: Direct Interspecies Electron Transfer. Annu. Rev. Microbiol. 71, 643–664. https://doi.org/10.1146/annurev-micro-030117-020420

Lovley, D.R., Coates, J.D., Blunt-Harris, E.L., Phillips, E.J.P., Woodward, J.C., 1996. Humic substances as electron acceptors for microbial respiration. Lett. Nat. 445–446.

Luna-delRisco, M., Orupõld, K., Dubourguier, H.C., 2011. Particle-size effect of CuO and ZnO on biogas and methane production during anaerobic digestion. J. Hazard. Mater. 189, 603–608. https://doi.org/10.1016/j.jhazmat.2011.02.085

Luo, G., Angelidaki, I., 2012. Integrated biogas upgrading and hydrogen utilization in an anaerobic reactor containing enriched hydrogenotrophic methanogenic culture. Biotechnol. Bioeng. 109, 2729–2736. https://doi.org/10.1002/bit.24557

Madigan, M., Martinko, J.., Stahl, D., Clark, D.P., 2012. Brock biology of microorganisms, 13th ed.

McAllister, M.J., Li, J.L., Adamson, D.H., Schniepp, H.C., Abdala, A.A., Liu, J., Herrera-Alonso, M., Milius, D.L., Car, R., Prud'homme, R.K., Aksay, I.A., 2007. Single sheet functionalized graphene by oxidation and thermal expansion of graphite. Chem. Mater. 19, 4396–4404. https://doi.org/10.1021/cm0630800

Nethravathi, C., Nisha, T., Ravishankar, N., Shivakumara, C., Rajamathi, M., 2009. Graphene–nanocrystalline metal sulphide composites produced by a one-pot reaction starting from graphite oxide. Carbon N. Y. 47, 2054–2059. https://doi.org/https://doi.org/10.1016/j.carbon.2009.03.055

Niemann, M.U., Srinivasan, S.S., Phani, A.R., Kumar, A., Goswami, D.Y., Stefanakos, E.K., 2008. Nanomaterials for hydrogen storage applications: a

review. J. Nanomater. 2008. https://doi.org/10.1155/2008/950967

Patel, V.B., Patel, A.R., Patel, M.C., Madamwar, D.B., 1993. Effect of metals on anaerobic digestion of water hyacinth-cattle dung. Appl. Biochem. Biotechnol. 43, 45–50. https://doi.org/10.1007/BF02916429

Peigney, A., Laurent, C., Flahaut, E., Bacsa, R.R., Rousset, A., 2001. Specific surface area of carbon nanotubes and bundles of carbon nanotubes. Carbon N. Y. 39, 507–514. https://doi.org/https://doi.org/10.1016/S0008-6223(00)00155-X

Ram, M.S., Singh, L., Suryanarayana, M.V.S., Alam, S.I., 1999. Effect of iron, nickel and cobalt on bacterial activity and dynamics during anaerobic oxidation of organic matter. Water, Air Soil Pollut. 305–312.

Reyhani, A., Mortazavi, S.Z., Mirershadi, S., Moshfegh, A.Z., Parvin, P., Golikand, A.N., 2011. Hydrogen storage in decorated multiwalled carbon nanotubes by Ca, Co, Fe, Ni, and Pd nanoparticles under ambient conditions. J. Phys. Chem. C 115, 6994–7001. https://doi.org/10.1021/jp108797p

Reyhani, A., Mortazavi, S.Z., Moshfegh, A.Z., Golikand, A.N., Amiri, M., 2009. Enhanced electrochemical hydrogen storage by catalytic Fe-doped multi-walled carbon nanotubes synthesized by thermal chemical vapor deposition. J. Power Sources 188, 404–410. https://doi.org/https://doi.org/10.1016/j.jpowsour.2008.11.131

Roden, E.E., Kappler, A., Bauer, I., Jiang, J., Paul, A., Stoesser, R., Konishi, H., Xu, H., 2010. Extracellular electron transfer through microbial reduction of solid-phase humic substances. Nat. Geosci. 3, 417–421. https://doi.org/10.1038/ngeo870

Ryckebosch, E., Drouillon, M., Vervaeren, H., 2011. Techniques for transformation of biogas to biomethane. Biomass and Bioenergy 35, 1633–1645. https://doi.org/10.1016/j.biombioe.2011.02.033

Sherif, S.A., Barbir, F., Veziroglu, T.N., 2005. Wind energy and the hydrogen economy-review of the technology. Sol. Energy 78, 647–660. https://doi.org/10.1016/j.solener.2005.01.002

Simon, K., Rittmann, M.., 2015. A critical assessment of microbiological biogas to

biomethane upgrading systems, in: Biogas Science and Technology. pp. 117–135.

Siriwongrungson, V., Zeng, R.J., Angelidaki, I., 2007. Homoacetogenesis as the alternative pathway for H2 sink during thermophilic anaerobic degradation of butyrate under suppressed methanogenesis. Water Res. 41, 4204–4210. https://doi.org/10.1016/j.watres.2007.05.037

Soni, M., Kumar, P., Pandey, J., Sharma, S.K., Soni, A., 2018. Scalable and site specific functionalization of reduced graphene oxide for circuit elements and flexible electronics. Carbon N. Y. 128, 172–178. https://doi.org/https://doi.org/10.1016/j.carbon.2017.11.087

Srinivas, G., Zhu, Y., Piner, R., Skipper, N., Ellerby, M., Ruoff, R., 2010. Synthesis of graphene-like nanosheets and their hydrogen adsorption capacity. Carbon N. Y. 48, 630–635. https://doi.org/10.1016/j.carbon.2009.10.003

Stookey, L.L., 1970. Ferrozoine-a new spectrophotometric reagent for iron. Anal. Chem. 42, 779–781.

Su, L., Shi, X., Guo, G., Zhao, A., Zhao, Y., 2013. Stabilization of sewage sludge in the presence of nanoscale zero-valent iron (nZVI): Abatement of odor and improvement of biogas production. J. Mater. Cycles Waste Manag. 15, 461–468. https://doi.org/10.1007/s10163-013-0150-9

Sundman, A., Vitzthum, A.L., Adaktylos-Surber, K., Figueroa, A.I., van der Laan, G., Daus, B., Kappler, A., Byrne, J.M., 2020. Effect of Fe-metabolizing bacteria and humic substances on magnetite nanoparticle reactivity towards arsenic and chromium. J. Hazard. Mater. 384, 121450. https://doi.org/10.1016/j.jhazmat.2019.121450

Thanh, P.M., Ketheesan, B., Yan, Z., Stuckey, D., 2016. Trace metal speciation and bioavailability in anaerobic digestion: A review. Biotechnol. Adv. 34, 122–136. https://doi.org/10.1016/j.biotechadv.2015.12.006

Thanikaivelan, P., Narayanan, N.T., Pradhan, B.K., Ajayan, P.M., 2012. Collagen based magnetic nanocomposites for oil removal applications. Sci. Rep. 2, 230.

Titelman, G.I., Gelman, V., Bron, S., Khalfin, R.L., Cohen, Y., Bianco-Peled, H., 2005. Characteristics and microstructure of aqueous colloidal dispersions of

graphite oxide. Carbon N. Y. 43, 641–649. https://doi.org/10.1016/j.carbon.2004.10.035

Valenzuela, Edgardo, I., Davo-Prieto, A., López-Lozano, Nguyen, E., Hernández-Eligio, A., Vega-Alvarado, L., Júarez, K., García-González, A.S., López, Mercedes, G., Cervantes, Francisco, J., 2017. Anaerobic methane oxidation driven by microbial reduction of natural organic matter in tropical wetland. Appl. Environ. Microbiol. 83, e00645-17. https://doi.org/10.1128/AEM.00645-17

Wang, L., Lee, K., Sun, Y.Y., Lucking, M., Chen, Z., Zhao, J.J., Zhang, S.B., 2009. Graphene oxide as an ideal substrate for hydrogen storage. ACS Nano 3, 2995–3000. https://doi.org/10.1021/nn900667s

Wei, Y., Yin, G., Ma, C., Huang, Z., Chen, X., Liao, X., Yao, Y., Yin, H., 2013. Synthesis and cellular compatibility of biomineralized Fe3O4 nanoparticles in tumor cells targeting peptides. Colloids Surfaces B Biointerfaces 107, 180–188. https://doi.org/https://doi.org/10.1016/j.colsurfb.2013.01.058

Yang, L., Ge, X., Wan, C., Yu, F., Li, Y., 2014. Progress and perspectives in converting biogas to transportation fuels. Renew. Sustain. Energy Rev. 40, 1133–1152. https://doi.org/10.1016/j.rser.2014.08.008

Yang, Y., Guo, J., Hu, Z., 2013. Impact of nano zero valent iron (NZVI) on methanogenic activity and population dynamics in anaerobic digestion. Water Res. 47, 6790–6800. https://doi.org/10.1016/j.watres.2013.09.012

Zacharia, R., Kim, K.Y., Fazle Kibria, A.K.M., Nahm, K.S., 2005. Enhancement of hydrogen storage capacity of carbon nanotubes via spill-over from vanadium and palladium nanoparticles. Chem. Phys. Lett. 412, 369–375. https://doi.org/https://doi.org/10.1016/j.cplett.2005.07.020

Zaidi, A.A., RuiZhe, F., Shi, Y., Khan, S.Z., Mushtaq, K., 2018. Nanoparticles augmentation on biogas yield from microalgal biomass anaerobic digestion. Int. J. Hydrogen Energy 43, 14202–14213. https://doi.org/https://doi.org/10.1016/j.ijhydene.2018.05.132

Zhang, J., Wang, Z., Wang, Y., Zhong, H., Sui, Q., 2017. Effects of graphene oxide on the performance, microbial community dynamics and antibiotic resistance

genes reduction during anaerobic digestion of swine manure. Bioresour. Technol. 245, 850–859.
https://doi.org/dx.doi.org/10.1016/j.biortech.2017.08.217

Chapter III: Nanostructured complex of reduced graphene oxide adorned with magnetite as an adsorbent for inhibitor compounds in wood hydrolysates

Itzel Covarrubias-García, Carlos S. Osorio-González, Antonio Avalos Ramírez, José Luis Rodríguez-López, Satinder Kaur Brar, Sonia Arriaga. Nanostructured complex of reduced graphene oxide adorned with magnetite as an adsorbent for inhibitor compounds in wood hydrolysates. *Microporous and Mesoporous Materials*, Volume 310, 2021, 110592, ISSN 1387-1811.
https://doi.org/10.1016/j.micromeso.2020.110592.
https://www.sciencedirect.com/science/article/pii/S1387181120305928

Graphical Abstract

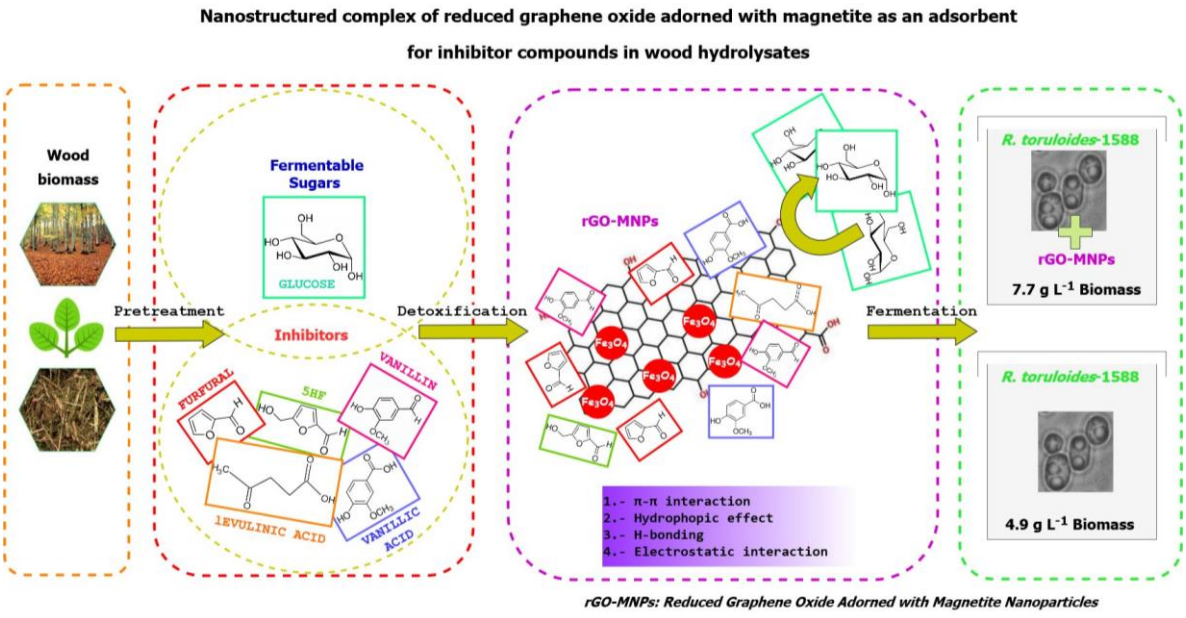

Abstract

Lignocellulosic biomass is an abundant and renewable feedstock for biofuels, biochemicals and biomaterials. To make this recalcitrant biomass more susceptible to hydrolysis and microbial conversion a pretreatment is required. Many pretreatments have resulted in high sugar yields; however, they can generate microbial inhibitory compounds in the fermentation step. Therefore, the detoxification of hydrolysates is necessary. This study shows that reduced graphene oxide adorned with magnetite nanoparticles (rGO-MNPs) can adsorb inhibitory

compounds such as furfural. Adsorption tests were performed in both aqueous solutions (furfural and furfural-glucose) and wood hydrolysate. rGO-MNPs (20 mg) removed 68% of furfural when it was alone, 49% of furfural when it was mixed with glucose and 20% of furfural in the wood hydrolysate. Among the adsorption of furfural in wood hydrolysate, rGO-MNPs adsorbed other lignin derivate compounds. Finally, no toxic effect of rGO-MNPs on *R. toruloides*-1588 was observed during the fermentation using detoxified wood hydrolysate.

Keywords: reduced graphene; magnetite; adsorption; furfural; wood hydrolysate

1. Introduction

Lignocellulosic biomass is one of the most abundant renewable resources available on the planet. It is mainly composed of cellulose, hemicellulose and lignin. Chemical, physicochemical or biological hydrolysis can be used to make cellulose and hemicellulose accessible for bioconversion. However, these processes can generate by-products other than sugars, such as furans, aliphatic acids, and phenolic compounds which can cause microbial inhibition (Palmqvist and Hahn-Hägerdal, 2000b). The amount of these inhibitors depends specifically on the kind of biomass and pretreatment conditions used. These compounds decrease the activity of several enzymes, break down the DNA and inhibit protein and RNA synthesis in microorganisms (Jung et al., 2014, 2013; Liu et al., 2004; Palmqvist and Hahn-Hägerdal, 2000a; Taherzadeh et al., 2000). Furfural is one important by-product presented at high concentration in wood hydrolysates, from 0.4 to 220 mg L^{-1}. It is mainly produced by hydrolysis and dehydration of xylan, from hemicellulose. Furfural can also affect the metabolism of yeasts, such as *Rhodosporidium sp* which grows slower and produces less lipids in the presence of furfural (Carlos S Osorio-González et al., 2019).

In order to decrease the amount of toxic compounds in wood hydrolysates, several detoxification methods have been studied such as overliming, ion exchange, membranes, enzymatic hydrolysis, microorganisms and adsorption using polymeric sorbents or activated carbon (Grzenia et al., 2010; Ludwig et al., 2013; Myoung et

al., 2010; K. Zhang et al., 2011). The main drawback of detoxification processes is the simultaneous removal of fermentable sugars resulting in a decrease of final products (Almeida et al., 2009; Deng and Aita, 2018; Li et al., 2013; Myoung et al., 2010). Activated carbon (AC) is the most common adsorbent used for detoxification. Either stand-alone or in combination with chemicals, such as alkali and ion exchange resins, the AC was found to be effective for removing furfural, 5-hydroxymethyl furfural, and phenolic compounds from several matrices such as softwood diluted in sulfuric acid, hemicellulosic hydrolysate of rice straw and hydrolysate from hardwood chips (Hodge et al., 2009; Mussatto and Roberto, 2001; Myoung et al., 2010). For instance, Myoung et al., (2010) developed a detoxification process for wood hydrolysate obtained from hardwood chips; they removed 96% of hydroxymethylfurfural, 93% of furfural, 42% of formic acid, 14% of acetic acid and 8.9% of sugar using a concentration of AC of 2.5 w/w%. However, the AC can retain up to 30% of fermentable sugars (Carvalho et al., 2006). Furthermore, the main inconvenience to use AC is its high price. The AC is commonly regenerated by thermal reactivation and 10% of AC granules are lost during each regenerating cycle (Ranjan et al., 2009). During the last decade, some studies have been performed to remove furfural from hydrolysates before their fermentation. Zhang et al., (2011) studied furfural adsorption with commercial and poly derived AC from water solution during bioethanol production; they explained that carbonyls and carboxyls groups of AC play a key role in the sorbent selectivity between furfural and sugar, being the poly derived AC with 1% oxygen more efficient. Moreover, furfural has been removed by adsorption from other matrices, for example Li et al. (2013) used bamboo charcoal for furfural removal from bio-oil; and surfactant nanoporous materials (Anbia and Mohammadi, 2009), chitosan-coated with magnetite particles (He et al., 2014) and zero valent iron nanoparticles (Fazlzadeh et al., 2018) from wastewater systems.

Graphene-based materials have been successfully applied to remove organic pollutants like dyes, polycyclic aromatic hydrocarbons and gasoline (Gupta et al., 2012; Xu et al., 2012). Different structures of graphene such as sponges, beads, fibres, membranes and crumpled nanosheets have been studied to remove a wide

range of organic substances from water and air (Yousefi et al., 2019). For instance, graphene aerogel has been used to separate oil and organic solvent from water (Ren et al., 2019). Likewise, it has been studied the reduction degree of graphene oxide for tuning the adsorption of phenolic compounds, finding that the adsorption capacities increase with the increment of the reduction degree (X. Wang et al., 2014a). The hydrophobic behavior of the reduced form of graphene oxide enhances the adsorption of hydrophobic molecules and has been utilized to fabricate super-hydrophobic and super-oleophilic materials (Kemp et al., 2013). However, this material has the characteristic of aggregate through via π-π stacking, which greatly hinders its application (J. Liu et al., 2012). In this sense, to solve the aggregation problem, stabilization and functionalization of reduced graphene *via* modification of the material are necessary. A potential and attractive alternative is the adorning of magnetite nanoparticles over the surface of reduced graphene oxide. This functionalization prevents the aggregation efficiently and disrupting the arrangement of their sheets (Yan et al., 2016). Moreover, magnetite nanoparticles present unique characteristics, including magnetic, electric, catalytic, cellular biocompatibility and low toxicity propertiess (He and Gao, 2010; Thanikaivelan et al., 2012; Wei et al., 2013), which seem appropriate for biological applications.

So far, no research has attempted to remove furfural or another type of microbial growth inhibitor from wood hydrolysate using reduced graphene oxide. This work aimed to remove furfural from wood hydrolysate using reduced graphene oxide adorned with magnetite nanoparticles (rGO-MNPs) as an adsorbent matrix. In order to determine the best detoxification conditions to less sugar removal, adsorption experiments using the nanocomposite were performed firstly in a furfural solution and secondly in a furfural-glucose solution, to finally validate the furfural adsorption under real conditions using a wood hydrolysate. Also, toxicity assays of the effect of rGO-MNPs were performed on *R. toruloides*-1588.

2. Experimental

2.1 Synthesis of rGO-MNPs

The nanocomposite was synthesized in three main steps: i) graphene oxide was prepared and reduced, ii) magnetite nanoparticles were formed, and iii) reduced graphene was adorned with magnetite nanoparticles. Graphene oxide was prepared with commercial microcrystal graphite powder (2-15 μm) according to modified Hummer's method (Covarrubias-García et al., 2020; Esfandiar et al., 2011). The reduction of graphene oxide, the formation of magnetite nanoparticles and the adorning of reduced graphene oxide with magnetite nanoparticles was carried out by the methodology previously reported by Covarrubias-García et al. (2020). In brief, ethylene glycol was used as a reducing agent of graphene oxide; this mixture was incubated at 110°C for 15 min; reduced graphene oxide was washed with Milli-Q water by centrifugation at 9000 *x g* by 15 minutes. The supernatant was discarded and reduced graphene oxide was dried at 60°C by 24 hours.

Magnetite nanoparticles were synthesized by co-precipitation using a solution of ferrous chloride ($FeCl_2$) and ferric chloride ($FeCl_3$) in a ratio 2:1 respectively. The solution was kept under a nitrogen atmosphere and vigorously stirred with a nitrogen flux at room temperature. Subsequently, 80 mL of 0.2 N sodium hydroxide solution was added drop-wise and precipitated nanoparticles were washed with Milli-Q water and separated with a magnet. The supernatant was discarded and nanoparticles were dried at 60°C for 18 hours.

The reduced graphene oxide was adorned with magnetite nanoparticles by dispersing them in Milli-Q water (1%w/v). Reduced graphene oxide solution was kept in a sonicator bath and the magnetite solution was added drop-wise. rGO-MNPs nanocomposite was recovered by centrifugation at 9000 *x g* by 15 min. Finally, the supernatant was discarded and precipitate was dried at 60°C by 18 hours.

2.2 Adsorption assays

The adsorption of furfural by rGO-MNPs was determined for the following cases: a) using 20 mg and 50 mg rGO-MNPs to analyze the effect of rGO-MNPs mass, with an initial furfural concentration of 1000 mg L^{-1} at 25°C; b) varying the initial

concentration of furfural (250, 300, 500 and 1000 mg L^{-1}), with 20 mg of rGO-MNPs at 25°C; c) varying the temperature (25°C and 50°C), with an initial furfural concentration of 500 mg L^{-1} and 20 mg of rGO-MNPs; and, d) using a mixture of glucose 10 g L^{-1} and furfural 300 mg L^{-1}, to verify if there is a competition for the adsorption sites of rGO-MNPs.

At the same time, an adsorption isotherm of single furfural and the detoxification of wood hydrolysates were performed. The sorption isotherm was conducted by varying the initial concentration of furfural (250 to 1000 mg L^{-1}) while the adsorbent mass in each sample was fixed at 20 mg. For the experiments in wood hydrolysate, a mass of adsorbent of 10, 20 and 50 mg rGO-MNPs at 25°C and the initial concentration of inhibitor present in the hydrolysates were used. All experiments were performed in conical flasks of 250 mL containing 25 mL of solution. Flasks were maintained in the dark, at pH 5 and 200 rpm. The adsorption kinetics was performed in a period from 0 to 120 min, considering time zero the moment of nanostructure addition.

To measure the residual furfural concentration, an aliquot was taken after a magnet was used to separate the nanocomposite from the flask bottom. This aliquot was centrifuged at 13148 *x g* for 2 min to ensure the complete separation of the nanocomposite. Residual furfural was measured by liquid chromatography as it is described below.

The sorption capacity (q) was calculated by **Equation 1**:

$$q = \frac{V*(C_0 - C_f)}{M} \quad (1)$$

Where q is the sorption capacity (mg g^{-1}), V is the volume of furfural solution (L), C_o and C_f are the initial and final furfural concentrations (mg L^{-1}) respectively and M is the adsorbent mass (g).

For furfural removal (FR) and glucose removal (GR), **Equation 2** was used:

$$FR\ or\ GR(\%) = \left(1 - \frac{C_f}{C_0}\right) x\ 100 \quad (2)$$

Where C_o and C_f are the initial and final furfural or glucose concentrations (mg L^{-1}).

The sorption isotherm was modeled by using Langmuir (**Equation 3**) and Freundlich (**Equation 4**) equations described below.

$$C_e/q_e = \left(1/q_m b\right) + \left(1/q_m\right)C_e \quad (3)$$

Where C_e is the equilibrium concentration (mg L^{-1}), q_e is the adsorption capacity in the equilibrium (mg g^{-1}), q_m is the maximum adsorption capacity to form a monolayer (mg g^{-1}) and b is a constant of adsorption energy (L mg^{-1}).

$$\mathrm{In}\, q_e = In\, K_f + \left(1/n\right) In\, C_e \quad (4)$$

Where q_e is the adsorption equilibrium concentration (mg g^{-1}), K_f is the Freundlich adsorption capacity parameter, 1/n is the adsorption intensity parameter and C_e is the equilibrium concentration (mg L^{-1}).

2.3 Wood hydrolysate

Wood hydrolysate obtained from poplar (Greenfield Global Inc., Canada) with six-carbon sugars (glucose mainly) was used to validate the furfural removal in a real fermentation feedstock.

2.4 Microorganism and inoculum

Oleaginous yeast *Rhodosporidium toruloides*-1588 (Agricultural Research Service (NRRL) Culture Collection (USA) was preserved in YM agar (yeast extract 3 g L^{-1}; malt extract 3 g L^{-1}; peptone 5 g L^{-1}; glucose 10 g L^{-1}; agar 15 g L^{-1}). The seed culture was prepared according to Osorio-Gonzalez *et al.* (2019).

2.5 Yeast growth in wood hydrolysate treated with rGO-MNPs as a substrate

To determine the rGO-MNPs nanocomposite effect on microbial growth and sugar consumption experiments in 125 mL conical flasks were performed. The flasks contained 25 mL of wood hydrolysate (10 g L^{-1} of glucose), 1 g L^{-1} of ammonium sulfate as nitrogen source and initial pH of 6. Flasks were inoculated with 0.1 OD 600nm. All flasks were incubated during 126 h at 25°C and 200 rpm.

2.6 Characterization of the synthesized materials

Graphene oxide, reduced graphene oxide, magnetite and rGO-MNPs were characterized by Fourier Transform Infrared Spectroscopy (FTIR) using a Cary 670 FTIR Spectrometer (Thermo Fisher). The spectra were obtained at a resolution of 4 cm^{-1}, in the range of 4000-400 cm^{-1}. Spectra was constructed with 16 replicates per sample.

Microstructural analysis of rGO-MNPs was carried out using Scanning Electron Microscopy (SEM, FIB Dual Beam Helios Nanolab 600) and Scanning Transmission Electron Microscopy (STEM, FEI Tecnai F30). Micrographic grids were prepared by placing a drop of diluted sample dispersed in ethanol onto a carbon-coated copper grid and dried at room temperature. Surface area and the pore size distributions were calculated by adsorption-desorption isotherms of nitrogen gas in a Micromeritics ASAP 2020 instrument at 77 K. The surface area was calculated using the Brunauer-Emmett-Teller (BET) equation and the pore size distribution was determined by using the density functional theory (DFT), protocol established in this equipment.

2.7 Cell growth, glucose content and inhibitors concentration

Cell growth was determined in terms of biomass density as a function of time. The biomass density (g L^{-1}) was determined by drying cells previously separated from samples of culture media. The concentration of glucose, residual furfural and other inhibitor compounds were determined by liquid chromatography (LC-MS, Liquid TSQ Quantum Access Mass Spectrometer, Thermo Scientific) using the methods reported by Osorio-Gonzalez et al. (2019a, and 2019b) (Carlos S. Osorio-González et al., 2019a, 2019b). For glucose, a 5 µm, 150mm ID, 4.6mm df column with acetonitrile: water (89:11 v/v) was used as a mobile phase. In the case of residual furfural and other inhibitory compounds, a BetaBasic-18 100mm x 2.1mm; 3µm column was used with water: methanol (80:20 v/v) as the mobile phase. All data presented are average values from duplicate samples.

3. Results and discussion

3.1 SEM and STEM micrographs of rGO-MNPs nanocomposite

The morphology and structure of rGO-MNPs are shown in **Figure 1**.

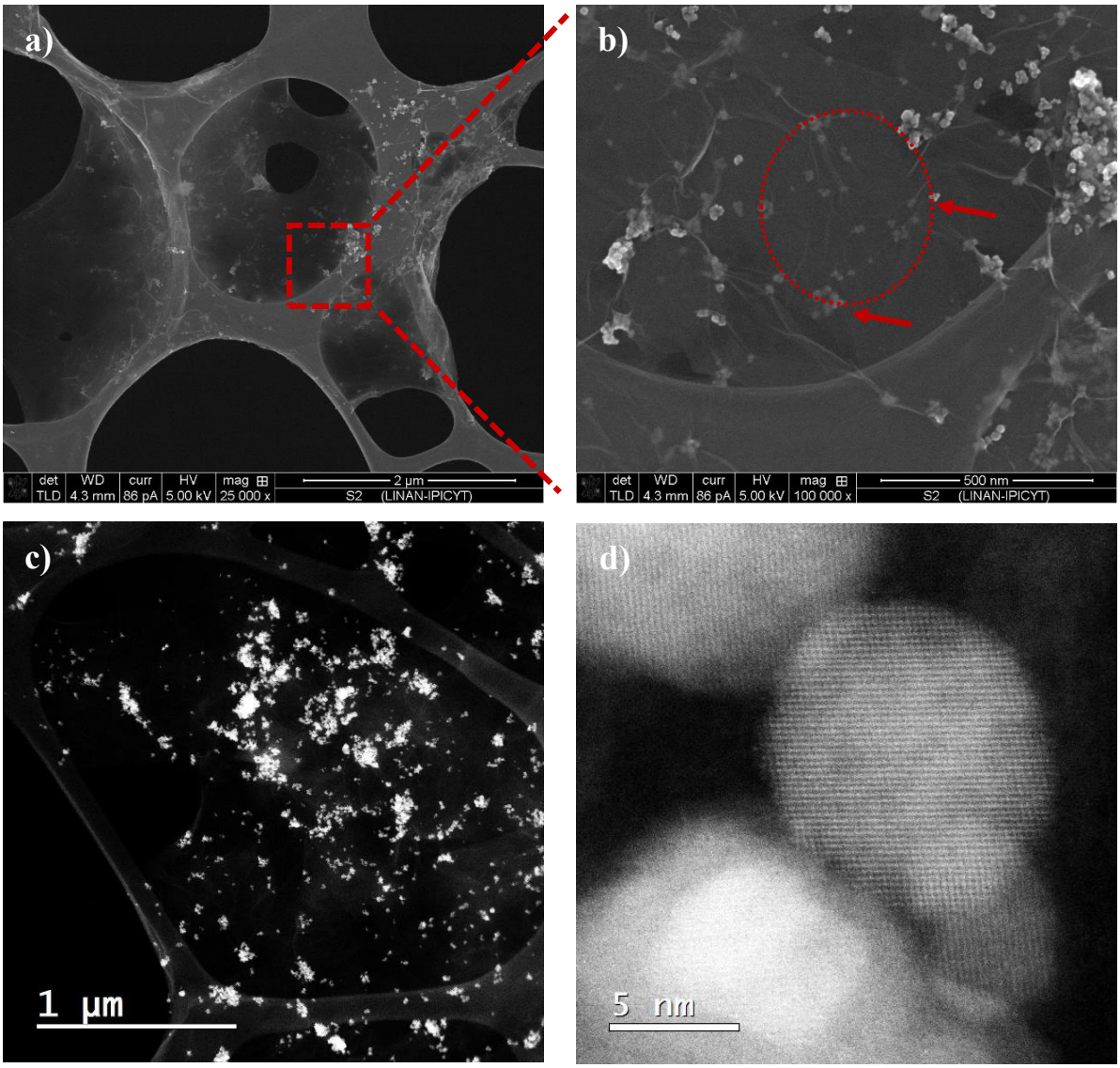

Figure 1. Scanning Electron Microscopy (SEM) and Scanning Transmission Electron Microscopy (STEM) analysis. a) and b) SEM micrographs of rGO-MNPs, c) STEM micrograph of rGO-MNPs and d) STEM micrograph of magnetite nanoparticles.

As can be seen in SEM micrographs, Figure 1a-b and in STEM micrograph, Figure 1c, magnetite nanoparticles are randomly distributed over the surface of graphene. The red circle and arrows at Figure 1c show that magnetite nanoparticles are internalized between the sheets of graphene. This morphology observed was similar

to other studies reported in literature (Chandra et al., 2010; Covarrubias-García et al., 2020; Hou et al., 2011). Figure 1d shows the magnification STEM image of magnetite nanoparticle and clearly shows its spherical form with an average size of 9.3±1.6 nm.

3.2 Adsorption of furfural on rGO-MNPs nanocomposite

Prior to the detoxification experiments in wood hydrolysate, the kinetics behavior of rGO-MNPs nanocomposite was analyzed with model molecules at different conditions. **Figure 2**a shows the mass effect of rGO-MNPs on furfural adsorption. The adsorption capacity of rGO-MNPs (q) was 312.9±11.2 and 404.8±14.0 mg g^{-1}, for 50 and 20 mg of adsorbent at 120 min, respectively. The higher adsorption capacity of furfural with a mass of 20 mg was probably due to electrostatic interactions among the particles, which let to expose more functional groups per unit area. In the case of 50 mg of rGO-MNPs the electrostatic interactions between the graphene particles should have been higher but agglomeration between small particles led to decrease the adsorption sites and the adsorbent surface area. In terms of furfural removal (FR), the highest FR was with 50 mg of adsorbent (62.7±2.6%) than with 20 mg (35.2±1.4%). The higher adsorbate removal with the increase of adsorbent can be explained by the greater exposed surface area and thus the more adsorption sites available. The FR can be used to estimate the final concentration after an adsorption process.

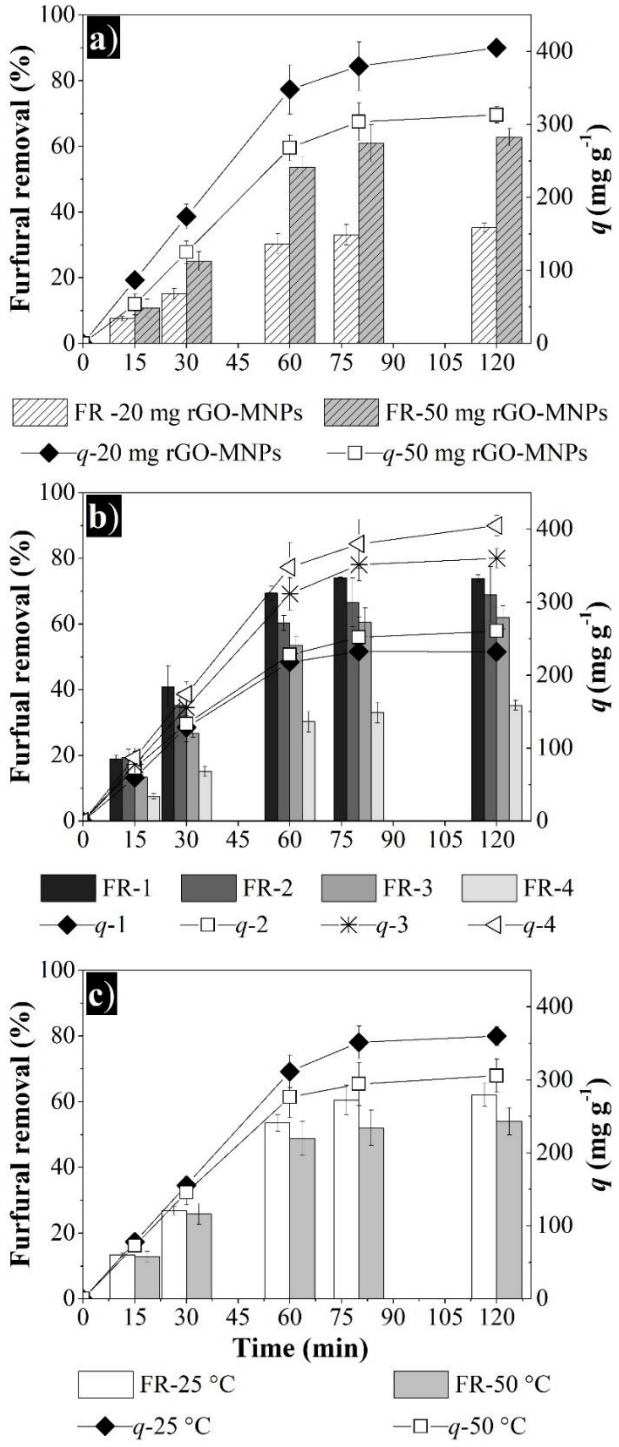

Figure 2. Effect of main parameters on furfural adsorption: a) Effect of rGO-MNPs mass, b) Effect of furfural initial concentration, 1=250, 2=300, 3=500 and 4=1000 mg L^{-1}, and c) Effect of temperature. FR=Furfural removal

The effect of adsorbent mass on furfural adsorption has been previously studied using bamboo charcoal with a mass from 0.2 to 20 g in 100 mL solution and initial furfural concentration of 10 g L^{-1}. The removal increased rapidly with the bamboo mass, until 7.5 g, then a slow adsorption was observed with the further increase of bamboo mass (Li et al., 2013). The *q* ranged from 57 to 98 mg g^{-1}, which is smaller than the *q* obtained with 20 and 50 mg of rGO-MNPs in the present study. The parameter that determines the highest adsorption capacity is commonly the specific surface area. In the present study, the nitrogen adsorption-desorption isotherm of the nanocomposite is shown in **Figure S1**. As can be seen at Figure S1 and according to the IUPAC (International Union of Pure and Applied Chemistry) classification, the nitrogen adsorption-desorption isotherm exhibited type IV curve and H3 hysteresis loop, indicating a mesoporous structure with a specific surface area of 19.0915 ± 0.0728 m^2 g^{-1} and a pore size of 0.02934 cm^3 g^{-1}. Similar BET specific surface areas of composites of reduced graphene oxide with magnetite nanoparticles have been reported with values of 14 and 26.76 m^2 g^{-1} (Khatamian et al., 2017; Yoon et al., 2017) and others with areas of 66.8 and 213 m^2 g^{-1} (Karimi-Maleh et al., 2020; Liu et al., 2020; Muthukannan et al., 2015; Shan et al., 2018). The difference in surface areas is mainly attributed to the synthesis method. Additionally, it has been reported that surface area measurement of graphene by nitrogen or dye adsorption is underrated, due to the overlap of the exfoliated sheets and due to agglomeration (McAllister et al., 2007). The specific surface area reported for bamboo biochar in the study mentioned above was 42.8 m^2 g^{-1}, two times greater than the specific surface area herein calculated. The lower surface area and the higher adsorption capacity of rGO-MNPs for furfural adsorption can be explained by the higher affinity of the nanocomposite; such affinity is presented with more active sites in the surface area of rGO-MNPs than biochar for furfural adsorption.

Figure 2b shows the effect of the initial concentration of furfural on its adsorption by rGO-MNPs. The adsorbent mass of 20 mg was selected for this and next assays, in the application field, the operation costs of adsorption units are highly influenced by the mass of adsorbent. The *q* ranged from 77.8±5.5 to 427.0±13.7 mg g^{-1}. Likewise, the removal of furfural decreased when its initial concentration increased. For

instance, when the initial concentration of the furfural solution increased from 250 to 500 mg L^{-1}, the removal of furfural at 60 min decreased from 68.9±6.1 to 53.6±2.5%, and at 1000 mg L^{-1}, it was 26.4±2.1%. This is explained by the saturation of the adsorbent. The nanocomposite reached a dynamic equilibrium with furfural molecules of the medium and with the increment of furfural concentration was less and less able to remove it. According to literature, the furfural concentration in wood hydrolysate is in the range of 0.40 to 220 mg L^{-1} (Carlos S Osorio-González et al., 2019), which is smaller than the concentrations tested in this assay. Therefore, the rGO-MNPs could be an alternative to effectively remove inhibitory compounds at their typical concentrations using small quantities of rGO-MNPs. The removal of furfural using engineered materials has been studied showing similar tendencies, this means that small amount of adsorbent is necessary to remove high concentrations of furfural, as reported by Fazlzadeh et al. (2018); they used 500 mg of zero-valent iron nanoparticles synthesized from nettle extract with initial furfural concentrations ranging from 100 to 1000 mg L^{-1} obtaining removal efficiencies from 96 to 16%, with the decrease of furfural concentration at 70 minutes.

Figure 2c shows the temperature effect on furfural adsorption onto rGO-MNPs. The furfural removal and q were not different until 60 min adsorption point. At 60 min ahead, the furfural removal and q were lower at 50°C than 25°C. For example, at 120 min FR and q were: FR=62.1±3.5%, q=360.1±13.0 mg g^{-1} and FR=54.0±4.2%, q=305.7±22.7, for 25 and 50 °C, respectively. This is probably because the molecular movement of furfural molecules increases with temperature, and furfural molecules begin to escape from the adsorption sites, making the desorption dominant. Sahu et al., (2008) found that the decrease in temperature, favorably influenced the adsorption of furfural onto activated carbon, indicating an exothermic and spontaneous nature of furfural adsorption. Thus, the furfural adsorption on rGO-MNPs may be also exothermic, since the lower temperature of 25°C is better than 50°C. Considering this fact and the operating cost, 25°C can be chosen over 50°C for furfural detoxification.

The equilibrium adsorption is a physical-chemical property for evaluating the sorption process and plays a key role in designing an adsorption system. The adsorption

isotherm of furfural by rGO-MNPs nanocomposite and the fitted data scheme with Langmuir and Freundlich models are shown in the Supplementary material (**Figures S2-S4**).

According to the calculated parameters, Langmuir model presented a higher regression coefficient (R^2=0.99), than the Freundlich model (R^2=0.95). This suggests monolayer adsorption of a homogeneous surface. The constant of maximum adsorption capacity (q_m), which is a measure of the adsorption capacity to form a monolayer was 450.4 mg g^{-1}. The constant b, which denotes the adsorption energy, was equal to 0.015 L mg^{-1}. In the Supplementary material is presented the *qm* values of other studies using other adsorbents (**Table S1**). The most closely q_m was reported by Fazlzadeh et al.(2018), using zero-valent iron nanoparticles and obtaining a q_m of 454.4 mg g^{-1}. Hence, the rGO-MNPs nanocomposite could be a promising adsorbent for furfural removal. Another important factor to analyze is the adsorption contact time. From a practical point of view, a shorter contact time represents an advantage, since, in the real application, longer time in a downstream process i.e; hydrolysis, detoxification, or fermentation, may not be cost-effective. In the present study, a maximum adsorption capacity was reached in 120 min.

3.3 Adsorption of furfural *vs* glucose

To determine the sugar loss during furfural removal, an adsorption test using a model binary solution furfural-glucose was performed under the best conditions previously obtained for temperature and mass, this means 25°C and 20 mg of the adsorbent. A higher furfural concentration of 300 mg L^{-1} than reported by Osorio-González et al., (2019) was used. **Figure 3** shows the adsorption of furfural and glucose.

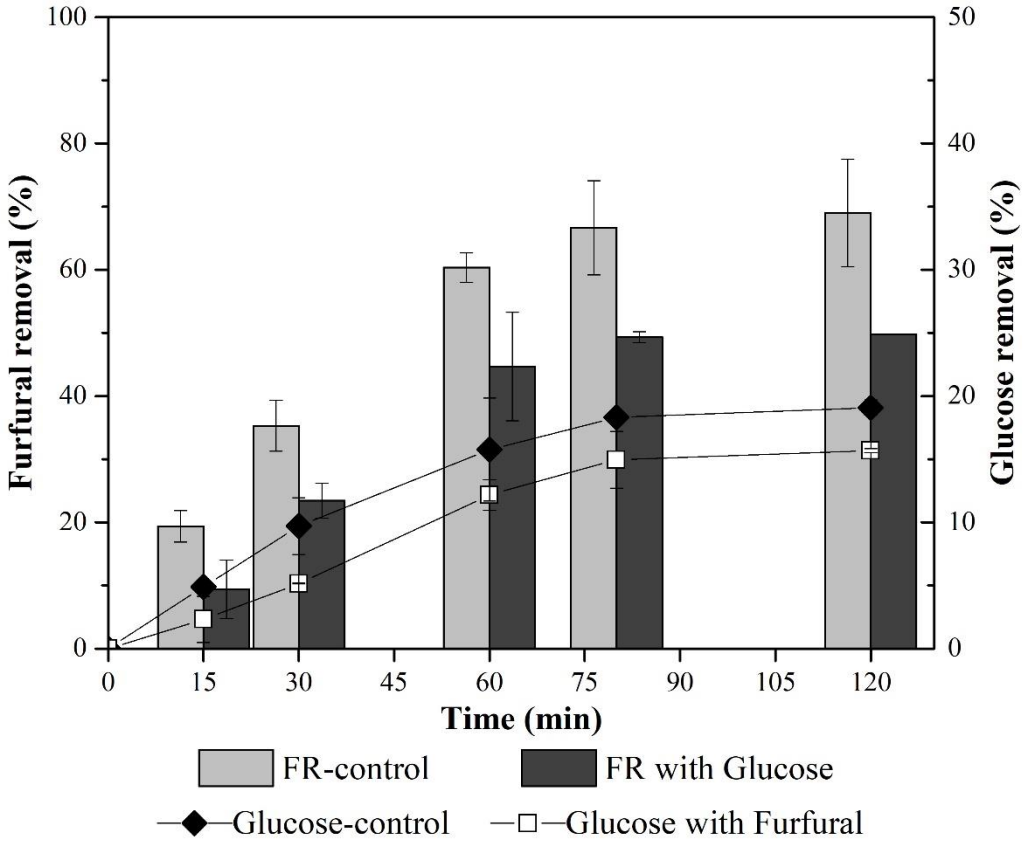

Figure 3. Adsorption study of glucose *vs* furfural (initial furfural concentration 300 mg L^{-1}, glucose concentration 10 g L^{-1} and 20 mg of rGO-MNPs).

Furfural removal decrease from 69.0±8.5% alone to 49.8±0.05% with glucose at 120 min treatment. On the other hand, the glucose removed by rGO-MNPs nanocomposite was 19.1±0.6% for glucose alone, and 15.7±0.2% for glucose with furfural at 120 min treatment, representing a decrease of 3.4%. These results suggest a competition between the adsorption sites of the nanomaterial. This behavior could be explained by the molecular size of furfural and glucose (0.57 nm, and 0.8 nm, respectively) (Adang and Spence, 1983; Karinen et al., 2011). Glucose could block the active sites of rGO-MNPs for furfural adsorption due to its bigger size and furfural could present a better diffusivity in the medium due to its smaller size; therefore, furfural could be easier attached to the adsorption sites of rGO-MNPs.

The adsorption competition between furfural and glucose have been also observed in other types of adsorbents. For instance, (Li et al. 2013), observed that the

adsorption of furfural decreased around 5% in the presence of glucose using bamboo charcoal. This was explained by the furfural selectivity into the adsorbent because of smaller molecular diameter of furfural and the functional groups in their different chemical structures. Even though the low sugar adsorption, it is worth mentioning that they used the same concentration of furfural and glucose (10000 mg L^{-1}) and a higher amount of adsorbent (7.5 g), which represents a disadvantage compared with the lower use of adsorbent utilized in the present study. Thus, the use of rGO-MNPs nanocomposite as an adsorbent is an attractive solution since the removal of furfural is 49.8±0.05% with only 20 mg of the nanocomposite.

Likewise, the higher attraction of furfural over glucose could be attributed to the hydrophobicity of the nanomaterial and furfural, rather than the hydrophilic glucose. The influence on the sorbent selectivity between furfural and sugar by the oxygen functional groups on carbon samples has been previously reported by Zhang et al., (2011). Oxygen groups tend to increase the hydrophilicity of carbon surface, making carbon adsorb more hydrophilic sugar, rather than hydrophobic furfural. The hydrophobic nature of rGO-MNPs was corroborated with the decrease in oxygenated groups of graphene oxide by Fourier-transform infrared spectroscopy (FTIR) in **Figure 4**.

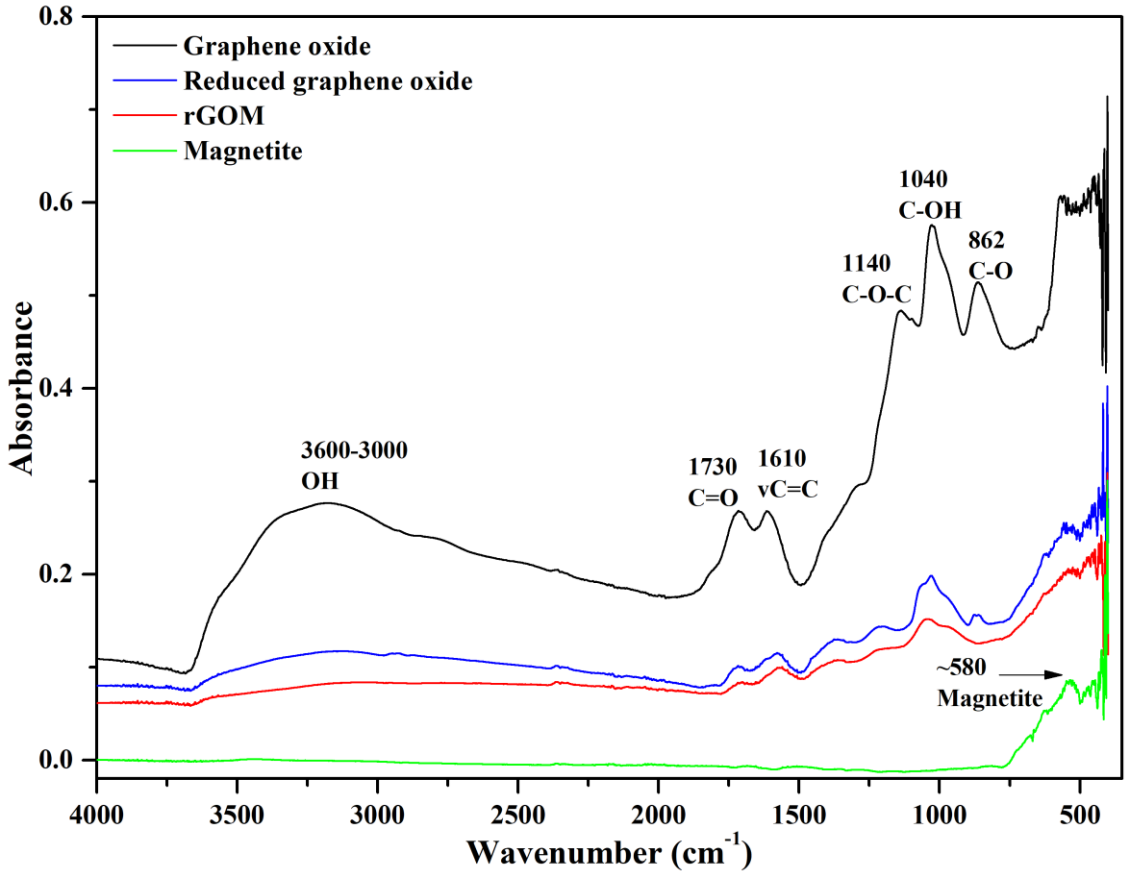

Figure 4. Fourier-transform infrared spectroscopy (FTIR) characterization of graphene oxide, reduced graphene oxide and reduced graphene oxide decorated with magnetite nanoparticles (rGO-MNPs).

Furthermore, FTIR showed that the oxygenated groups did not disappear completely, thus rGO-MNPs can still attract the hydrophilic glucose forming hydrogen bonds with the remained oxygenated groups. The infrared spectrum of graphene oxide presented the following characteristic peaks. The broadband ranging from 3600 to 3000 cm^{-1} corresponds to the O-H stretching vibrations of adsorbed water molecules on the basal planes (Szabó et al., 2005). The bands at 1730 and 1040 cm^{-1} are assigned to the C=O and C-OH stretching vibrations of COOH groups (carboxylic acids), respectively (Titelman et al., 2005). The band at 1610 cm^{-1} corresponds to the contributions from the skeletal vibrations of un-oxidized graphitic domains (vC=C). A signal presented at 862 cm^{-1} corresponds to vibrations of C–O from epoxy and hydroxyl groups (Eigler et al., 2012). As observed, in the spectra of reduced graphene oxide, the peaks decreased dramatically and

some of them disappeared completely, which indicated a successful reduction of the material. The characteristic peak of magnetite was seen at 580 cm^{-1}, this signal being previously reported at 583.1 cm^{-1} (Liu and Wang, 2004).

3.4 Furfural adsorption in the wood hydrolysate

Figure 5 shows furfural adsorption in the wood hydrolysate.

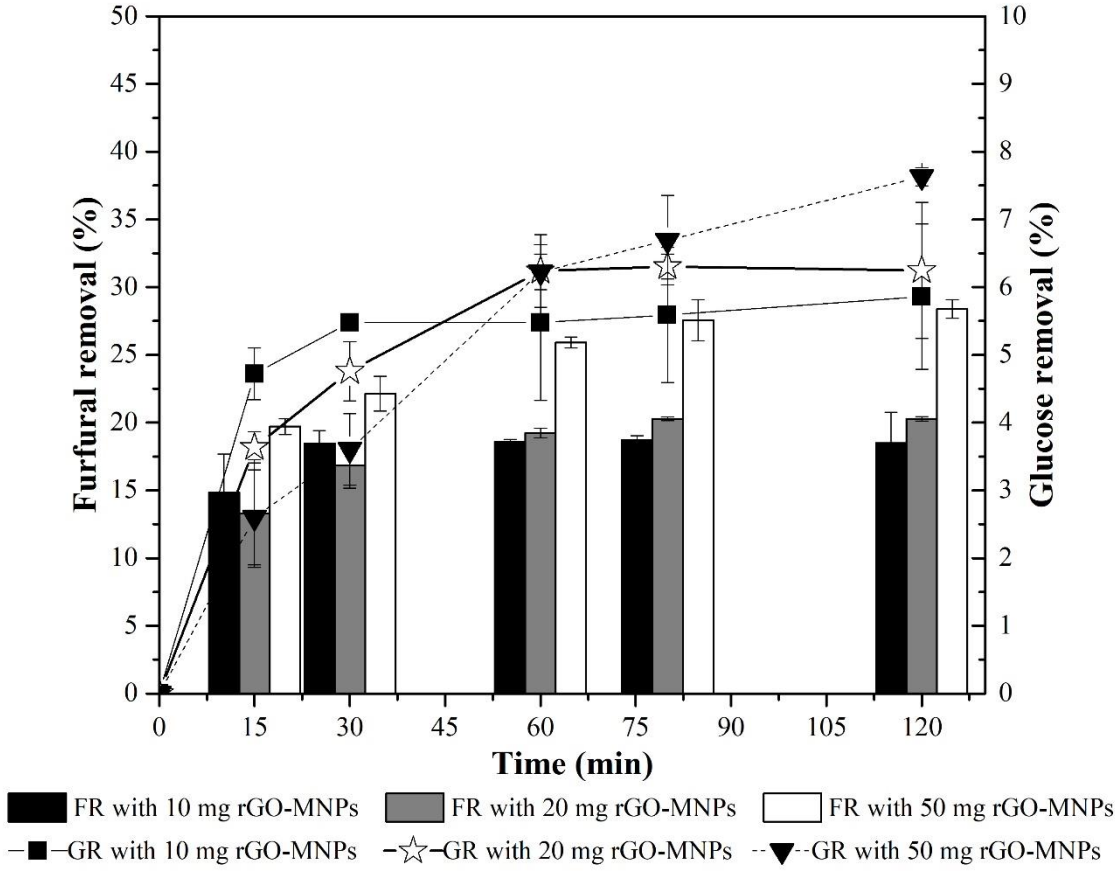

Figure 5. Furfural adsorption in wood hydrolysates. GR=Glucose removal, FR=Furfural removal. Initial furfural concentration of 379.3±4.4 mg L^{-1}, the mass of adsorbent 10, 20 and 50 mg rGO-MNPs.

The highest removal of furfural reached a value of 28.4±0.7% for 50 mg of rGO-MNPs at an adsorption time of 120 min. Likewise, the removal with 20 and 10 mg of rGO-MNPs was 20.3±0.2 and 18.5±2.3 %, respectively. Regarding glucose removal (**GR**), at 120 min the GR was nearly similar for the three masses tested, being 5.9±1.1, 6.2±1.0 and 7.6±0.1, for 10, 20 and 50 mg of rGO-MNPs, respectively. This

observation seems favorable since it is expected to have a minimal loss of fermentable sugar during the detoxification process. The fact that rGO-MNPs nanocomposite did not present a resemblance in glucose removal suggests that other hydrophobic inhibitors present in the hydrolysate may be competing for the nanocomposite.

In order to prove this assumption, other inhibitors in the wood hydrolysate were identified and quantified at time zero and during the kinetics assay of furfural adsorption. The initial concentration of inhibitors present in the wood hydrolysate is shown in **Table 1**.

Table 1. Initial concentration of inhibitors in the wood hydrolysate.

Inhibitor	**Concentration (mg L^{-1})**
Furfural	379.3±4.4
5-hydroxymethyl-furfural	40.3±0.2
Levulinic acid	39.3±0.3
Vanillic acid	48.3±0.2
Vanillin	6.2±0.05

The concentration profile of the four other inhibitors is shown in **Figure 6**a and b. The figure is a plot of C/C_0 as a function of time, where C is the inhibitor concentration at any time and C_0 is the initial inhibitor concentration in the hydrolysate. The removal of the other inhibitors was slightly affected by the mass of adsorbent. The 5-hydroxymethyl furfural (5-HMF) presented the highest removal of 72.5, 76.7 and 76.6%; followed by levulinic acid, with removal of 61.3, 63.1 and 60.5%; and vanillic acid, with removal of 57.5, 54.4 and 54.3%. Finally, vanillin the smallest removal of 39.4, 42.7 and 44.8%, at 120 min, for 10, 20 and 50 mg of rGO-MNPs, respectively.

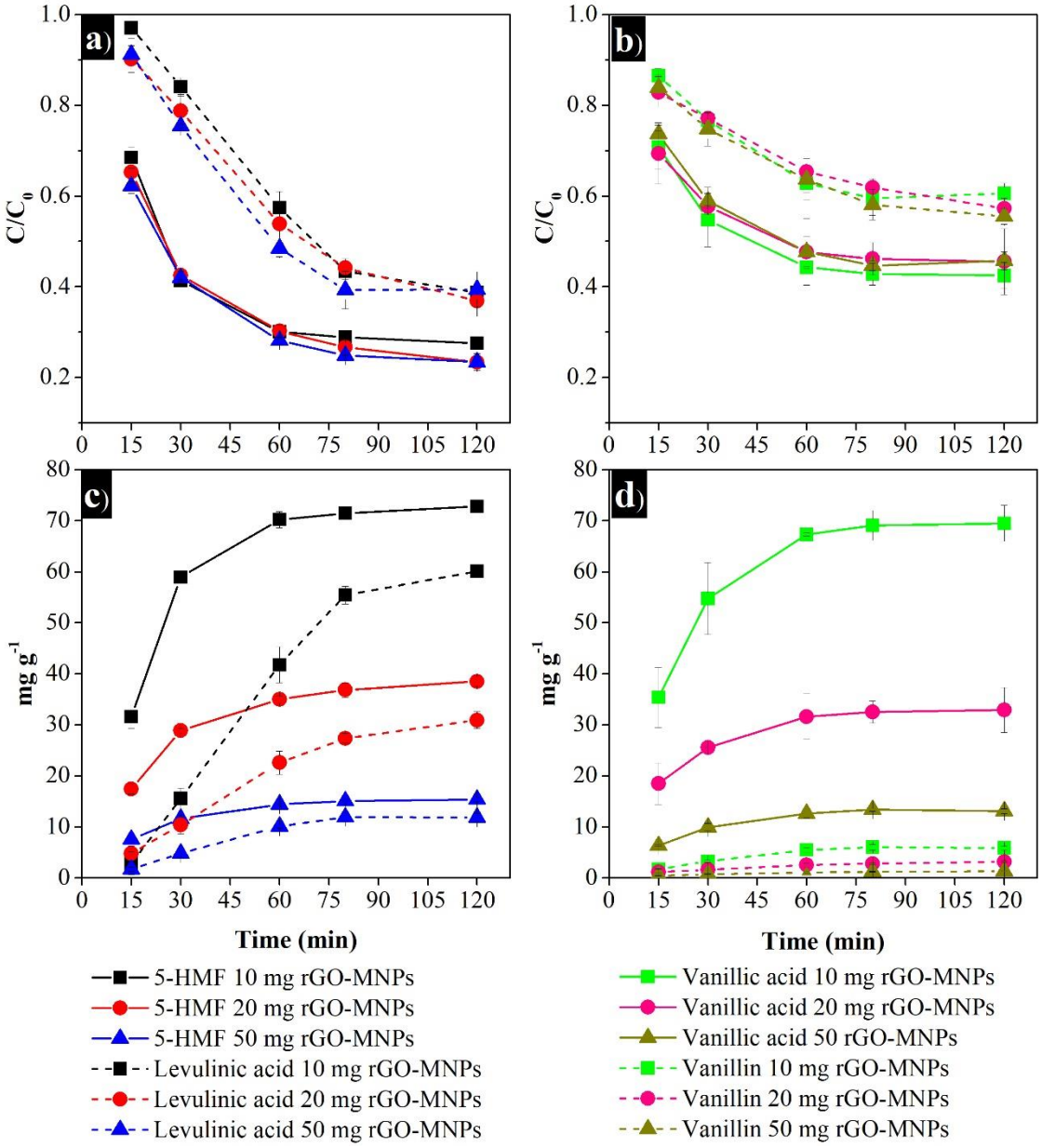

Figure 6. Adsorption assay of wood hydrolysate using rGO-MNPs nanocomposite: a) and b) concentration decay profile from inhibitors; c) and d) mg of inhibitor adsorbed by g of adsorbent. (5HMF=5-hydroxymethylfurfural, the mass of adsorbent 10, 20 and 50 mg rGO-MNPs).

Different adsorption factors can be involved in the arrangement of adsorption molecules to active sites of the nanocomposite. An important factor would be inhibitor concentration when the inhibitor concentration is high in the medium, a higher interaction with active sites of rGO-MNPs nanocomposite could exist,

increasing the adsorption ratio. This assumption may explain vanillin behavior, which presented lower removal since it was at the lowest concentration in the hydrolysate (6.2±0.05mg L^{-1}). Considering the hydrophobic interactions between organic chemicals and the nanostructure, the adsorption could be explained using the hydrophobic parameters of the compounds, such as K_{OW} (octane-water distribution coefficient). The K_{OW} value of the inhibitors is in the order of levulinic acid < 5-HMF < furfural < vanillin < vanillic acid, where the more hydrophobic is vanillic acid (Supplementary material **Table S2**). As mention above, 5-HMF presented the highest removal, following by levulinic acid, the second with the highest removal. These inhibitors are more hydrophilic compared with furfural, vanillin and vanillic acid. The more hydrophilic nature of levulinic acid and 5-HMF could be the reason they presented the higher removal followed by furfural since it is very likely that most of the hydrophobic sites of rGO-MNPs nanocomposite were occupied by the more hydrophobic compound (furfural). Thus, the hydrophilic sites of rGO-MNPs were available to absorb 5-HMF and levulinic acid. Otherwise, vanillic acid is the most hydrophobic among the identified inhibitors. It could be stated that should be adsorbed by the hydrophobic nature of rGO-MNPs, but as mention above was the penultimate with the highest removal (57.5, 54.4 and 54.3% for 10, 20 and 50 mg of adsorbent). This discloses that other mechanisms besides the hydrophobic interaction are involved. Overall, π-π interaction, hydrophobic effect, H-bonding and electrostatic interaction have been commonly applied to interpret the adsorption mechanisms of aromatic organic pollutants onto carbon-based materials such as graphene (Chen and Chen, 2015; J. Wang et al., 2014; Zhao et al., 2011).

Figure 6c and d shows the milligrams of inhibitor adsorbed by gram of adsorbent. Considering the *q*, it can be seen that the adsorption capacity did change with the mass of adsorbent for these inhibitors. For 5-HMF, levulinic acid, vanillic acid and vanillin, the highest *q* was present at 60 min treatment and such value shows similar trend in further detoxified treatments of 80 and 120 min, regardless of the adsorbent mass. This behavior can be correlated with the fraction removal in Figure 6a and b, where all inhibitors reached a stationary state of removal. Thus, a detoxification treatment by adsorption with rGO-MNPs at 60 min would be enough. Likewise, as

can be seen, a higher *q* is presented by 10 mg than 20 and 50 mg of rGO-MNPs in all inhibitors. The higher adsorption capacity of inhibitors with a lower amount of mass could be probably due to electrostatic interactions among the particles and to the concentration of each inhibitor in the hydrolysate solution. The electrostatic interactions between the graphene particles and the adorned nanoparticles of magnetite under high amounts of adsorbent led higher agglomeration and reducing the adsorption sites and the adsorbent surface area. In fact, it has been reported that magnetite nanoparticles display a great tendency for intrinsic agglomeration due to inter-particle magnetic dipolar interaction, London attractive and van der Walls forces (Krishna et al., 2016). In this sense, the higher amount of rGO-MNPs means a higher amount of adorned magnetite nanoparticles on the reduced graphene surface, leading agglomeration. In addition, the lower concentration of inhibitors compared with furfural and glucose concentration is also a factor that affects the adsorption of the inhibitors to the active sites of the nanocomposite due to the pseudo-adsorption-desorption balance if the concentration is to low, the desorption are the same.

3.5 Effect of rGO-MNPs nanocomposite on *R. toruloides*-1588

In order to test the effectivity of rGO-MNPs to detoxify real hydrolysates in a model fermentation process with the strain *R. toruloides*-1588, the level of toxicity of rGO-MNPs was determined in terms of yeast growth and sugar consumption. Fig. 7 shows the glucose consumption and biomass production by *R. toruloides*-1588 in presence of rGO-MNPs nanocomposite with the adsorbed inhibitors in a fermentation process of 126 h. The wood hydrolysate used was the one detoxified by adsorption at 120 min. Glucose consumption was 90% during the first 72 hours of fermentation flasks in the presence of 10 and 20 mg of rGO-MNPs (**Figure 7**a).

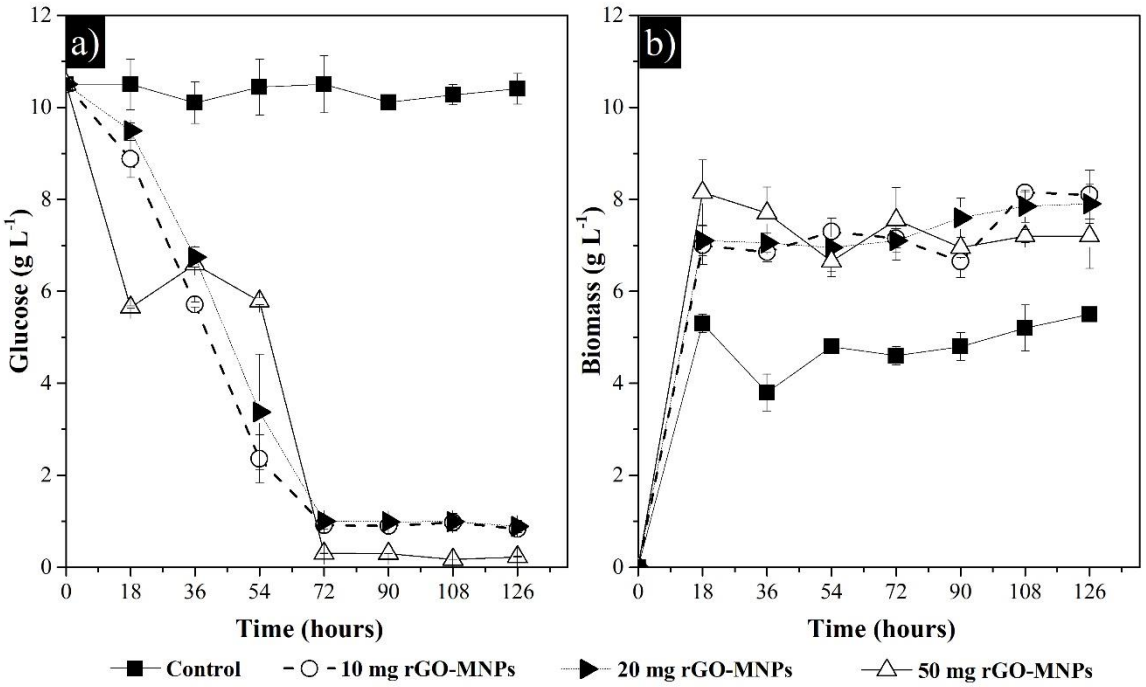

Figure 7. Performance of *R. toruloides*-1588 in presence of rGO-MNPs. Shaking speed 200 rpm at 25 °C. a) Sugar consumption for 10, 20 and 50 mg of rGO-MNPs; b) Biomass production for 10, 20 and 50 mg of rGO-MNPs.

Furthermore, when 50 mg of rGO-MNPs were added, glucose consumption was nearly 99% at the same time. Figure 7b shows biomass production during the fermentation process. The biomass production was around 7.7±0.5 g L^{-1} when rGO-MNPs was added (independently of the mass) and 4.9±0.5 g L^{-1} without rGO-MNPs. The higher biomass production in the assays with rGO-MNPs can be explained by two facts: i) *R. toruloides*-1588 show tolerance to oxidative stress of the still exposed nanosheets of graphene and ii) adorning with magnetite nanoparticles decreases the physical damage that the sharp edges of graphene can cause to the cell membrane.

To the best of our knowledge, few studies have evaluated the effects of nanostructures on yeasts. Peng et al. (2018) assessed the effect of magnetite nanoparticles on the growth of *Saccharomyces cerevisiae* yeast at concentrations of 100, 200, 400, 800 and 1600 mg L^{-1} with an initial yeast number of $1x10^6$ cells mL^{-1} after 12 h. They found an inhibitory effect from nanoparticles on yeast growth when the concentration reached up to 200 mg L^{-1}, and the effect became greater as the

concentrations increased. The inhibition was attributed to the nanoparticle interaction with the mitochondria, which led to disruption of the mitochondrial respiratory chain and consequently the attenuation of ATP production. On the other hand, Zhu et al. (2017), studied the toxicity of graphene oxide on the same yeast at concentrations of 25, 50, 100, 200, 400 and 600 mg L^{-1} with an initial yeast number of 1-2x10^5 cells mL^{-1} for 24 hours. The results showed that cell proliferation was inhibited at a half-maximal inhibitory concentration of 352.7 mg L^{-1}. The effects were related to mitochondria-mediated apoptosis and oxidative stress. Concentrations used in the present study were 400, 800 and 2000 mg L^{-1}, which correspond to 10, 20 and 50 mg of rGO-MNPs. In this sense, the fact that the nanocomposite herein studied did not present an inhibitory effect on biomass growth of *R. toruloides*-1588 may be attributed also to the different resistances of the yeasts, the concentrations used, the size, the shape, type and the chemical structure of the nanostructure.

Considering that the removed inhibitors are still present, but adsorbed onto the nanostructure, these results indirectly prove that detoxification with rGO-MNPs of inhibitors was satisfactory since they were not desorbed during the fermentation assay.

Some of the advantages of the use of rGO-MNPs nanocomposite as an adsorbent for large-scale inhibitors removal over existing methods for fermentation of hydrolysates, is that this adsorbent can be easily extracted before the fermentation or after fermentation, by applying an external magnetic force. Thus, rGO-MNPs can be easily recovered, minimizing their release to the environment. This study highlights the advantage of using a lower amount of adsorbent for detoxification of wood hydrolysates, achieving a high adsorption capacity.

4. Conclusions

Reduced graphene oxide adorned with magnetite nanoparticles (rGO-MNPs) can be a potential adsorbent for the removal of fermentation inhibitors such as, furfural, 5-hydroxymethyl-furfural, levulinic acid, vanillic acid and vanillin from wood hydrolysates with a minimal sugar loss of 5.9, 6.2 and 7.6%, for 10, 20 and 50 mg of

the adsorbent. This study also explored the effect of rGO-MNPs in a fermentation process with *R. toruloides*-1588, finding no toxicity with the nanostructure.

5. Supplementary data

Figure S1. N_2 adsorption/desorption isotherm of rGO-MNPs nanocomposite

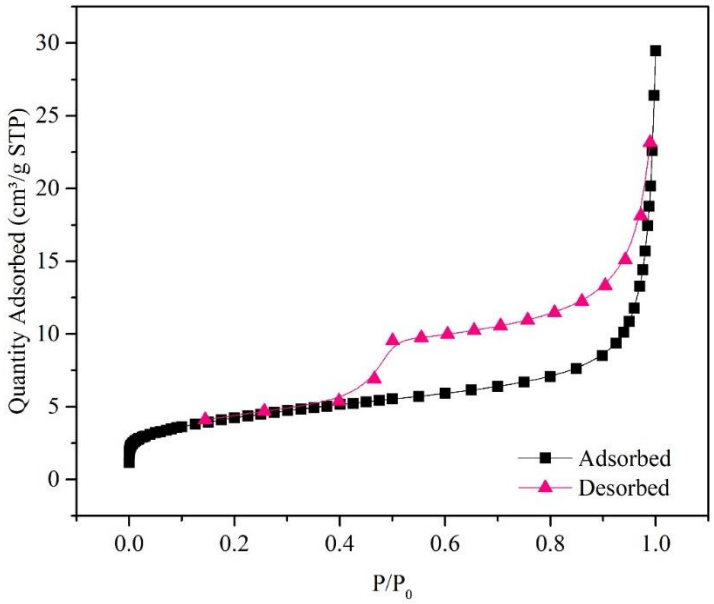

Figure S2. Adsorption isotherm of furfural using rGO-MNPs. (Contact time=120 min, adsorbent amount= 20 mg)

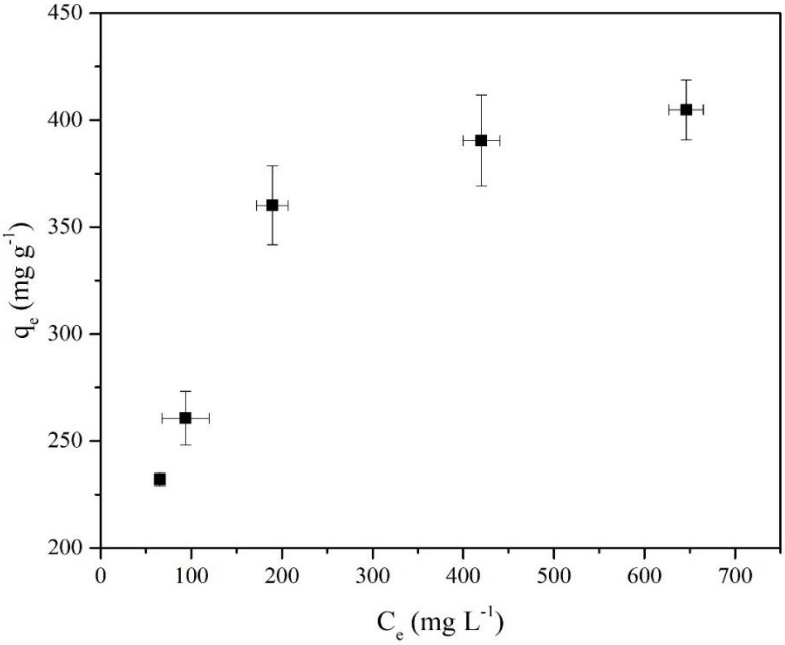

Figure S3. Langmuir model of isotherm for adsorption of furfural onto rGO-MNPs.

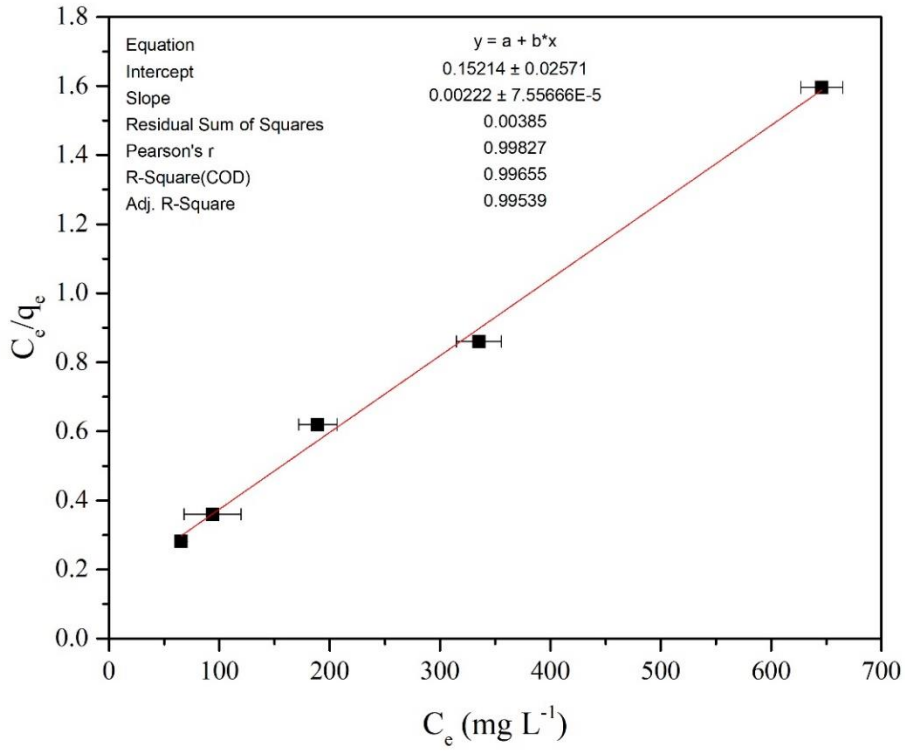

Figure S4. Freundlich model of isotherm for adsorption of furfural onto rGO-MNPs.

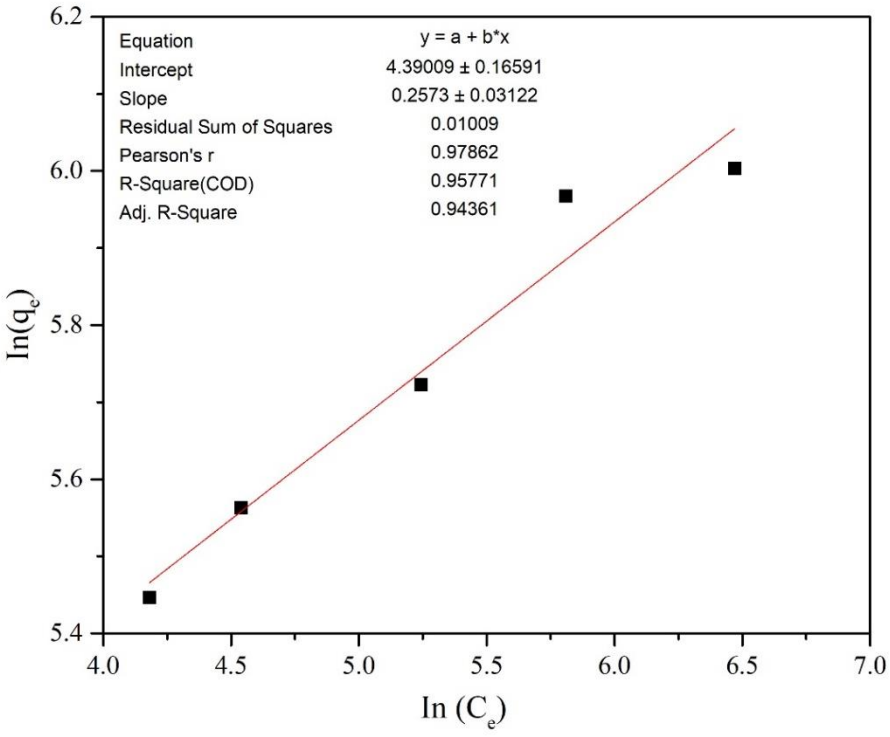

Table S1. Studies reported of furfural removal using various adsorbents.

Material	Mass Adsorbent (mg)	q_m (mg g^{-1})	Furfural Concentration (mg L^{-1})	V (mL)	Time (min)	pH	T (°C)	rpm	Application	Reference
MCM-48	100	196.1	1000	25	60	6	25	150	WW Treatment	Anbia and Mohammadi (2009)
Activated Carbon	200	250-280	100-4000	20	10	x	25	x	Ethanol production	Zhang et al. (2011)
Pyrolitic char (Bamboo charcoal)	200-20000	57-98	5000-20000	100	24(h)	5.6	25-55	100	Ethanol production	Li et al. (2013)
Chitosan coated magnetite particles	50	121.7	100-1400	40	5(h)	8	25	200	WW Treatment	He et al. (2014)
Torrefied biomass	1000	38	300-6000	20	12 (h)	3.6	20	150	Torrefaction condensate	Doddapaneni et al. (2018)
Zero valent Iron	500	454.4	100-1000	250	70	2	25	200	WW Treatment	Fazlzadeh et al. (2018)
rGO-MNPs	**20**	**450.4**	**250-1000**	**25**	**120**	**5**	**25**	**200**	**Fermentation**	**This study**

Table S2. K_{OW} (Octane-water distribution coefficient) of inhibitors at 25°C.

Inhibitor	KOW	Reference
Furfural	log Kow= 0.41	Hansch, C., Leo, A., D. Hoekman. Exploring QSAR - Hydrophobic, Electronic, and Steric Constants. Washington, DC: American Chemical Society., 1995., p. 11
5-hydroxymethyl -furfural	log Kow = -0.09	http://www.epa.gov/oppt/exposure/pubs/episuitedl.htm
Levulinic acid	log Kow= -0.49	http://www.gfbiochemicals.com/_media/Document/2015/9/21/ACIDO%20LEVULINICO_sds_ENG_rev3.pdf
Vanillic acid	log Kow = 1.43	https://comptox.epa.gov/dashboard/dsstoxdb/results?search=DTXSID6059522#properties
Vanillin	log Kow = 1.37	Hansch, C., Leo, A., D. Hoekman. Exploring QSAR - Hydrophobic, Electronic, and Steric Constants. Washington, DC: American Chemical Society., 1995., p. 42

6. References

Adang, M.J., Spence, K.D., 1983. Permeability of the peritrophic membrane of the Douglas fir tussock moth (Orgyia pseudotsugata). Comp. Biochem. Physiol. Part A Physiol. 75, 233–238. https://doi.org/https://doi.org/10.1016/0300-9629(83)90075-0

Almeida, J.R.M., Bertilsson, M., Gorwa-Grauslund, M.F., Gorsich, S., Lidén, G., 2009. Metabolic effects of furaldehydes and impacts on biotechnological processes. Appl. Microbiol. Biotechnol. 82, 625–638. https://doi.org/10.1007/s00253-009-1875-1

Anbia, M., Mohammadi, N., 2009. A nanoporous adsorbent for removal of furfural from aqueous solutions. DES 249, 150–153. https://doi.org/10.1016/j.desal.2008.06.027

Carvalho, G.B.M., Mussatto, S.I., Cândido, E.J., e Silva, J.B., 2006. Comparison of different procedures for the detoxification of eucalyptus hemicellulosic hydrolysate for use in fermentative processes. J. Chem. Technol. Biotechnol. 81, 152–157. https://doi.org/10.1002/jctb.1372

Chandra, V., Park, J., Chun, Y., Lee, J.W., Hwang, I., Kim, K.S., 2010. Water-

dispersible magnetite-reduced graphene oxide composites for arsenic removal. ACS Nano 4, 3979–3986. https://doi.org/10.1021/nn1008897

Chen, X., Chen, B., 2015. Macroscopic and spectroscopic investigations of the adsorption of nitroaromatic compounds on graphene oxide, reduced graphene oxide, and graphene nanosheets. Environ. Sci. Technol. 49, 6181–6189. https://doi.org/10.1021/es5054946

Covarrubias-García, I., Quijano, G., Aizpuru, A., Sánchez-García, J.L., Rodríguez-López, J.L., Arriaga, S., 2020. Reduced graphene oxide decorated with magnetite nanoparticles enhance biomethane enrichment. J. Hazard. Mater. 397, 1–12. https://doi.org/10.1016/j.jhazmat.2020.122760

Deng, F., Aita, G.M., 2018. Detoxification of dilute ammonia pretreated energy cane bagasse enzymatic hydrolysate by soluble polyelectrolyte flocculants. Ind. Crops Prod. 112, 681–690. https://doi.org/https://doi.org/10.1016/j.indcrop.2017.12.061

Doddapaneni, T.R.K.C., Jain, R., Praveenkumar, R., Rintala, J., Romar, H., Konttinen, J., 2018. Adsorption of furfural from torrefaction condensate using torrefied biomass. Chem. Eng. J. 334, 558–568. https://doi.org/10.1016/j.cej.2017.10.053

Eigler, S., Dotzer, C., Hirsch, A., 2012. Visualization of defect densities in reduced graphene oxide. Carbon N. Y. 50, 3666–3673. https://doi.org/10.1016/j.carbon.2012.03.039

Esfandiar, A., Akhavan, O., Irajizad, A., 2011. Melatonin as a powerful bio-antioxidant for reduction of graphene oxide. J. Mater. Chem. 21, 10907. https://doi.org/10.1039/c1jm10151j

Fazlzadeh, M., Ansarizadeh, M., Leili, M., 2018. Data in Brief Data of furfural adsorption on nano zero valent iron (NZVI) synthesized from Nettle extract. Data Br. 16, 341–345. https://doi.org/10.1016/j.dib.2017.11.035

Grzenia, D.L., Schell, D.J., Wickramsinghe, S.R., 2010. Detoxification of biomass hydrolysates by reactive membrane extraction. J. Memb. Sci. 348, 6–12. https://doi.org/10.1016/j.memsci.2009.10.035

Gupta, S. Sen, Sreeprasad, T.S., Maliyekkal, S.M., Das, S.K., Pradeep, T., 2012.

Graphene from Sugar and its Application in Water Purification. ACS Appl. Mater. Interfaces 4, 4156–4163. https://doi.org/10.1021/am300889u

He, H., Gao, C., 2010. Supraparamagnetic, Conductive, and Processable Multifunctional Graphene Nanosheets Coated with High-Density Fe3O4 Nanoparticles. ACS Appl. Mater. Interfaces 2, 3201–3210. https://doi.org/10.1021/am100673g

He, Y., Pei, M., Du, Y., Yu, F., Wang, L., Guo, W., 2014. Synthesis, characterization and application of chitosan coated Fe3O4 particles as an adsorbent for the removal of furfural from aqueous solution. RSC Adv. 4, 30352–30357. https://doi.org/10.1039/c4ra04098h

Hodge, D.B., Andersson, C., Berglund, K.A., Rova, U., 2009. Detoxification requirements for bioconversion of softwood dilute acid hydrolyzates to succinic acid. Enzyme Microb. Technol. 44, 309–316. https://doi.org/https://doi.org/10.1016/j.enzmictec.2008.11.007

Hou, C., Zhang, Q., Zhu, M., Li, Y., Wang, H., 2011. One-step synthesis of magnetically-functionalized reduced graphite sheets and their use in hydrogels. Carbon N. Y. 49, 47–53. https://doi.org/10.1016/j.carbon.2010.08.040

Jung, Y.H., Kim, I.J., Kim, H.K., Kim, K.H., 2013. Dilute acid pretreatment of lignocellulose for whole slurry ethanol fermentation. Bioresour. Technol. 132, 109–114. https://doi.org/https://doi.org/10.1016/j.biortech.2012.12.151

Jung, Y.H., Park, H.M., Kim, I.J., Park, Y., Seo, J., Kim, K.H., 2014. One-pot pretreatment, saccharification and ethanol fermentation of lignocellulose based on acid–base mixture pretreatment 55318–55327. https://doi.org/10.1039/c4ra10092a

Karimi-Maleh, H., Shafieizadeh, M., Taher, M.A., Opoku, F., Kiarii, E.M., Govender, P.P., Ranjbari, S., Rezapour, M., Orooji, Y., 2020. The role of magnetite/graphene oxide nano-composite as a high-efficiency adsorbent for removal of phenazopyridine residues from water samples, an experimental/theoretical investigation. J. Mol. Liq. 298. https://doi.org/10.1016/j.molliq.2019.112040

Karinen, R., Vilonen, K., Niemelä, M., 2011. Biorefining: Heterogeneously Catalyzed Reactions of Carbohydrates for the Production of Furfural and Hydroxymethylfurfural. ChemSusChem 4, 1002–1016. https://doi.org/10.1002/cssc.201000375

Kemp, K.C., Seema, H., Saleh, M., Le, N.H., Mahesh, K., Chandra, V., Kim, K.S., 2013. Environmental applications using graphene composites: Water remediation and gas adsorption. Nanoscale 5, 3149–3171. https://doi.org/10.1039/c3nr33708a

Khatamian, M., Khodakarampoor, N., Saket-Oskoui, M., 2017. Efficient removal of arsenic using graphene-zeolite based composites. J. Colloid Interface Sci. 498, 433–441. https://doi.org/10.1016/j.jcis.2017.03.052

Krishna, R., Dias, C., Ventura, J., Titus, E., 2016. Green and facile decoration of Fe3O4 nanoparticles on reduced graphene oxide. Mater. Today Proc. 3, 2807–2813. https://doi.org/10.1016/j.matpr.2016.06.030

Li, Y., Shao, J., Wang, X., Yang, H., Chen, Y., Deng, Y., Zhang, S., Chen, H., 2013. Upgrading of bio-oil: Removal of the fermentation inhibitor (furfural) from the model compounds of bio-oil using pyrolytic char. Energy and Fuels 27, 5975–5981. https://doi.org/10.1021/ef401375q

Liu, J., Tang, J., Gooding, J.J., 2012. Strategies for chemical modification of graphene and applications of chemically modified graphene. J. Mater. Chem. 22, 12435–12452. https://doi.org/10.1039/c2jm31218b

Liu, Z., Gao, Z., Xu, L., Hu, F., 2020. Efficient and rapid adsorption of rare earth elements from water by magnetic Fe3O4/MnO2 decorated reduced graphene oxide. J. Mol. Liq. 313, 113510. https://doi.org/10.1016/j.molliq.2020.113510

Liu, Z.L., Slininger, P.J., Dien, B.S., Berhow, M.A., Kurtzman, C.P., Gorsich, S.W., 2004. Adaptive response of yeasts to furfural and 5-hydroxymethylfurfural and new chemical evidence for HMF conversion to 2,5-bis-hydroxymethylfuran. J. Ind. Microbiol. Biotechnol. 31, 345–352. https://doi.org/10.1007/s10295-004-0148-3

Liu, Z.L., Wang, X., 2004. Synthesis of magnetite nanoparticles in W/O microemulsion. J. Mater. Sci. 39, 2633–2636.

Ludwig, D., Amann, M., Hirth, T., Rupp, S., Zibek, S., 2013. Bioresource Technology Development and optimization of single and combined detoxification processes to improve the fermentability of lignocellulose hydrolyzates. Bioresour. Technol. 133, 455–461. https://doi.org/10.1016/j.biortech.2013.01.053

McAllister, M.J., Li, J.L., Adamson, D.H., Schniepp, H.C., Abdala, A.A., Liu, J., Herrera-Alonso, M., Milius, D.L., Car, R., Prud'homme, R.K., Aksay, I.A., 2007. Single sheet functionalized graphene by oxidation and thermal expansion of graphite. Chem. Mater. 19, 4396–4404. https://doi.org/10.1021/cm0630800

Mussatto, S.I., Roberto, I.C., 2001. Hydrolysate detoxification with activated charcoal for xylitol production by Candida guilliermondii. Biotechnol. Lett. 23, 1681–1684. https://doi.org/10.1023/A:1012492028646

Muthukannan, V., Praveen, K., Natesan, B., 2015. Fabrication and characterization of magnetite/reduced graphene oxide composite incurred from iron ore tailings for high performance application. Mater. Chem. Phys. 162, 400–407. https://doi.org/10.1016/j.matchemphys.2015.06.006

Myoung, J., Venditti, R.A., Jameel, H., Kenealy, W.R., 2010. Detoxification of woody hydrolyzates with activated carbon for bioconversion to ethanol by the thermophilic anaerobic bacterium Thermoanaerobacterium saccharolyticum. Biomass and Bioenergy 35, 626–636. https://doi.org/10.1016/j.biombioe.2010.10.021

Osorio-González, Carlos S, Hegde, K., Brar, S.K., Kermanshahipour, A., Avalos-Ramírez, A., 2019. Challenges in lipid production from lignocellulosic biomass using Rhodosporidium sp.; A look at the role of lignocellulosic inhibitors. Biofuels, Bioprod. Biorefining 13, 740–759. https://doi.org/10.1002/bbb.1954

Osorio-González, Carlos S., Hegde, K., Brar, S.K., Kermanshahipour, A., Avalos-Ramírez, A., 2019a. Data set of green extraction of valuable chemicals from lignocellulosic biomass using microwave method. Data Br. 26, 1–6. https://doi.org/10.1016/j.dib.2019.104347

Osorio-González, Carlos S., Hegde, K., Ferreira, P., Brar, S.K., Kermanshahipour, A., Soccol, C.R., Avalos-Ramírez, A., 2019b. Lipid production in

Rhodosporidium toruloides using C-6 and C-5 wood hydrolysate: A comparative study. Biomass and Bioenergy 130, 105355. https://doi.org/10.1016/j.biombioe.2019.105355

Palmqvist, E., Hahn-Hägerdal, B., 2000a. Fermentation of lignocellulosic hydrolysates. II: inhibitors and mechanisms of inhibition. Bioresour. Technol. 74, 25–33. https://doi.org/https://doi.org/10.1016/S0960-8524(99)00161-3

Palmqvist, E., Hahn-Hägerdal, B., 2000b. Fermentation of lignocellulosic hydrolysates. I: inhibition and detoxification. Bioresour. Technol. 74, 17–24. https://doi.org/https://doi.org/10.1016/S0960-8524(99)00160-1

Peng, Q., Huo, D., Li, H., Zhang, B., Li, Y., Liang, A., Wang, H., Yu, Q., Li, M., 2018. ROS-independent toxicity of Fe3O4 nanoparticles to yeast cells: Involvement of mitochondrial dysfunction. Chem. Biol. Interact. 287, 20–26. https://doi.org/10.1016/j.cbi.2018.03.012

Ranjan, R., Thust, S., Gounaris, C.E., Woo, M., Floudas, C.A., Keitz, M. von, Valentas, K.J., Wei, J., Tsapatsis, M., 2009. Adsorption of fermentation inhibitors from lignocellulosic biomass hydrolyzates for improved ethanol yield and value-added product recovery. Microporous Mesoporous Mater. 122, 143–148. https://doi.org/https://doi.org/10.1016/j.micromeso.2009.02.025

Ren, R.P., Wang, Z., Ren, J., Lv, Y.K., 2019. Highly compressible polyimide/graphene aerogel for efficient oil/water separation. J. Mater. Sci. 54, 5918–5926. https://doi.org/10.1007/s10853-018-03238-1

Sahu, A.K., Srivastava, V.C., Mall, I.D., Lataye, D.H., 2008. Adsorption of furfural from aqueous solution onto activated carbon: Kinetic, equilibrium and thermodynamic study. Sep. Sci. Technol. 43, 1239–1259. https://doi.org/10.1080/01496390701885711

Shan, D., Deng, S., Jiang, C., Chen, Y., Wang, B., Wang, Y., Huang, J., Yu, G., Wiesner, M.R., 2018. Hydrophilic and strengthened 3D reduced graphene oxide/nano-Fe3O4 hybrid hydrogel for enhanced adsorption and catalytic oxidation of typical pharmaceuticals. Environ. Sci. Nano 5, 1650–1660. https://doi.org/10.1039/c8en00422f

Szabó, T., Berkesi, O., Dékány, I., 2005. DRIFT study of deuterium-exchanged

graphite oxide. Carbon N. Y. 43, 3186–3189.

Taherzadeh, M.J., Gustafsson, L., Niklasson, C., Lidén, G., 2000. Physiological effects of 5-hydroxymethylfurfural on Saccharomyces cerevisiae. Appl. Microbiol. Biotechnol. 53, 701–708. https://doi.org/10.1007/s002530000328

Thanikaivelan, P., Narayanan, N.T., Pradhan, B.K., Ajayan, P.M., 2012. Collagen based magnetic nanocomposites for oil removal applications. Sci. Rep. 2, 230.

Titelman, G.I., Gelman, V., Bron, S., Khalfin, R.L., Cohen, Y., Bianco-Peled, H., 2005. Characteristics and microstructure of aqueous colloidal dispersions of graphite oxide. Carbon N. Y. 43, 641–649. https://doi.org/10.1016/j.carbon.2004.10.035

Wang, J., Chen, Z., Chen, B., 2014. Adsorption of polycyclic aromatic hydrocarbons by graphene and graphene oxide nanosheets. Environ. Sci. Technol. 48, 4817–4825. https://doi.org/10.1021/es405227u

Wang, X., Huang, S., Zhu, L., Tian, X., Li, S., Tang, H., 2014a. Correlation between the adsorption ability and reduction degree of graphene oxide and tuning of adsorption of phenolic compounds. Carbon N. Y. 69, 101–112. https://doi.org/https://doi.org/10.1016/j.carbon.2013.11.070

Wang, X., Huang, S., Zhu, L., Tian, X., Li, S., Tang, H., 2014b. Correlation between the adsorption ability and reduction degree of graphene oxide and tuning of adsorption of phenolic compounds. Carbon N. Y. 69, 101–112. https://doi.org/10.1016/j.carbon.2013.11.070

Wei, Y., Yin, G., Ma, C., Huang, Z., Chen, X., Liao, X., Yao, Y., Yin, H., 2013. Synthesis and cellular compatibility of biomineralized Fe3O4 nanoparticles in tumor cells targeting peptides. Colloids Surfaces B Biointerfaces 107, 180–188. https://doi.org/https://doi.org/10.1016/j.colsurfb.2013.01.058

Xu, J., Wang, L., Zhu, Y., 2012. Decontamination of Bisphenol A from Aqueous Solution by Graphene Adsorption. Langmuir 28, 8418–8425. https://doi.org/10.1021/la301476p

Yan, J., Gao, W., Dong, M., Han, L., Qian, L., Nathanail, C.P., Chen, M., 2016. Degradation of trichloroethylene by activated persulfate using a reduced graphene oxide supported magnetite nanoparticle. Chem. Eng. J. 295, 309–

316. https://doi.org/10.1016/j.cej.2016.01.085

Yoon, D., Hwang, J., Chang, W., Kim, J., 2017. Uniform one-pot anchoring of Fe3O4 to defective reduced graphene oxide for enhanced lithium storage. Chem. Eng. J. 317, 890–900. https://doi.org/10.1016/j.cej.2017.02.108

Yousefi, N., Lu, X., Elimelech, M., Tufenkji, N., 2019. Environmental performance of graphene-based 3D macrostructures. Nat. Nanotechnol. 14, 107–119. https://doi.org/10.1038/s41565-018-0325-6

Zhang, K., Agrawal, M., Harper, J., Chen, R., Koros, W.J., 2011. Removal of the Fermentation Inhibitor, Furfural, Using Activated Carbon in Cellulosic-Ethanol Production 14055–14060. https://doi.org/10.1021/ie2013983

Zhao, G., Jiang, L., He, Y., Li, J., Dong, H., Wang, X., Hu, W., 2011. Sulfonated Graphene for Persistent Aromatic Pollutant Management. Adv. Mater. 23, 3959–3963. https://doi.org/10.1002/adma.201101007

Zhu, S., Luo, F., Zhu, B., Wang, G.X., 2017. Toxicological effects of graphene oxide on: Saccharomyces cerevisiae. Toxicol. Res. (Camb). 6, 535–543. https://doi.org/10.1039/c7tx00103g

Chapter IV. Use of reduced graphene oxide adorned with magnetite nanoparticles to enhance the production of metabolites of interest from syngas fermentation

"To be submitted, 2021"

Graphical Abstract

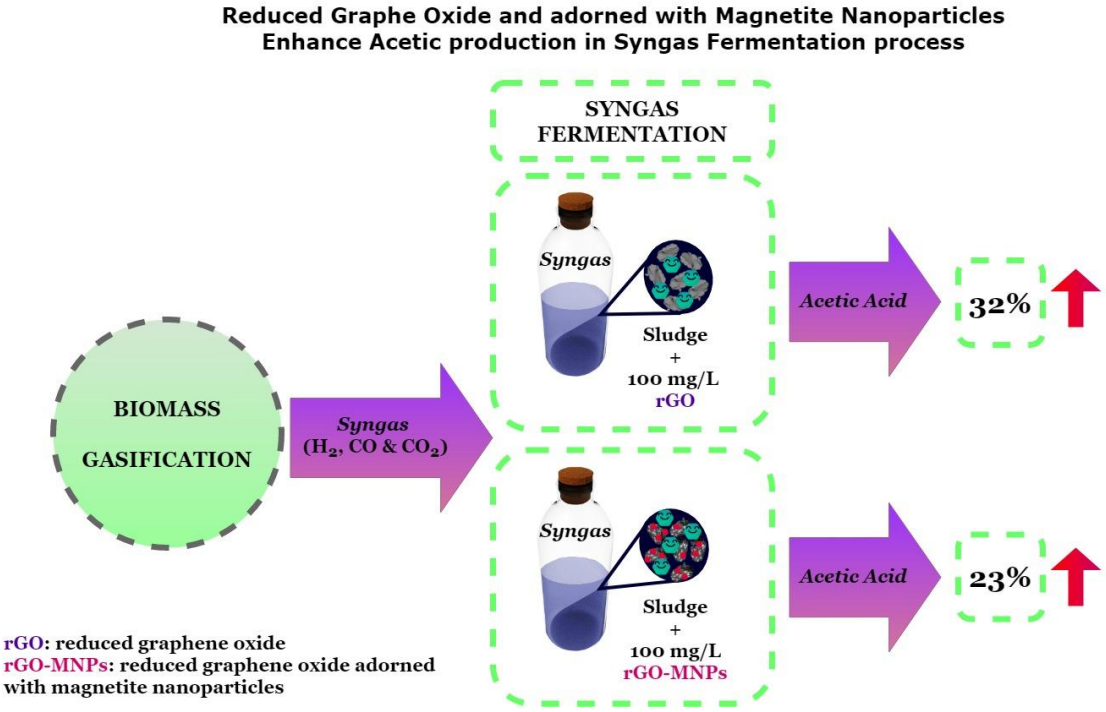

Abstract

Syngas is produced from biomass gasification and also it is a byproduct of several industrial processes. It is carrier of a high amount of energy and carbon that cannot be stored (due to high content of H_2 and CO) unless it is processed. One attractive alternative is its fixation by fermentation into a platform chemicals (e.g. medium chain fatty acids or alcohols). Such compounds can present high economic values due to their wider range of applications in the chemical industry. The main drawbacks in the syngas fermentation process are, the slow gas-liquid mass transfer and the need of work in sterile conditions due to the pure culture used. Hence, this study investigated the addition of reduced graphene oxide (rGO) and reduced graphene oxide adorned

with magnetite nanoparticles (rGO-MNPs) to an acclimatized consortium sludge in a syngas fermentation process. Results showed that rGO and rGO-MNPs enhanced the acetic acid production by 32% and 23% with 100 mg/L of nanomaterial added, respectively. The improvement was linked to the higher electron shuttling capacity, the sorption capacity and the dosing of dissolved iron in the medium.

Keywords: carbon monoxide; syngas fermentation; reduced graphene; magnetite; acetic acid.

1. Introduction

Gasification itself is considered a clean, efficient and environment-friendly process (Li et al., 2018; Yang et al., 2018). Synthesis gas (syngas) is the product of gasification of different types of coal, biomass, solid municipal waste or solid recovered fuels. Syngas is a mixture of (carbon monoxide) CO and H_2 in the first place, and can also contain smaller amounts of CO_2, CH_4, N_2 or Sulphur. Syngas composition depends on the gasification process parameters (Lin and Weng, 2017; Mishra et al., 2018). In biorefineries, CO-rich syngas is a major compound found in waste gases from some industries such as steel producing plants and it is (Abubackar et al., 2011; Xie et al., 2014, 2012). The synthesis gas production, transport and storage could lead to problems related to the hazards of H_2 and and CO due to their flammable and toxic properties (Stolecka and Rusin, 2020). Syngas can be used in energy production process; It can be used as a feedstock for the production of bulk chemicals such as acetic acid, butyric acid or biofuels (e.g. ethanol and butanol) either by chemical catalytic conversion (e.g. Fischer-Tropsch) or biological conversion processes (Drzyzga et al., 2015). Biological processes are considered more attractive because they provide several advantages compared with the chemical processes. The main advantages of using bacteria as biocatalysts for syngas fermentation are: the use of temperatures and pressures which are closer to standard environmental conditions; the biological catalysts is less sensitive to the ratio of CO to H_2 of syngas compared with traditional/commercial catalysts that require a specific ratio of CO to H_2 and that biocatalysts is less sensitive to trace

amounts of contaminants of syngas compared with the chemical catalysts (Acharya et al., 2014; Bengelsdorf et al., 2013; Munasinghe and Khanal, 2010). CO can be converted anaerobically by acetogenic bacteria into a spectrum of commercially useful metabolites. Several acetogenic bacteria assimilating CO are also able to metabolize CO_2 and H_2 as well as syngas, *e.g*. *Clostridium ljungdahlii, Clostridium autoethanogenum, Clostridium ragsdalei, Clostridium carboxidivorans* (Fernández-Naveira et al., 2017; Phillips et al., 2015). Recent research on CO, CO_2/H_2 and syngas fermentation has focused on the production of different end-products, such as ethanol, higher alcohols such as butanol or hexanol, 2,3-butanediol, biomethane or biopolymers, e.g., polyhydroxyalkanoates (Fernández-Naveira et al., 2017; Köpke et al., 2011; Lagoa-Costa et al., 2017; Navarro et al., 2016; Phillips et al., 2015). Many studies have been done with available pure cultures and only a few with mixed cultures (Singla et al., 2014; Xu et al., 2015). The main advantages in mixed culture fermentation are a lower energy consumtion and a better stability under environmental changes (Kleerebezem and van Loosdrecht, 2007). Another benefit is that the bioprocess works under non-sterile conditions. Accordingly, it is important to develop the implementation of biotechnological processes that work with mixed or enriched cultures, which own a higher microbial diversity.

Likewise, the overall reaction rate of syngas fermentation is limited by the slow gas–liquid mass transfer (Munasinghe and Khanal, 2010; Zhu et al., 2010), which results in low productivity on the end-products. Thus, the use of a nanomaterial that presents a high affinity to these gases (H_2, CO and CO_2) is particularly relevant. Carbon based materials are promising candidates due to their unique characteristics, such as their high chemical stability, low density, large-scale production suitability, wide range of synthesis approaches and structural shapes (Srinivas et al., 2010). Moreover, if the nanomaterial is a material with high conductivity, it can play a significant role in promoting the direct interspecies electron transfer (DIET). All these characteristics could stimulate the microorganisms involved in the syngas fermentation process, leading to higher yields of the end-products.

The aim of this work was to explore the use of conductive nanomaterials, such as reduced graphene oxide and reduced graphene oxide adorned with magnetite nanoparticles in order to investigate the production of volatile fatty acids, commodities that can present higher economic values, owing to their wide range of applications in the chemical industry.

2. Materials and Methods

2.1 Synthesis of nanomaterials

Magnetite nanoparticles (MNPs), reduced graphene oxide (rGO) and reduced graphene oxide adorned with magnetite nanoparticles (rGO-MNPs) were prepared as previously reported (Covarrubias-García et al., 2021, 2020). Briefly, MNPs were synthetized by chemical co-precipitation of Fe(II) and Fe(III) chloride salts (2:1), under a N_2 atmosphere at room temperature with the addition of NaOH (0.2N). MNPs were washed with Milli-Q water and separated with a magnet. Graphene oxide was prepared by the modified Hummer's method (Esfandiar et al., 2011) and the reduction of graphene oxide (rGO) was carried out with ethylene glycol at 110°C for 15 min. The preparation of the nanocomposite rGO-MNPs was carried out in a sonicator. The solution of MNPs was added dropwise to the solution of rGO that was stand inside a sonicator. MNPs relation to rGO was 10% (w/w). All nanomaterials were dried at 60°C overnight.

2.2 Mineral salt medium

Mineral unautoclaved medium was used as described by Covarrubias-García et al., (2020). The composition of the mineral salt medium was: (0.25 g) K_2HPO_4; (0.28 g) NH_4Cl; (0.83 g) $MgCl_2.6H_2O$; (0.01 g) $CaCl_2$; (2.5 g) $NaHCO_3$; and (0.1 g) of yeast extract. No vitamin solution was added, as some CO fermenting cultures have been shown to be able to metabolize gases in the absence of vitamins (Abubackar et al., 2015, Abubackar et al., 2016).

2.3 Inoculum

The inoculum used was anaerobic granular sludge from an anaerobic digester treating tequila *vinasse* obtained from the Casa Herradura tequila industry wastewater treatment plant, located in Guadalajara, Jalisco, Mexico.

2.4 Sludge acclimation

Sludge acclimation was carried out in 120 mL serological flasks sealed with rubber stoppers and aluminum rings (working volume of 80 mL). Flasks contained 32 mL of mineral medium and 48 mL of inoculum. The headspace was flushed with N_2 and the excess of N_2 was released to balance the system to ambient pressure with a needle connected to a deionized water solution. Then, the bottles were sparged each 2 or 3 days with custom-made artificial syngas mixture of CO, CO_2, H_2 and N_2 in the ratio 20:20:10:50 % v/v, respectively. Cultures were placed in a shaking incubator at 37°C and 150 rpm.

The consumption/production of H_2, CO, CH_4 and CO_2 was measured from the headspace of the bottles by gas chromatography to corroborate the acclimatization of the sludge.

2.5 Fermentation tests of acclimatized sludge provided with nanomaterial

Batch assays with nanomaterial were performed in 60 mL serological flasks, sealed with rubber stoppers and aluminum rings. The flasks contained 1.6 mL of the acclimatized sludge, and 18.4 mL of mineral medium. The final concentration was 3 g/L of volatile suspended solids in a working volume of 20 mL. Two concentrations of each nanomaterial were tested (50 and 100 mg/L). Assays were incubated under the same conditions as the acclimatized sludge (37°C, 150 rpm). CO, CO_2, H_2 and N_2 in the ratio 20:20:10:50 % v/v were added in the headspace at the beginning of the experiment in each treatment.

2.6 Analytical methods

Gas composition (H_2, CO, CH_4 and CO_2) was determined by gas chromatography with TCD detector 6890N (Agilent Technologies, Germany). The column used was

a Hayesep D (Alltech, Deerfield, Illinois, USA) with the following dimensions: 10' x 1/80'' x 0.085''. Temperatures of the injection port, oven and the detector were 250, 60 and 250°C, respectively. Nitrogen was used as carrier gas with a flow-rate of 12 mL/min. Liquid samples were centrifuged at 12000 rpm for 2 min to separate the sludge and the nanomaterial. Then the supernatant was filtered through a 0.22 membrane (Millipore, Bedford, Massachusetts, USA). The carboxylic acids (formic, acetic, propionic and butyric) of the filtered samples were quantified by capillary electrophoresis 1600A (Agilent Technologies, Germany) in the same run (Soga and Ross, 1999).

The dissolved iron Fe^{2+} of the medium was determined by ferrozine assay (Stookey, 1970). The complex obtained is measured by absorption at 562 nm in a spectrophotometer (Cary 60, Agilent Technologies). The calibration curve was performed as previously reported (Covarrubias-García et al., 2020). Fe^{2+} was measured in the fermentation assays of the nanomaterials that contained iron (magnetite and reduced graphene oxide adorned with magnetite nanoparticles). The electron shuttling capacity (ESC) was measured in the fermentation assays that were provided with the conductive materials (reduced graphene oxide and reduced graphene oxide adorned with magnetite nanoparticles. The ESC was determined according to methodologies previously reported (Covarrubias-García et al., 2020; Lovley et al., 1996; Valenzuela, Edgardo et al., 2017).

The pH of the medium was monitored with a potentiometer (Thermo Scientific ORION VERSTAR PRO).

3. Results and discussion

3.1 Acclimation

The gas composition in the headspace was analyzed when fresh syngas was added (day 39) and three days later (day 42). As can be seen in **Table 1**, H_2 and CO were totally and almost totally consumed, respectively, at day 42. However, CH_4 and CO_2 production was observed, with a volume produced of 12 and 4 mL, respectively.

Table 1. Headspace gas composition of sludge after 39 days of acclimation.

	H_2	CO	CH_4	CO_2
DAY	**mL**	**mL**	**mL**	**mL**
39	4.1±0.5	8.2±0.2	0.48±0.3	7.9±0.1
42	0±0.0	0.3±0.1	12.5±0.2	11.97±0.2

According with this results, it was opted to eliminate the remaining organic matter, which could be the reason of CO_2 and CH_4 production. This was done at day 46. The washing consisted in placing the sludge in 1.6 L of deionized water over a stirring rack for 12 minutes. Subsequently, the sludge and deionized water were passed through a 250 µm sieve to decant the excess of water and retain the sludge. This was carried out three consecutive times. Finally, the acclimatization process was mounted again as previously described.

Different strategies have been carried out to ferment C1 gases to ethanol and others metabolites, applying specific conditions such as the alternation of high and low pH values of the bioreactor medium or the addition of a specific inhibitor of methanogens (Chakraborty et al., 2019). In literature, several chemical substances have been reported to inhibit the CH_4 formation or methanogenic archaea with optimum inhibition concentrations (Ungerfeld et al., 2004; Valdez-Vazquez and Poggi-Varaldo, 2009; Xu et al., 2010). Among these chemicals, 2-bromoethanesulfonate (BES) and chloroform ($CHCl_3$) are the most common additives due to their high effectiveness and wide availability (Xu et al., 2010). According, $CHCl_3$ was chosen as an additive to inhibit the CH_4 formation in the acclimatized sludge. The concentration added was 40 µL of $CHCl_3$, which corresponds to 0.05% (v/v) of the working volume. This percentage was selected according to literature values that effectively inhibit CH_4 production without affecting the efficiency of hydrolysis and acidification (Xu et al., 2010). The effect of the addition of $CHCl_3$ was observed in the acclimatized sludge for 17 days (corresponding to day 49 to 66). For this, the atmosphere of the bottles was replaced with pure N_2 and the headspace gas composition was measured to visualize the CH_4 inhibition. A control was carried out without the addition of $CHCl_3$.

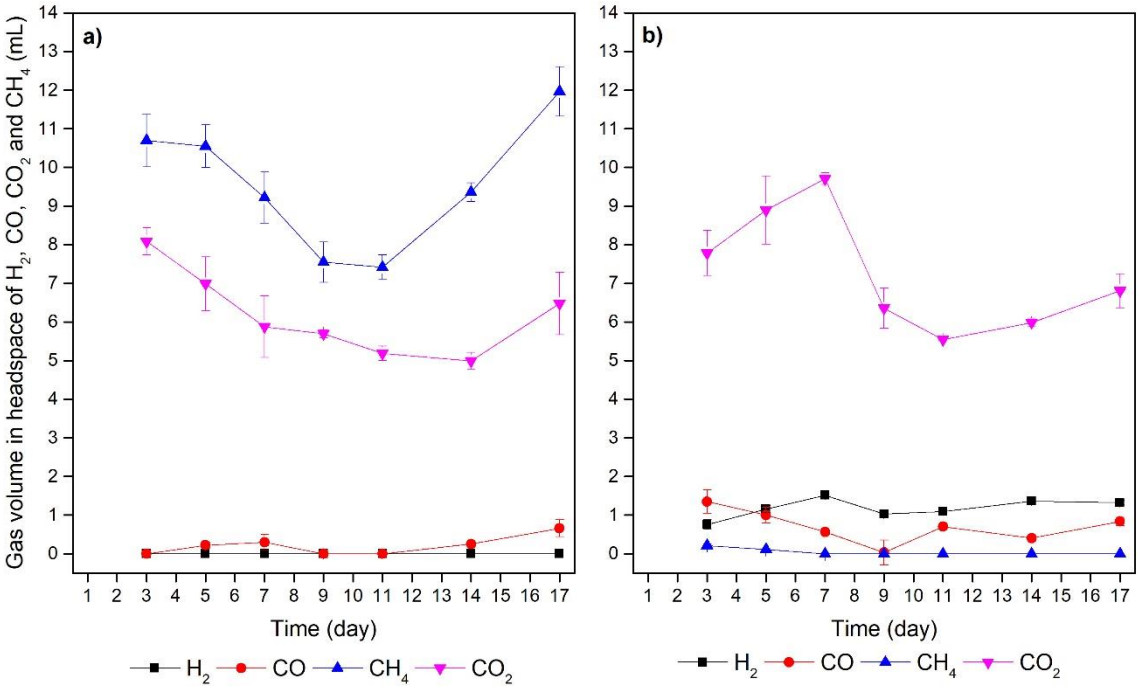

Figure 1. Headspace gas composition, a) without the addition of $CHCl_3$ and, b) with the addition of 40 µL of $CHCl_3$ of the acclimatized sludge.

Figure 1a) shows the flasks that were not exposed to $CHCl_3$. CH_4 production reached a volume as high as 12±0.6 mL, while CO_2 production decreased up to values of 6.5±0.8 mL, both at day 17. Regarding H_2 and CO, these gases did not seem to change along the time. The decrement of CH_4 from the beginning to day 9 could be attributed to the lack of substrate; then, the increment from day 10 to 17 it may be due to the endogenous respiration from the remaining organic matter. Figure 1b) clearly shows that the addition of $CHCl_3$ inhibits the CH_4 production. Also, this graph does not show an evolution of H_2 and CO content along the time. Contrary to what was expected, CO_2 increased until day 7 and then dropped until values around 6.8±0.4 mL at the end of the assay. Interestingly, the CO_2 content at both treatments was very similar at the end of the assay, with values around 6 mL of CO_2. This suggest that amount of $CHCl_3$ added was not toxic to the to the consortium, since CH_4 production was inhibited and the CO_2 was not lower than the control.

The results of the assays of the acclimatized sludge that was not exposed to $CHCl_3$ can be explained by the different metabolic pathways presented in **Figure 2**. This Figure also shows the pathways that can be blocked by the presence of inhibitor $CHCl_3$, totally or partially (crossed out lines). Since, the CO_2 consumption was not observed we can assume that CH_4 production may come from CO and also by acetate as an intermediate metabolite. This pathway has been previously reported (Navarro et al., 2014; O';Brien et al., 1984; Sipma et al., 2003). Also, H_2 consumption is linked to CH_4 production by hydrogenotrophic methanogenesis pathway. At this point, the acclimatization with syngas is not complete, since CO_2 has not been consumed. CO_2 is a fully oxidized molecule and can only act as a carbon source, thus, the consumption of CO_2 would be feasible by supplying additional reducing power, i.e. H_2, or CO. It is very likely that from day 6 ahead some hydrogenotrophic methanogens are acting with the help of H_2 or CO to form CH_4. H_2 is an electron donor and therefore acts as an energy source, CO can act both as an energy source and a carbon source. Overall, this allows a diverse consortium of microbes to grow syntrophically on this gaseous substrate depending on their preferred energy and carbon source and the occurring metabolites.

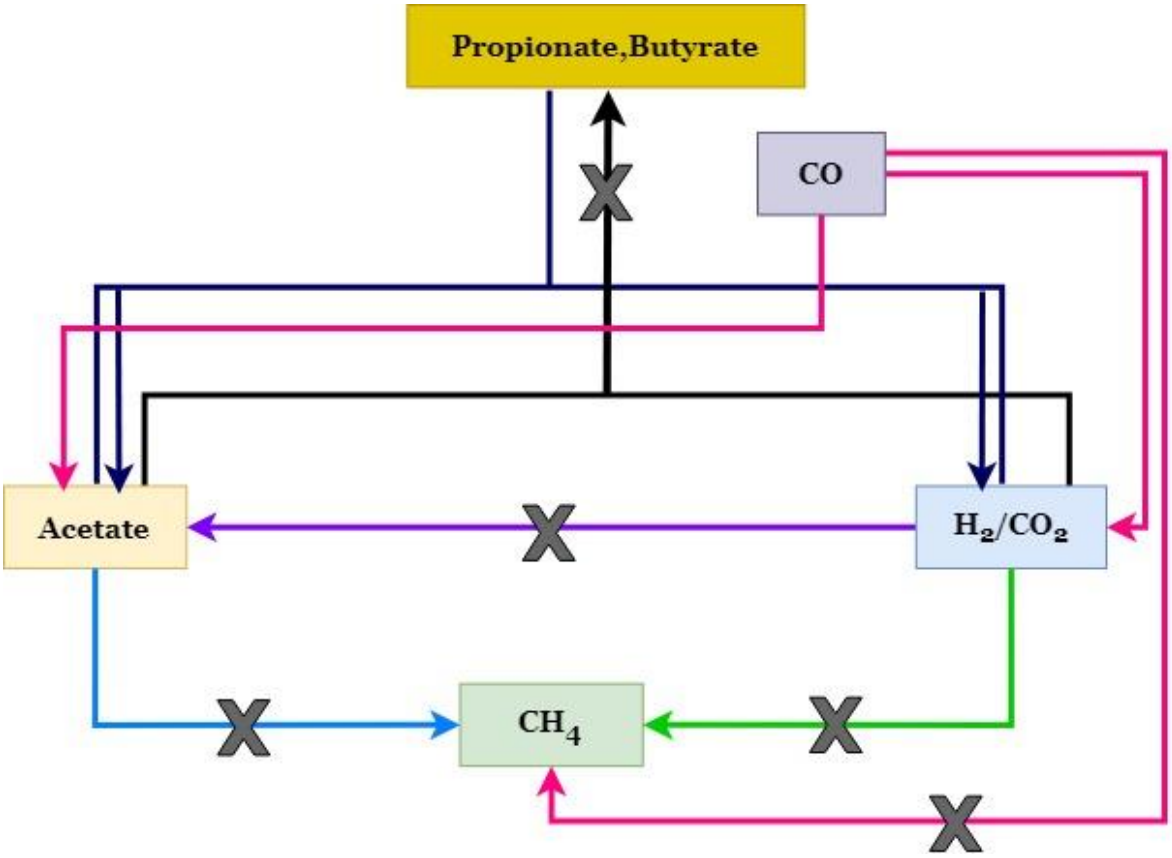

Figure 2. Carbon flow scheme to CH_4. The crossed out lines indicate the totally or partially blocked pathways in presence of $CHCl_3$ inhibitor.

Regarding the acclimatized sludge that were exposed to $CHCl_3$, we can discuss the following. $CHCl_3$ is known to block the function of conrrinoid enzymes and to inhibit *methyl-coenzyme M* reductase of methanogens. It not only inhibits methanogenesis, but also inhibits partially acetate-dependent reduction and probably acetogenesis (Conrad and Klose, 2000). In addition, it has been reported to inhibit H_2 consumption without affecting CO_2 (Conrad and Klose, 2000). All these statements are in agreement with the results of the assays of acclimatized sludge that were exposed to $CHCl_3$ in this study.

Subsequently of corroborate the inhibition of CH_4 by $CHCl_3$ addition; fresh syngas were added to those bottles at day 18 (corresponds to 67 days of acclimatization). The syngas composition in the headspace of these assays is depicted in **Figure 3**.

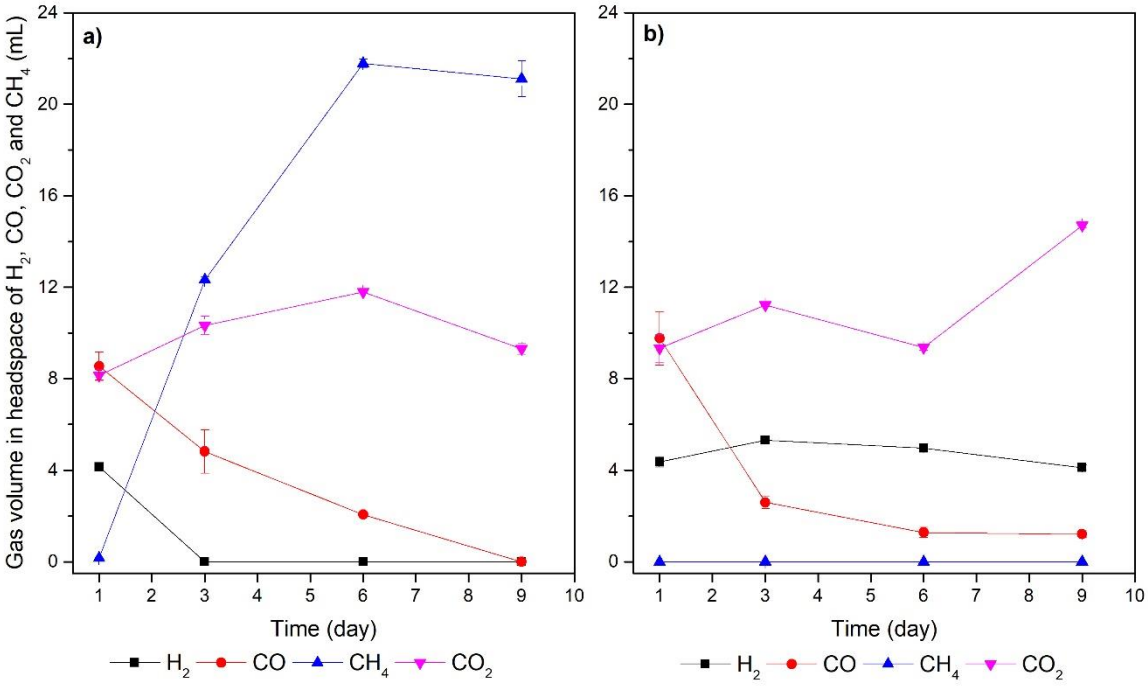

Figure 3. Headspace gas composition. Day 1 corresponds to fresh syngas composition.

a) Assays that were not exposed to $CHCl_3$ and, b) assays that were exposed to 40 µL of $CHCl_3$.

As depicted in Figure 3a), H_2 was completed depleted at day 3 in the assays that were not exposed to $CHCl_3$. Contrary, H_2 was not consumed in the assays that were exposed to $CHCl_3$. CO was consumed in both treatments, being completely depleted at day 9 in the assays without $CHCl_3$ addition, and presenting the lower value of 1.2±0.2 mL in the treatment with $CHCl_3$ addition at day 6. CH_4 produced presented a value as high as 21.8±0.2 mL in the assays without $CHCl_3$ at day 6 (Figure 3a) and was not produced in the assays with $CHCl_3$ (Figure 3b). Regarding CO_2, this gas is still present in the two treatments.

3.2 Fermentation of syngas provided with nanomaterials

Fermentation assays of syngas were carried out with the addition of MNPs, rGO and rGO-MNPs at two concentrations (50 and 100 mg/L) and the acclimatized sludge

that was exposed to $CHCl_3$. Headspace gas composition of the treatments are shown in **Figure 4**.

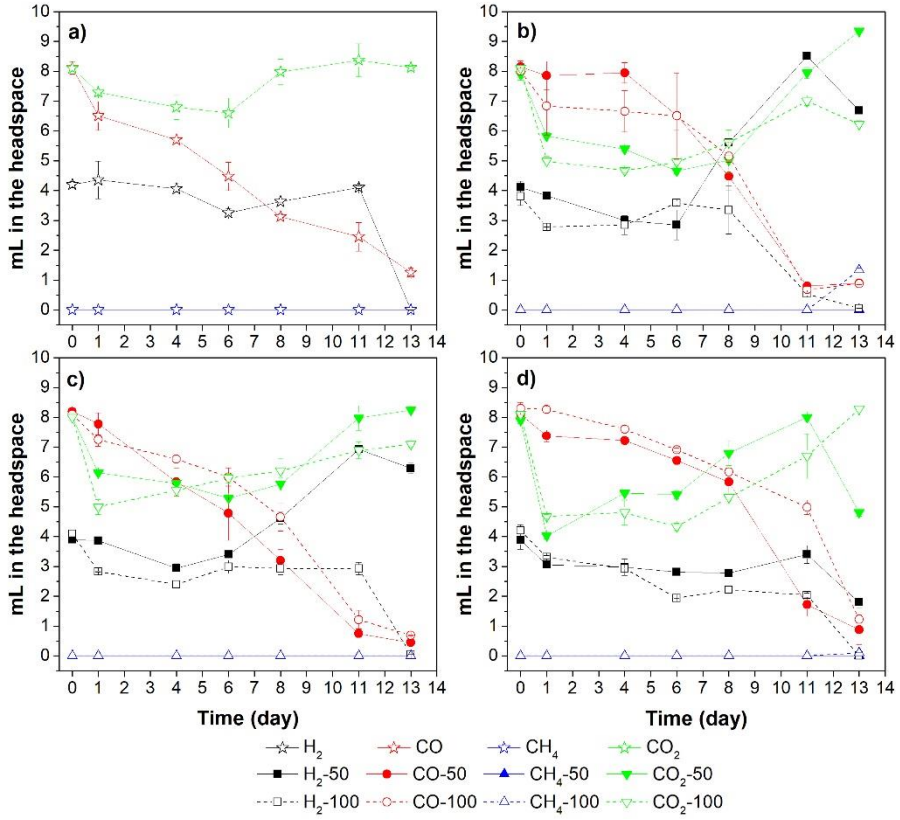

Figure 4. Headspace gas composition of syngas fermentation with nanomaterials. a) Control, b) Magnetite, c) Reduced graphene oxide and d) Reduced graphene oxide adorned with magnetite. 50= 50 mg/L and 100= 100 mg/L of nanomaterial, respectively

As it is observed, H_2 was completely consumed in the control and in treatments with 100 mg/L at day 13 for MNPs, rGO and rGO-MNPs (Figure 4a-d). On the other hand, in the treatment with 50 mg/L of MNPs (Figure 4b), H_2 started to increase form day 6 onwards until day 11 (8.5±0.1 mL) and then dropped. H_2 also presented the higher value, 6.9±0.1 and 5.9±0.5 mL, for 50 mg/L of rGO (Figure 4c) and rGO-MNPs (Figure 4d), respectively, at day 11 and then dropped. As can be seen, CO was almost depleted in all treatments; the lowest values of CO for 50 mg/L of MNPs (Figure 4b), and rGO (Figure 4c) were reached at day 11, whereas, the lowest values for 100 mg/L of MNPs (Figure 4b), rGO (Figure 4c), rGO-MNPs (Figure 4d) and the

control (Figure 4a) were reached at day 13. For 50 mg/L of rGO-MNPs (Figure 4d), CO increased at day 13 and then dropped until the end of the assay. According to literature, fermentation with syngas containing CO, CO_2 and H_2, typically shows simultaneous uptake of both CO and H_2 (Maddipati et al., 2011; Phillips et al., 1993), which happens in the present study until day 13 for control and most of the treatments. Additionally, it has been reported that, CO was always preferred over H_2 as substrate for syngas fermentation by thermodynamics study (Hu et al., 2011), which is in agreement since, the consumption of CO is faster than the H_2 consumption.

Regarding CO_2 profile, CO_2 did not change significantly for control (Figure 4a) until day 13, then dropped. The treatments with all the nanomaterials at both concentration disclosed a CO_2 consumption until day 8 for 50 mg/L of MNPs, rGO; until day 1 for 100 mg/L of MNPs, rGO and rGO-MNPs; and until day 6 for 50 mg/L of rGO-MNPs. Onwards those days in each treatment, CO_2 increased until day 13 and then dropped. Interestingly, CO_2 was lower during the assay compared with the control until day 8.

As can be seen, CO consumption was higher in the control than the treatments with nanoparticles until day 8. On the other hand, for H_2 and CO_2, their consumption was higher in the treatments with nanomaterial than the control until day 11. This could be explained due to the solubility of the gases and the hydrophobic nature of the nanomaterials. The Henry´s law constant are: 140262, 121561 and 4240 kPa L/mol for H_2, CO and CO_2, respectively, at 37°C (Hougen et al., 1954).

Calculating the solubility from saturated concentration of the pure gas in water at 100 kPa, it is obtained: 0.00071, 0.00082 and 0.0236 mol/L, for H_2, CO and CO_2, respectively. Thus, H_2 and CO present a similar solubility, whereas CO_2 is 33 and 32 times more soluble in water than H_2 and CO, respectively. Likewise, the higher decrease of H_2 could be explained by the hydrophobic nature of the nanomaterials. The sorption capacity of H_2 of the nanomaterials used in the present study and the same mineral medium are presented in **Table 2**. As can be seen, all used nanomaterials present a sorption capacity for H_2 being the lower for MNPs, then rGO-MNPs and finally the higher Q for rGO. The difference in Q are attributed mainly

to agglomeration. The main benefit of the use of nanomaterials that present a Q for a substrate, i.e. H_2, is that they can act as vectors transfer where H_2 can be released continuously for microbial consumption, leading to a new pseudo-equilibrium of adsorption and desorption and thus improving the process.

Table 2. Sorption capacity (Q) of H_2 in mineral medium with nanoparticles (Covarrubias-García et al., 2020).

Nanomaterial	Concentration	Q
	mg/L	mg H_2/g sorbent
MNPs	50	104.30
	100	59.60
rGO	50	572.97
	100	225.07
rGO-MNPs	50	326.96
	100	193.26

Regarding the CH_4, this gas continued to be inhibited by the $CHCl_3$ action until day 11 for 100 mg/L of MNPs and until day 13 for all other treatments with nanomaterials including the control.

3.2.1 Volatile fatty acid profile of fermentation of syngas provided with nanomaterials

Since, the aim of this work is to produce metabolites of interest by syngas fermentation, and it has been reported that $CHCl_3$ can stimulate the production of propionate and butyrate on rice roots incubated under anoxic conditions (Conrad and Klose, 2000), the following experiments were to analyze the volatile fatty acids (VFAs) profile from the syngas fermentation process of previous experiment (Fermentation tests of acclimatized sludge provided with nanomaterial).

As can be observed at Figure 5a), acetic, propionic and butyric acids were produced from day 4 onwards in the control. Acetic acid was the commodity that was produced at higher amount (470.06±5.2 mg/L) at day 13. Propionic acid did not change significantly from day 6 ahead; the highest amount of propionic reached a value of 104.7±4.0 mg/L. Butyric acid reached its higher at the end of the assay with a value

at 115.7±8.2 mg/L. Formic acid was consumed along the kinetic assay, reaching the lowest value at 253.4±4.7 mg/L at day 13, then increased until the end. Acetate can be syntrophically oxidized to formic acid of H_2/CO_2, and subsequently converted to CH_4 (Tabatabaei et al., 2010). This could be the reason of the increment of formic acid, the decrement of acetic acid and the production of CH_4 at day 25.

Figure 5b) shows the VFA profile of the assays provided with 50 and 100 mg/L of MNPs. Formic acid presented the lowest concentration of 220±7.2 mg/L at day 11 for 50 mg/L of MNPs and 240.0±9.6 mg/L at day 6 for 100 mg/L of MNPs; then, formic increased. Regarding the other VFAs, acetic, propionic and butyric acids were different from zero compared to control until day 4. Assays provided with 50 mg/L of MNPs presented a concentration of 100.8±9.0 mg/L of acetic, 84.8±6.5 of propionic and 130.1±7.4 mg/L of butyric. Whereas, assays provided with 100 mg/L of MNPs presented a concentration of 130.25±8.26 mg/L of acetic, 48.3±5.3 of propionic and 48.7.12±2.1 mg/L of butyric. All these acids dropped at day 6, but then increased again with values very similar of day 4, except of acetic acid. Acetic acid presented its highest concentration at day 13 for 50 mg/L of M (290.1±8.7) and at day 11 for 100 mg/L of MNPs (309.3±9.9 mg/L). Such values are lower than the control, thus the addition of 50 or 100 mg/L of MNPs is not improving the process for acetic production comparing with the control. However, values of propionic and butyric are higher than the control the first 4 days.

Figure 5c) shows the VFA profile of the assays provided with 50 and 100 mg/L of rGO. Acetic and propionic acids were different from zero compared with the control. Butyric acid was very close to zero for 50 and 100 mg/L of rGO along the assay. Acetic acid was the commodity that was produced at higher amounts; 195.3±6.7 and 398.1±20.4 mg/L for 50 mg/L of rGO at day 13 and 25, respectively and 620.2±9.7 and 229.6±5.1 mg/L for 100 mg/L of rGO at day 13 and 25, respectively. Formic acid was also consumed until day 6; for 50 mg/L of rGO, formic acid changed slightly after day 6. For 100 mg/L of rGO, formic acid increased presenting its highest value of 616.1±15.3 mg/L, then dropped.

Figure 5d) depicts the VFA profile of syngas fermentation of assays provided with 50 and 100 mg/L of rGO-MNPs. As can be seen, formic acid went up and down, and

at the end reached the lowest value of 298.5±10.7 mg/L for 50 mg/L of rGO-MNPs and 267.8±13.1 mg/L for 100 mg/L at day 25. Acetic acid was different from zero compared with the control until day 6 for both concentration of rGO-MNPs, then increased, reaching a value as high as 260.4±15.5 mg/L at day 13 for 50 mg/L of rGO-MNPs (then dropped) and the highest of 578.4±13.3 mg/L at day 13 for 100 mg/L of rGO-MNPs (then dropped). Propionic and butyric acids were not very different from zero compared with the control until day 6, then increased slightly.

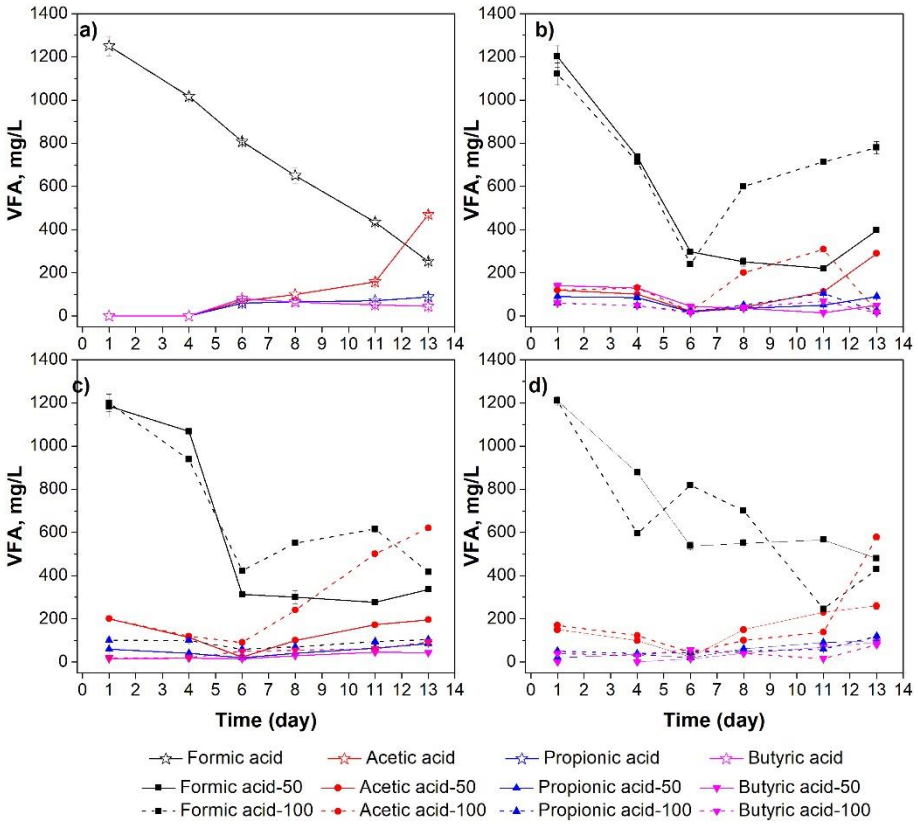

Figure 5. VFA profile: a) Control, b) Magnetite, c) Reduced graphene oxide and d) Reduced graphene oxide adorned with magnetite. 50= 50 mg/L and 100= 100 mg/L of nanomaterial, respectively.

A 32% higher production of acetic acid was presented for 100 mg/L of rGO with a value of 620.2±9.7 mg/L and an improvement of 23% was presented for 100 mg/L of rGO-MNPs with a value of 578.4±13.3 mg/L, compared with the control, both at day 13. Acetic acid is a very important commodity, and is used as a starting material for vinyl acetate and acetic anhydride synthesis (Yoneda et al., 2001).

As mention above, the main advantages in mixed culture fermentation is that they consume less power and is more stable to environmental changes (Kleerebezem and van Loosdrecht, 2007). Mixed culture syngas fermentations for the production of ethanol and acetic acid and conversion of organic acids have been previously reported (Liu et al., 2014a, 2014b). For instance, Liu et al., (2014b) found that the mixed culture converted 50% more carboxylic acid into their corresponding alcohols than the monocultures. They reached concentration of acetic acid of 4.2 g/L in a yeast extract medium and 6.4 g/L in a medium with corn steep liquor of acetic acid at 80 h fermentation in semi-continuous mode. After reaching this maximum concentration, acetic acid slowly decreased around 100 h due to acetic acid conversion to ethanol. On the other hand, Liu et al., (2014a) obtained a mixed culture that produced a maximum of 8 g/L of ethanol, 6 g/L of propanol and 1 g/L of n-butanol in a continuous reactor and 3.4 g/L of acetic acid.

The pH graph of the fermentation of acclimatized sludge provided with nanomaterials is presented in **Figure 6**. As can be seen, the pH variation did not change along the assay. This could be attributed to the low concentration of the formed products (i.e. acetate, propionate and butyrate). However, looking closer, the drop of pH at day 6 matches with the day were a higher volume of CO_2 was measured in the headspace (Figure 4c). This can be explained by the release of CO_2 of the liquid medium, thus the pH increased after day 6. At the same time, the decrease in pH until day 6 and then the increase onwards matches with the production of acetic acid and the consumption of formic acid until day 13 in all treatments and the control (Figure 5). The decrease in pH have been reported by the production of acetic acid in syngas fermentation previously (Liu et al., 2014b), but in the present study, we cannot observe such decrement due to the consumption of formic acid. According to this, the system present a dynamic behavior where the microorganisms produce and consume metabolites that can change the pH.

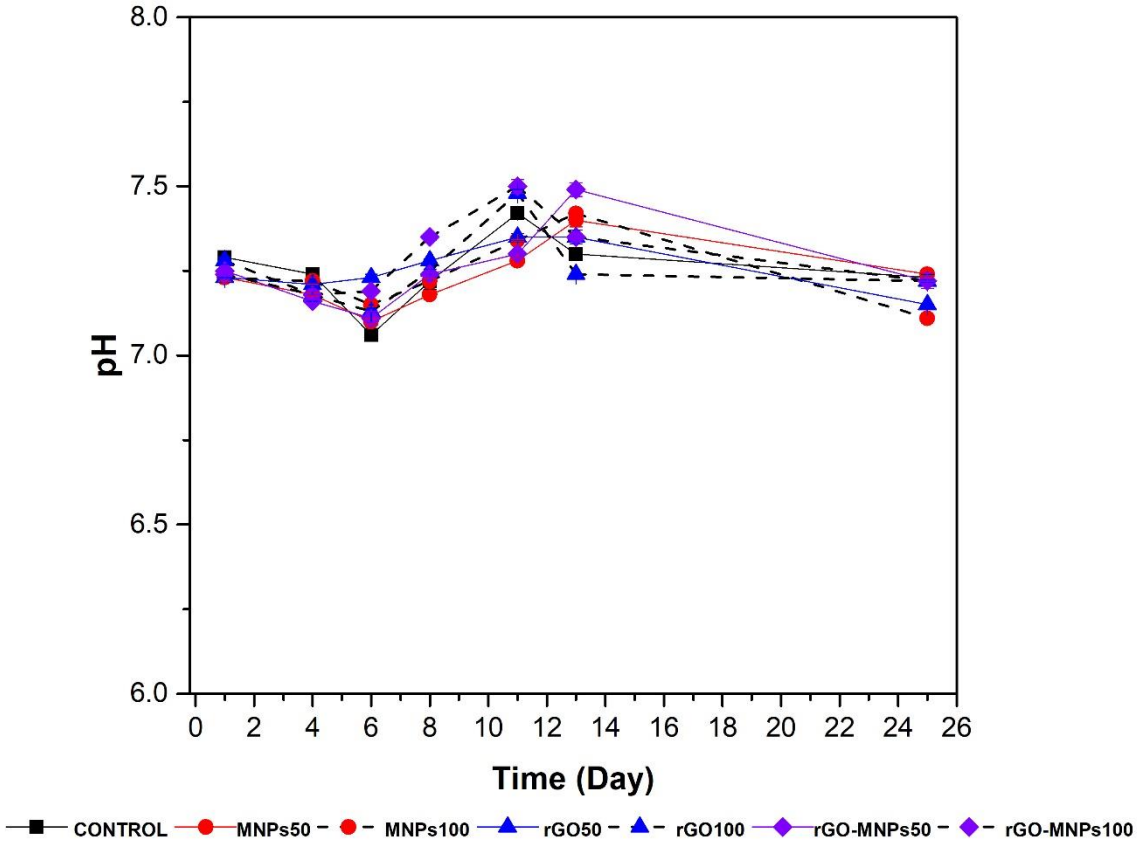

Figure 6. pH of assays of acclimatized sludge provided with nanomaterials. MNPs=assays of magnetite, rGO=assays of reduced graphene oxide, rGO-MNPs=assays with reduced graphene oxide adorned with magnetite nanoparticles. 50= 50 mg/L and 100= 100 mg/L of nanomaterial, respectively.

3.2.3 Electron shuttling capacity and dissolved Fe^{2+} in syngas fermentation tests provided with nanomaterial

Figure 7 shows the dissolved iron Fe^{2+} measured in the syngas fermentation assays provided with MNPs and rGO-MNPs (left axis). Also, shows the electron shuttling capacity (ESC) measured in the syngas fermentation assays provided with rGO and rGO-MNPs (right axis).

Dissolved Fe^{2+} ranged from 15.25±1.25 mg/L (day 1) to 40.25±1.28 mg/L (day 25) and 33.26±2.1 mg/L (day 1) to 50.15±1.78 mg/L (day 25) for 50 and 100 mg/L of MNPs, respectively. For 50 mg/L of rGO-MNPs, the dissolved Fe^{2+} ranged from

9.44±0.88 mg/L (day 1) to 30.26±1.58 mg/L (day 25). Finally, dissolved Fe^{2+} ranged from 20.45±0.73 (day 1) to 37.15±1.79 mg/L (day 25) for 100 mg/L of rGO-MNPs. Makes sense that rGO-MNPs released a lower amount of Fe^{2+} into the medium, since magnetite is decorating the rGO. It has been reported that Fe^{2+} released in the media form an adorned reduced graphene oxide decorated with magnetite nanoparticles act like a dietary supply for the microorganisms improving their microbial activity for biogas enrichment (Covarrubias-García et al., 2020), but not for syngas fermentation. In syngas fermentation process efficient mechanisms for nutrient uptake are required for the microorganisms to thrive especially in the environment with very low nutrient concentrations (Phillips et al., 2017). Therefore, the use of a nanomaterial that can improve the process by dosing a micronutrient could be attractive. The micronutrient such as Fe^{2+} act as a catalyst to the enzymes improving the kinetics of the metabolites involved in the process.

ESC is measured indirectly by the total amount of Fe^{3+} reduced to Fe^{2+}, which is the total electron accepting capacity that the material can provide to the process. Results showed that the higher ESC was presented at day 13 for all treatments (Figure 7). All values of ESC for 50 mg/L of rGO were lower than the ESC values of 100 mg/L of rGO. Moreover, all values of ESC of rGO-MNPs were higher than ESC values of rGO at the two concentration, and the ESC values of 100 mg/L of rGO-MNPs were higher than those values of ESC with 50 mg/L of rGO-MNPs.

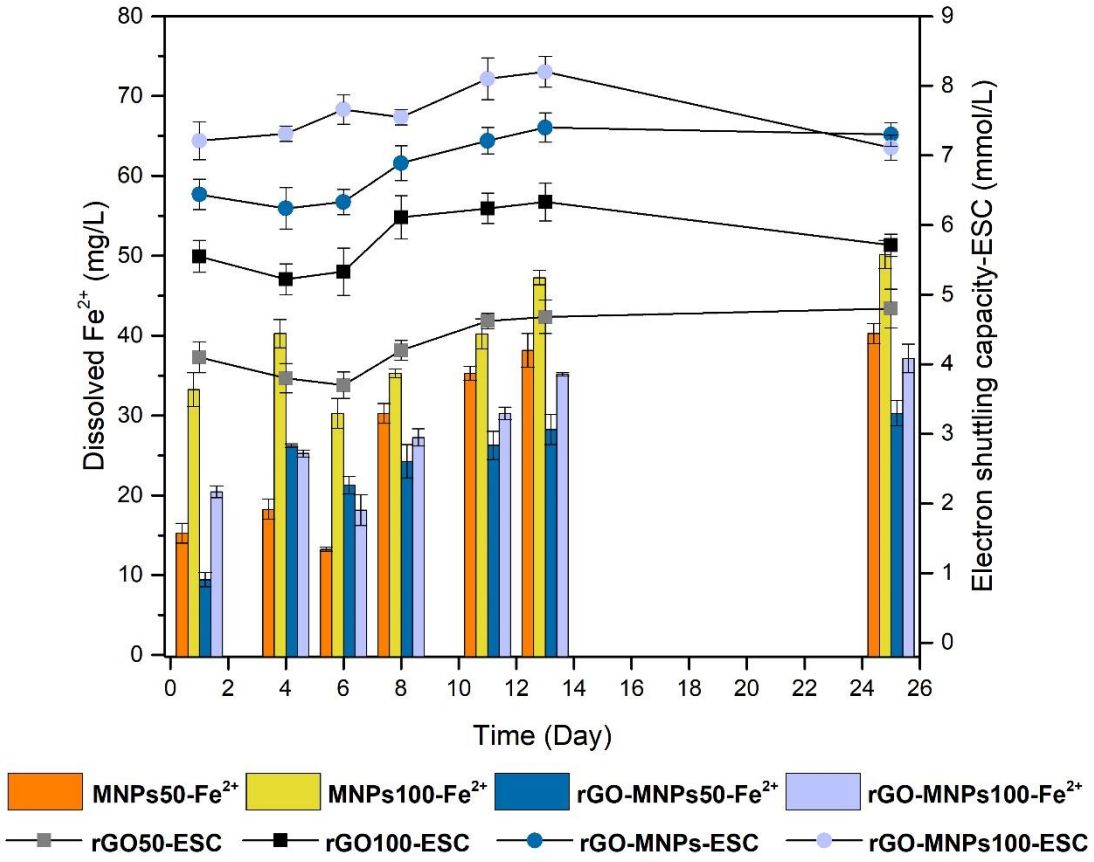

Figure 7. Left axis, dissolved iron Fe^{2+} in the syngas fermentation assays provided with 50 and 100 mg/L of MNPs and rGO-MNPs. Right axis, electron shuttling capacity (ESC) of syngas fermentation assays provided with 50 and 100 mg/L of rGO and rGO-MNPs.

As shown in Figure 7, rGO-MNPs presented higher ESC than rGO alone, which confirms that MNPs nanoparticles can improve the redox properties of rGO. This observation has been previously reported by Covarrubias-García et al., (2020) where de decoration of reduced graphene oxide with magnetite improved the ESC and thus promoted the electron transfer in a enrichment process of CH_4 provided with graphene material. Moreover, it has been established that, the DIET process can be facilitated by magnetite particles. Magnetite nanoparticles, which are smaller than microbial cells can attach to individual cells and the multiple partner cells can attach to conductive carbon materials, such as granular activated carbon, biochar and carbon cloth (Chen et al., 2014a, 2014b; F. Liu et al., 2012). Therefore as both

rGO and rGO-MNPs can shuttle electrons between them and the microorganisms due to their redox properties, enhancing the capacity of microorganisms to reduce electron acceptors, such as insoluble Fe^{3+} oxide, organic matter or H_2.

4. Conclusions

Chloroform inhibited CH_4 production in the acclimatized sludge. However, chloroform did not help to CO_2 consumption. Even if CO_2 is not being consumed by microorganisms, acclimatized sludge is producing fatty acids (i.e., acetate, propionate and butyrate). The addition of reduced graphene oxide (rGO) and reduced graphene oxide adorned with magnetite nanoparticles (rGO-MNPs) improved the production of acetic acid, 32% with 100 mg/L of rGO and 23% with 100 mg/L of rGO-MNPs, compared with the control at day 13. rGO and rGO-MNPs could be an attractive alternative to enhance the production of acetic acid. The improvement of the syngas fermentation process with those materials is linked to their unique properties, the higher electron shuttling capacity, the sorption capacity and the dosing of dissolved iron, which boosted the microbial activity.

5. Supplementary data

6. References

Abubackar, H.N., Veiga, M.C., Kennes, C., 2011. Biological conversion of carbon monoxide: rich syngas or waste gases to bioethanol. Biofuels, Bioprod. Biorefining 5, 93–114. https://doi.org/10.1002/bbb.256

Acharya, B., Roy, P., Dutta, A., 2014. Review of syngas fermentation processes for bioethanol. Biofuels 5, 551–564. https://doi.org/10.1080/17597269.2014.1002996

Bengelsdorf, F.R., Straub, M., Dürre, P., 2013. Bacterial synthesis gas (syngas) fermentation. Environ. Technol. 34, 1639–1651. https://doi.org/10.1080/09593330.2013.827747

Chakraborty, S., Rene, E.R., Lens, P.N.L., Veiga, M.C., Kennes, C., 2019. Enrichment of a solventogenic anaerobic sludge converting carbon monoxide

and syngas into acids and alcohols. Bioresour. Technol. 272, 130–136. https://doi.org/10.1016/j.biortech.2018.10.002

Chen, S., Rotaru, A.E., Liu, F., Philips, J., Woodard, T.L., Nevin, K.P., Lovley, D.R., 2014a. Carbon cloth stimulates direct interspecies electron transfer in syntrophic co-cultures. Bioresour. Technol. 173, 82–86. https://doi.org/10.1016/j.biortech.2014.09.009

Chen, S., Rotaru, A.E., Shrestha, P.M., Malvankar, N.S., Liu, F., Fan, W., Nevin, K.P., Lovley, D.R., 2014b. Promoting interspecies electron transfer with biochar. Sci. Rep. 4. https://doi.org/10.1038/srep05019

Conrad, R., Klose, M., 2000. Selective inhibition of reactions involved in methanogenesis and fatty acid production on rice roots. FEMS Microbiol. Ecol. 34, 27–34. https://doi.org/10.1016/S0168-6496(00)00071-4

Covarrubias-García, I., Osorio-González, C.S., Avalos Ramírez, A., Rodríguez-López, J.L., Kaur Brar, S., Arriaga, S., 2021. Microporous and Mesoporous Materials Nanostructured complex of reduced graphene oxide adorned with magnetite as an adsorbent for inhibitor compounds in wood hydrolysates 310. https://doi.org/10.1016/j.micromeso.2020.110592

Covarrubias-García, I., Quijano, G., Aizpuru, A., Sánchez-García, J.L., Rodríguez-López, J.L., Arriaga, S., 2020. Reduced graphene oxide decorated with magnetite nanoparticles enhance biomethane enrichment. J. Hazard. Mater. 397, 1–12. https://doi.org/10.1016/j.jhazmat.2020.122760

Drzyzga, O., Revelles, O., Durante-Rodríguez, G., Díaz, E., García, J.L., Prieto, A., 2015. New challenges for syngas fermentation: Towards production of biopolymers. J. Chem. Technol. Biotechnol. 90, 1735–1751. https://doi.org/10.1002/jctb.4721

Esfandiar, A., Akhavan, O., Irajizad, A., 2011. Melatonin as a powerful bio-antioxidant for reduction of graphene oxide. J. Mater. Chem. 21, 10907. https://doi.org/10.1039/c1jm10151j

Fernández-Naveira, Á., Veiga, M.C., Kennes, C., 2017. H-B-E (hexanol-butanol-ethanol) fermentation for the production of higher alcohols from syngas/waste gas. J. Chem. Technol. Biotechnol. 92, 712–731.

https://doi.org/10.1002/jctb.5194

Hougen, O.A., Watson, K.M., Ragatz, R.A., 1954. Chemical Process Principles. Wiley, New York, USA.

Hu, P., Bowen, S.H., Lewis, R.S., 2011. A thermodynamic analysis of electron production during syngas fermentation. Bioresour. Technol. 102, 8071–8076. https://doi.org/https://doi.org/10.1016/j.biortech.2011.05.080

Kleerebezem, R., van Loosdrecht, M.C.M., 2007. Mixed culture biotechnology for bioenergy production. Curr. Opin. Biotechnol. 18, 207–212. https://doi.org/https://doi.org/10.1016/j.copbio.2007.05.001

Köpke, M., Mihalcea, C., Liew, F.M., Tizard, J.H., Ali, M.S., Conolly, J.J., Al-Sinawi, B., Simpson, S.D., 2011. 2,3-Butanediol production by acetogenic bacteria, an alternative route to chemical synthesis, using industrial waste gas. Appl. Environ. Microbiol. 77, 5467–5475. https://doi.org/10.1128/AEM.00355-11

Lagoa-Costa, B., Abubackar, H.N., Fernández-Romasanta, M., Kennes, C., Veiga, M.C., 2017. Integrated bioconversion of syngas into bioethanol and biopolymers. Bioresour. Technol. 239, 244–249. https://doi.org/10.1016/j.biortech.2017.05.019

Li, Z., Han, C., Gu, T., 2018. Economics of biomass gasification: A review of the current status. Energy Sources, Part B Econ. Planning, Policy 13, 137–140. https://doi.org/10.1080/15567249.2017.1410593

Lin, C.-L., Weng, W.-C., 2017. Effects of different operating parameters on the syngas composition in a two-stage gasification process. Renew. Energy 109, 135–143. https://doi.org/https://doi.org/10.1016/j.renene.2017.03.019

Liu, F., Rotaru, A.E., Shrestha, P.M., Malvankar, N.S., Nevin, K.P., Lovley, D.R., 2012. Promoting direct interspecies electron transfer with activated carbon. Energy Environ. Sci. 5, 8982–8989. https://doi.org/10.1039/c2ee22459c

Liu, K., Atiyeh, H.K., Stevenson, B.S., Tanner, R.S., Wilkins, M.R., Huhnke, R.L., 2014a. Continuous syngas fermentation for the production of ethanol, n-propanol and n-butanol. Bioresour. Technol. 151, 69–77. https://doi.org/10.1016/j.biortech.2013.10.059

Liu, K., Atiyeh, H.K., Stevenson, B.S., Tanner, R.S., Wilkins, M.R., Huhnke, R.L.,

2014b. Mixed culture syngas fermentation and conversion of carboxylic acids into alcohols. Bioresour. Technol. 152, 337–346. https://doi.org/10.1016/j.biortech.2013.11.015

Lovley, D.R., Coates, J.D., Blunt-Harris, E.L., Phillips, E.J.P., Woodward, J.C., 1996. Humic substances as electron acceptors for microbial respiration. Lett. Nat. 445–446.

Maddipati, P., Atiyeh, H.K., Bellmer, D.D., Huhnke, R.L., 2011. Ethanol production from syngas by Clostridium strain P11 using corn steep liquor as a nutrient replacement to yeast extract. Bioresour. Technol. 102, 6494–6501. https://doi.org/https://doi.org/10.1016/j.biortech.2011.03.047

Mishra, A., Gautam, S., Sharma, T., 2018. Effect of operating parameters on coal gasification. Int. J. Coal Sci. Technol. 5, 113–125. https://doi.org/10.1007/s40789-018-0196-3

Munasinghe, P.C., Khanal, S.K., 2010. Biomass-derived syngas fermentation into biofuels: Opportunities and challenges. Bioresour. Technol. 101, 5013–5022. https://doi.org/https://doi.org/10.1016/j.biortech.2009.12.098

Navarro, S.S., Cimpoia, R., Bruant, G., Guiot, S.R., 2016. Biomethanation of syngas using anaerobic sludge: Shift in the catabolic routes with the CO partial pressure increase. Front. Microbiol. 7, 1–13. https://doi.org/10.3389/fmicb.2016.01188

Navarro, S.S., Cimpoia, R., Bruant, G., Guiot, S.R., 2014. Specific inhibitors for identifying pathways for methane production from carbon monoxide by a nonadapted anaerobic mixed culture. Can. J. Microbiol. 60, 407–415. https://doi.org/10.1139/cjm-2013-0843

O';Brien, J.M., Wolkin, R.H., Moench, T.T., Morgan, J.B., Zeikus, J.G., 1984. Association of hydrogen metabolism with unitrophic or mixotrophic growth of Methanosarcina barkeri on carbon monoxide. J. Bacteriol. 158, 373 LP – 375.

Phillips, J.R., Atiyeh, H.K., Tanner, R.S., Torres, J.R., Saxena, J., Wilkins, M.R., Huhnke, R.L., 2015. Butanol and hexanol production in Clostridium carboxidivorans syngas fermentation: Medium development and culture techniques. Bioresour. Technol. 190, 114–121.

https://doi.org/10.1016/j.biortech.2015.04.043

Phillips, J.R., Huhnke, R.L., Atiyeh, H.K., 2017. Syngas fermentation: A microbial conversion process of gaseous substrates to various products. Fermentation 3. https://doi.org/10.3390/fermentation3020028

Phillips, J.R., Klasson, K.T., Clausen, E.C., Gaddy, J.L., 1993. Biological production of ethanol from coal synthesis gas. Appl. Biochem. Biotechnol. 39, 559–571. https://doi.org/10.1007/BF02919018

Singla, A., Verma, D., Lal, B., Sarma, P.M., 2014. Enrichment and optimization of anaerobic bacterial mixed culture for conversion of syngas to ethanol. Bioresour. Technol. 172, 41–49. https://doi.org/10.1016/j.biortech.2014.08.083

Sipma, J., Lens, P.N.L., Stams, A.J.M., Lettinga, G., 2003. Carbon monoxide conversion by anaerobic bioreactor sludges. FEMS Microbiol. Ecol. 44, 271–277. https://doi.org/10.1016/S0168-6496(03)00033-3

Soga, T., Ross, G.A., 1999. Simultaneous determination of inorganic anions, organic acids, amino acids and carbohydrates by capillary electrophoresis. J. Chromatogr. 837, 231–239.

Srinivas, G., Zhu, Y., Piner, R., Skipper, N., Ellerby, M., Ruoff, R., 2010. Synthesis of graphene-like nanosheets and their hydrogen adsorption capacity. Carbon N. Y. 48, 630–635. https://doi.org/10.1016/j.carbon.2009.10.003

Stolecka, K., Rusin, A., 2020. Analysis of hazards related to syngas production and transport. Renew. Energy 146, 2535–2555. https://doi.org/https://doi.org/10.1016/j.renene.2019.08.102

Stookey, L.L., 1970. Ferrozoine-a new spectrophotometric reagent for iron. Anal. Chem. 42, 779–781.

Tabatabaei, M., Rahim, R.A., Abdullah, N., Wright, A.-D.G., Shirai, Y., Sakai, K., Sulaiman, A., Hassan, M.A., 2010. Importance of the methanogenic archaea populations in anaerobic wastewater treatments. Process Biochem. 45, 1214–1225. https://doi.org/https://doi.org/10.1016/j.procbio.2010.05.017

Ungerfeld, E.M., Rust, S.R., Boone, D.R., Liu, Y., 2004. Effects of several inhibitors on pure cultures of ruminal methanogens. J. Appl. Microbiol. 97, 520–526. https://doi.org/10.1111/j.1365-2672.2004.02330.x

Valdez-Vazquez, I., Poggi-Varaldo, H.M., 2009. Hydrogen production by fermentative consortia. Renew. Sustain. Energy Rev. 13, 1000–1013. https://doi.org/10.1016/j.rser.2008.03.003

Valenzuela, Edgardo, I., Davo-Prieto, A., López-Lozano, Nguyen, E., Hernández-Eligio, A., Vega-Alvarado, L., Júarez, K., García-González, A.S., López, Mercedes, G., Cervantes, Francisco, J., 2017. Anaerobic methane oxidation driven by microbial reduction of natural organic matter in tropical wetland. Appl. Environ. Microbiol. 83, e00645-17. https://doi.org/10.1128/AEM.00645-17

Xie, Q., Borges, F.C., Cheng, Y., Wan, Y., Li, Y., Lin, X., Liu, Y., Hussain, F., Chen, P., Ruan, R., 2014. Fast microwave-assisted catalytic gasification of biomass for syngas production and tar removal. Bioresour. Technol. 156, 291–296. https://doi.org/https://doi.org/10.1016/j.biortech.2014.01.057

Xie, Q., Kong, S., Liu, Y., Zeng, H., 2012. Syngas production by two-stage method of biomass catalytic pyrolysis and gasification. Bioresour. Technol. 110, 603–609. https://doi.org/https://doi.org/10.1016/j.biortech.2012.01.028

Xu, K., Liu, H., Li, X., Chen, J., Wang, A., 2010. Typical methanogenic inhibitors can considerably alter bacterial populations and affect the interaction between fatty acid degraders and homoacetogens. Appl. Microbiol. Biotechnol. 87, 2267–2279. https://doi.org/10.1007/s00253-010-2708-y

Xu, S., Fu, B., Zhang, L., Liu, H., 2015. Bioconversion of H2/CO2 by acetogen enriched cultures for acetate and ethanol production: the impact of pH. World J. Microbiol. Biotechnol. 31, 941–950. https://doi.org/10.1007/s11274-015-1848-8

Yang, S., Yang, Y., Kankala, R.K., Li, B., 2018. Sustainability assessment of synfuels from biomass or coal: An insight on the economic and ecological burdens. Renew. Energy 118, 870–878. https://doi.org/https://doi.org/10.1016/j.renene.2017.11.073

Yoneda, N., Kusano, S., Yasui, M., Pujado, P., Wilcher, S., 2001. Recent advances in processes and catalysts for the production of acetic acid. Appl. Catal. A Gen. 221, 253–265. https://doi.org/https://doi.org/10.1016/S0926-

860X(01)00800-6

Zhu, H., Shanks, B.H., Choi, D.W., Heindel, T.J., 2010. Effect of functionalized MCM41 nanoparticles on syngas fermentation. Biomass and Bioenergy 34, 1624–1627. https://doi.org/10.1016/j.biombioe.2010.06.008

Chapter V. Conclusions, Perspectives and final remarks

Conclusions

To the best of our knowledge, few studies have attempted the addition of nanoparticles in the *ex situ* hydrogenotrophic process of biogas enrichment. In this thesis, I have presented the effect of the addition of magnetite nanoparticles (MNPs), reduced graphene oxide (rGO) and reduced graphene oxide adorned/decorated with magnetite nanoparticles (rGO-MNPs) on the performance of the hydrogenotrophic process of biomethane enrichment. The synergistic combination of rGO-MNPs did boost the CH_4 production by 47%, 28% and 33% at the three concentrations tested (50, 100 and 200 mg/L). This improvement was related with the ability of magnetite nanoparticles and conductive carbon materials to facilitate the electron shuttling capacity (ESC). At the same time, it was corroborated that rGO and rGO-MNPs served as reservoirs of hydrogen, which improved H_2 transport from the gas to the liquid phase in the hydrogenotrophic process. Additionally, significant structural changes occurred in the rGO-MNPs composite after hydrogenotrophic tests. Raman and XRD confirmed a greater disorder and lower crystallinity of rGO-MNPs after the biological assays. FTIR analysis indicated that rGO-MNPs were oxidized during the hydrogenotrophic tests. This study highlights the advantages of adding rGO-MNPs as a magnetic nanocomposite, since can be easily recovered, minimizing their release to the environment.

On the other hand, rGO-MNPs was proved to be an attractive alternative for detoxificate hydrolysates. Since the main drawback of detoxification processes is the simultaneous removal of fermentable sugars resulting in a decrease of final products. Graphene-based materials have been successfully applied to remove organic pollutants like dyes, polycyclic aromatic hydrocarbons and gasoline and recently the functionalization of graphene related materials has been explored with excellent results. In the thesis, adsorption tests with rGO-MNPs were performed with model molecules (furfural and furfural-glucose) and in wood hydrolysate obtained from poplar. Results showed that 68% of furfural was removed with furfural alone, 49% of furfural when it was mixed with glucose and 20% of furfural in the wood

hydrolysate using 20 mg of rGO-MNPs. Likewise, rGO-MNPs adsorbed other lignin derivative compounds. Finally, a study of the effect of rGO-MNPs with the adsorbed inhibitors was accomplished during the fermentation of on R. toruloides-1588 showing no toxic effect. The detoxification process with rGO-MNPs highlights that the nanostructure can be easily extracted before the fermentation or after fermentation, by applying an external magnetic force. Another advantage of the use of this nanostructure is the lower amount of adsorbent implemented compared with other adsorbents used.

Lastly, the syngas fermentation with and without the addition of MNPs, rGO and rGO-MNPs was accomplished. Results showed that the acetic acid production was improved by 32% and 23% with 100 mg/L of rGO and rGO-MNPs, respectively at day 13. rGO and rGO-MNPs could be an attractive alternative to enhance the production of acetic acid and then ethanol production. The improvement of the syngas fermentation process is linked to their unique properties, the higher electron shuttling capacity, the sorption capacity and the dosing of dissolved iron, which boosted the microbial activity.

Perspectives

- Due to, the synergistic combination of the reduced graphene oxide material adorned/decorated with magnetite nanoparticles (rGO-MNPs) boosted the CH_4 production by 47%, 28% and 33% relative to the control without nanomaterial for 50, 100 and 200 mg/L, respectively in batch assays. The next step would be scale-up the process in a bioreactor.
- As it was showed, the addition of reduced graphene oxide (rGO) and rGO-MNPs improved the production of acetic acid, 32% with 100 mg/L of rGO and 23% with 100 mg/L of rGO-MNPs, compared with the control at day 13. This results presented rGO and rGO-MNPs as an attractive alternative to enhance the production of acetic acid. However in the microbial pathway of syngas fermentation there could be a probability that alcohols are being produced simultaneously with acetic acid (i.e.; ethanol). Therefore, an analysis of this is needed.

- With the results obtained in the present thesis work, it was showed that rGO-MNPs composite performed satisfactory outcomes in all the biological processes for bioenergy production. However, the BET analysis showed that the surface area of rGO-MNPs was not as high as other reported in literature. The question would be; Does a higher surface area of the reduced graphene oxide adorned/decorated with magnetite nanoparticles could further enhance the bioenergy processes already studied. To answer this, would be interesting to explore other methods of synthesis or change the synthesis conditions in order to obtain a higher surface area. At the same time, from an economic point of view would be important make the synthesis method in less steps.
- In order to better understand the processes for bioenergy production and the complex interactions that could have with the nanomaterials, would be interesting to carry out molecular biology analyzes. In this way, could be elucidate the change in the microbial community structure with and without the addition of the nanomaterials and thus know the biodegradation pathways that could be followed or inhibited.
- As the rGO-MNPs is a magnetic material that can be recovered, another thing to study is to analyze the efficiency of rGO-MNPs after being recovered in each bioenergy production process (carry out the bioenergy processes in cycles).

Final remarks

Even though the improvement for biogas enrichment and syngas fermentation for the production of acetic acid in batch mode was demonstrated by the addition of rGO-MNPs and rGO materials, respectively. It is necessary a deep analysis of such processes to stablish the possibilities of scaling-up and the limitations/challenges faced such processes.

The addition of nanomaterials in industrial biotechnological processes in continuous or semicontinous mode will face problems because of the high cost of nanomateirlas and also because of drawbacks in the disposition of such materials in the

environment. Regarding, the alternatives proposed to scale up the nanomaterials application process in continuous mode, one is the immobilization of the nanomaterials to form filters or incorporated into conventional membranes in order to avoid losses of nanomaterials in the flow. Currently, the efficient immobilization of carbon nanomaterials for removal of pollutants has been reported in literature (Han et al., 2013; Mostafavi et al., 2009; Nie et al., 2021; Wang et al., 2021). On the other hand, other reactor configurations could be explored; such is the use of a continuous up-flow anaerobic sludge blanket reactor (UASB) with magnetic traps made with neodymium magnets. This kind of reactor at lab scale has been previously used to recover magnetic reduced graphene oxide nanosacks in a anaerobic full continuous system (Toral-Sánchez et al., 2018). Likewise, other configuration of reactor configuration could be implemented such is the case of an anaerobic reactor followed by a nanoparticle settler reactor. For instance, Li et al., (2014) conducted a study of the treatment of smelting wastewater using zero-valent iron nanoparticles. The process consisted of two sequential treatment at pilot scale; each had a reactor with the NPs, a clarifier and a NPs recirculation pump. NPs were mixed with wastewater in the reactor, settled in the clarifier and returned by recirculation pump. The experiment was operated at 400 L/h and 35,000 L of wastewater was treated using 75 kg zero-valent iron NPs. Their process was effective for arsenic removal from 520 mg/L to 0.5 mg/L. The large removal capacity was attributed to the large surface area of the NPs and to recirculation. The success of this pilot test approved the construction of a full-scale wastewater treatment plant in which was implemented the same process. In our case, the settler reactor could have a faster settling of the nanoparticles by the implementation at the bottom of a magnet, which could reduce operation time. Otherwise, the main parameters to be considered in the following studies for scale up process are, hydraulic retention time (HRT) of gas and liquid phases, recirculation (if the reactor design applies), settling time (if applies), fluxes, the amount of the recover nanocomposite, the cleaning of the composite if is needed to be used again, and the efficiency of the material after cycles of its recovery. Other factors that should be also addressed are, the disposal of the nanocomposite after its finite use and the possible environmental impact that they could make. Regarding

the leachate of Fe^{2+} to the medium, it is important to study if the nanocomposite would change its magnetic properties because of the release (losses) of the Fe^{2}+ in the medium, since in similar composites with graphene oxide-magnetite it has been proved to be stable with minimum leaching concentration of magnetite due to the strong Fe-O-carbon bonds (Zubir et al., 2015, 2014). Thus, as magnetite is present at low concentrations over the surface of rGO, the leaching effect and the magnetic property might be enough to achieve the desired improvement at certain number of cycles.

The challenges and limitations aforementioned are mainly related with operation, and the design of the process. Nevertheless, the main challenge in the application of nanomaterials is related with the cost. Iron and carbon materials are inexpensive in bulk form but reactive nanomaterials are much more expensive because of the materials and processes needed to make them. For example, the cost of carbon engineered nanomaterials varies widely depending on type (e.g. graphene, nanotubes, amorphous carbon nanomaterials, etc), purity level (wt.%), functionalization, and grade. Current price ranges are $2.50–1000/g (for graphene and derivatives), $0.10–25/g (for MWCNTs), and $25–300/g (for SWCNTs) (Adeleye et al., 2016; “Cheap Tubes Inc.,” n.d.). Otherwise, nano zero iron costs around $0.05–0.10/g whereas micro and bulk Fe^{0} cost less than $0.001/g to produce it (Crane and Scott, 2012). It has been reported that in order to compete against existing treatments methods, the price of iron NPs must be reduced to approximately <$0.01 per g (Müeller and Nowack, n.d.). As an example of the use of bulk powder zero valent iron, Charalambous and Vyrides (2021) investigated a new approach for biogas upgrading (increase of total CH_4) in conjunction with buffering acidification by using zero-valent iron powder in anaerobic granular sludge and cheese whey under mesophilic in lab scale batch conditions. They made a cost effective analysis to scaling the study considering the benefit due to electricity generation from biogas, the cost of NaOH addition, the cost of metallic iron addition and the cost for cheese whey transportation and disposal. The capital cost regarding reactor cost and other equipment as well as labor cost and maintenance cost were not taken into account. They conclude that biogas upgrading through anaerobic digestion of cheese whey

via in-situ anaerobic corrosion of 50 g/L scrap zero-valent iron was more cost-effective way (28,376 € annual profit).

Accordingly, a reactor of 200 m^3 operating with a working volume of 120 m^3 (60%) and a headspace capacity of 80 m^3 (40%) would need 6 kg of the nanocomposite rGO-MNPs (Table 1). The used price was $7485 for 100 g (74850/kg) of rGO and commercialized by Graphenea (About Us – Graphenea). Worth mentioning that 1 g of rGO is sell at $97; thus the higher amount bought might be valued at lower price.

Table 1. Cost of rGO in a 200 m^3 reactor at different working volumes.

Working volume		**Headspace Reactor**	**Composite needed**	**Cost rGO**
(%)	**(m^3)**	**(m^3)**	**(kg)**	**($)**
20	40	160	2	149700
40	80	120	4	299400
60	120	80	6	449100

As is noted, the cost of the nanocomposite does not include the decoration of rGO with magnetite. However, the same company sell other graphene materials such amine functionalized graphene oxide at the same cost of rGO without functionalization. Therefore the functionalization process can be quoted in the same company, where it would be evaluated how much more the composite would cost. As is seen, the cost of the nanocomposite is too high, however, cost-effectiveness of preparation nanomaterials will depend on the final product and its application. Higher cost of production is tolerable for high end use such as in drug delivery systems; and for other proceeses such as waste water treatment, or in our case of study, biogas enrichment and syngas fermentation, the use of low-cost chemicals during the synthesis and the purity of the nanomaterial may be less-sensitive. Thus, would be interesting to use a graphene not as pure as the one used in this thesis and using a chepear or the chepeast available to produce the same nanomaterials in the bioenergy process and see if the enhancement of 47% with 50 mg/L of the synthetized rGO-MNPs in the case of biogas enrichment and the enhancement of 32% with 100 mg/L of rGO in the case of syngas fermentation remain.

All above, it is a fact that the mass scale production with low cost is still necessary in order to make the process economical feasible. Therefore, before scaling the process, further studies should be focused on fast and economical production of graphene and graphene composites through green pathways such as the solvent-free synthesis, recycling of wastes to fabricate the composites and reuse/recovery of the nanomaterial, all this with the aim of fabricate nanomaterials through simple common industrial means. Worth to mention that the cost may be reduced if the nanomaterial is recoverable and reusable several times, which is an advantage since the studied nanocomposite is magnetic. Moreover as investigation advance it has been demonstrated the success performance of nanoadditives in pilot and lab scale processes which seems promising for their implementation of nanomaterials at industrial scale in future.

In summary, the main disadvantage of the use of these nanomaterials is the relatively high cost of manufacturing. However, the costs have decreased as technology improves and meantime there is lot of work to do.

References

Adeleye, A.S., Conway, J.R., Garner, K., Huang, Y., Su, Y., Keller, A.A., 2016. Engineered nanomaterials for water treatment and remediation: Costs, benefits, and applicability. Chem. Eng. J. 286, 640–662. https://doi.org/10.1016/j.cej.2015.10.105

Charalambous, P., Vyrides, I., 2021. In situ biogas upgrading and enhancement of anaerobic digestion of cheese whey by addition of scrap or powder zero-valent iron (ZVI). J. Environ. Manage. 280, 111651. https://doi.org/10.1016/j.jenvman.2020.111651

Cheap Tubes Inc., n.d.

Crane, R.A., Scott, T.B., 2012. Nanoscale zero-valent iron: Future prospects for an emerging water treatment technology. J. Hazard. Mater. 211–212, 112–125. https://doi.org/10.1016/j.jhazmat.2011.11.073

Han, Y., Xu, Z., Gao, C., 2013. Ultrathin Graphene Nanofiltration Membrane for

Water Purification. Adv. Funct. Mater. 23, 3693–3700. https://doi.org/https://doi.org/10.1002/adfm.201202601

Li, S., Wang, W., Liu, Y., Zhang, W. xian, 2014. Zero-valent iron nanoparticles (nZVI) for the treatment of smelting wastewater: A pilot-scale demonstration. Chem. Eng. J. 254, 115–123. https://doi.org/10.1016/j.cej.2014.05.111

Mostafavi, S.T., Mehrnia, M.R., Rashidi, A.M., 2009. Preparation of nanofilter from carbon nanotubes for application in virus removal from water. Desalination 238, 271–280. https://doi.org/https://doi.org/10.1016/j.desal.2008.02.018

Müeller, N.C., Nowack, B., n.d. Nano zero valent iron – THE solution for water and soil remediation? Report of the ObservatoryNANO.

Nie, L., Chuah, C.Y., Bae, T.-H., Lee, J.-M., 2021. Graphene-Based Advanced Membrane Applications in Organic Solvent Nanofiltration. Adv. Funct. Mater. 31, 2006949. https://doi.org/https://doi.org/10.1002/adfm.202006949

Toral-Sánchez, E., Rangel-Mendez, J.R., Hurt, R.H., Ascacio Valdés, J.A., Aguilar, C.N., Cervantes, F.J., 2018. Novel application of magnetic nano-carbon composite as redox mediator in the reductive biodegradation of iopromide in anaerobic continuous systems. Appl. Microbiol. Biotechnol. 102, 8951–8961. https://doi.org/10.1007/s00253-018-9250-8

Wang, Z., Ma, C., Xu, C., Sinquefield, S.A., Shofner, M.L., Nair, S., 2021. Graphene oxide nanofiltration membranes for desalination under realistic conditions. Nat. Sustain. https://doi.org/10.1038/s41893-020-00674-3

Zubir, N.A., Yacou, C., Motuzas, J., Zhang, X., Diniz da Costa, J.C., 2014. Structural and functional investigation of graphene oxide–Fe3O4 nanocomposites for the heterogeneous Fenton-like reaction. Sci. Rep. 4, 4594. https://doi.org/10.1038/srep04594

Zubir, N.A., Yacou, C., Motuzas, J., Zhang, X., Zhao, X.S., da Costa, J.C., 2015. The sacrificial role of graphene oxide in stabilising a Fenton-like catalyst GO–Fe3O4. Chem. Commun. 51, 9291–9293. https://doi.org/10.1039/C5CC02292D